NASA TECHNICAL MEMORANDUM

NASA TM X-62,167

NASA TM X-62,167

AERODYNAMIC CHARACTERISTICS OF A LARGE-SCALE LIFT-ENGINE FIGHTER MODEL WITH EXTERNAL SWIVELING LIFT ENGINES

Jerry P. Barrack and Jerry V. Kirk

Ames Research Center
Moffett Field, Calif. 94035

July 1972

AERODYNAMIC CHARACTERISTICS OF A LARGE-SCALE LIFT-ENGINE FIGHTER MODEL WITH EXTERNAL SWIVELING LIFT-ENGINES

BY

JERRY P. BARRACK AND JERRY V. KIRK

NASA-AMES RESEARCH CENTER
MOFFETT FIELD, CA. 94035

NOTATION

A	nozzle exit area, sq. m (sq. ft.), or wing aspect ratio
b	wing span, m (ft.)
$\bar{c}$	mean aerodynamic chord, m (ft.), $2/_S \int^{b/2} c^2 dy$
C_D	drag coefficient, D/qS
C_l	rolling moment coefficient, ℓ/qSb
C_L	lift coefficient, L/qS
C_m	pitching moment coefficient, $M/qS\bar{c}$
C_n	yawing moment coefficient, N/qSb
C_T	thrust coefficient, T/qS
C_Y	side force coefficient, Y/qS
D	drag, N (lb.)
i_t	horizontal tail incidence angle, deg.
ℓ	rolling moment, mN (ft. Lb.)
L	total lift on model, N (lb.)
M	pitching moment, mN (ft. lb.)
N	yawing moment, mN (ft. lb.)
q	free stream dynamic pressure, $N/_m 2$ (lb./ft.^{2})
S	wing area, sq. m (sq. ft.)
T	engine gross thrust, N (lb.)
v	air velocity, m/sec. (ft./sec.)
V	free stream velocity, m/sec. (knots or ft./sec.)

Y	side force, N (lb.)
α	angle of attack of the wing chord plane, deg.
β	angle of sideslip, deg.
ρ	density Kg/m^3 ($lb.-sec.^2/ft.^4$)
σ	thrust angle from horizontal, deg.
δ_f	flap deflection angle measured normal to the hinge line, deg.
δ_s	slat deflection angle measured normal to the hinge line, deg.

Subsripts

c	lift-cruise
L	lift
s	static
u	uncorrected

INTRODUCTION

Previous investigations have determined the exhaust gas reingestion, inlet flow distortion, and aerodynamic characteristics of various lift-engine VTOL configurations in the transition speed range. Both small-scale (Ref. 1 through 9) and large-scale (Ref. 10 through 17) models were used for these investigations. In general, these configurations incorporated either wing mounted lift-engine-pods or internally mounted lift-engines in the fuselage. In contrast, the model used for this investigation had lift engines mounted in pairs on each side of the fuselage and was representative of a high-performance supersonic fighter VTOL aircraft.

This report presents the aerodynamic characteristics of a six-engine (four (4) lift, two (2) lift-cruise) lift-engine model obtained in the Ames 40- by 80-foot wind tunnel. The model was an approximate one-half scale representation of a lift-engine VTOL fighter aircraft with a variable-sweep wing. The four (4) lift-engines were mounted in pairs on each side of the aircraft. The two (2) lift-cruise engines were housed in the aft fuselage with the inlets located above the wing.

Longitudinal and lateral-directional force and moment data are presented for a range of exhaust gas momentum ratios (thrust coefficients). Wind tunnel forward speed was varied from 0 to 140 knots corresponding to a maximum Reynolds number of 6.7 million. The data contained herein are presented without analysis.

MODEL DESCRIPTION

The model was representive of a variable sweep lift engine fighter aircraft and was approximately one-half scale. Six YJ85-5 turbojet engines (without after burners) were used as the propulsion system

(four (4) engines as direct lift and two (2) as lift-cruise engines) for this low-speed wind tunnel investigation. Photographs of the model mounted in the Ames 40- by 80-foot wind tunnel are given in Fig. 1. Figure 2 is a sketch of the model showing pertinent details.

Fuselage

The fuselage was slab sided with rounded corners. The maximum width and depth were 134.6 cm (53 in.) and 168.9 cm (66.5 in.), respectively. The aft fuselage housed the two lift-cruise engines. The lift-cruise engine inlets were on top of the fuselage just behind the wing leading edge.

Wing

The high-mounted wing represented a variable sweep configuration. However, the outer panels were fixed at a 25-percent-chord sweep angle of 13.75° for this investigation. The inboard fixed section (strake or glove) had a leading edge sweep of 70° and joined the fuselage at station 327.4 (128.9). The strake faired into the outer wing panel at fuselage station 565.2 (222.5) and wing station 128.5 (50.6). The wing span was 7.32 m (24 ft.); wing aspect ratio was 5.82 (based on panel dimensions); and the taper ratio was 0.36. An NACA 65-412 modified airfoil section was used for the wing.

High-Lift Devices

A 40% chord, trailing-edge, single-slotted flap extended from the fuselage juncture to 75% of the wing semispan (see Fig. 2b). Flap

deflections of 0° and 45° were tested. Twenty percent chord leading edge slats spanned the outer wing panel and were tested at 0° and 25° deflection.

Empennage

The vertical tail had an NACA 64-009 airfoil section. The horizontal tail was wedge shaped with an aspect ratio of 2.87 and a taper ratio of 0.18. The horizontal tail was remotely controlled to give deflection angles of -30° to +25°.

Propulsion System

Four YJ85-5 turbojet engines were mounted in pairs at the sides of the fuselage as direct-lift engines with the axis of rotation 70° from the streamwise direction. Rotation was remotely controlled and angles from 90° (thrust axis vertical) through 30° were tested in 15° increments. When the lift engines were vertical, the tops of the inlets were in the wing chord plane. Two lift-cruise engines were installed in the aft fuselage. The lift-cruise engine exit nozzles were manually positioned to correspond to the lift-engine angles.

TEST PROCEDURE

Longitudinal force and moment data were obtained with the model on the normal strut system in the 40- by 80-foot wind tunnel for an angle of attack range from -4° to 22°. Lateral-directional force and moment data were obtained at 0° and 8° angle of attack for sideslip angles ranging from -16° to +12°. Wind tunnel forward speed was 0 to 140 knots corresponding to a maximum Reynolds number of 6.7 million.

Tests at Constant Angle of Attack

As angle of attack and wind tunnel forward speed were held constant, the engine thrust was varied to give a range of thrust coefficients (exhaust gas momentum ratios) at each engine vector angle. At selected thrust coefficients, horizontal tail incidence was varied. Model sideslip angle was also varied at 0° and 8° angle of attack.

Tests with Variable Angle of Attack

Engine thrust and wind tunnel speed (thrust coefficient or momentum ratio) were held essentially constant as the angle of attack was varied. Horizontal tail on and off results were obtained for various thrust coefficients at each engine vector angle.

CORRECTIONS

All force and moment data obtained with the engines not operating (power-off) have been corrected for the effect of the wind tunnel walls using the following equations:

$$\alpha = \alpha_u + 0.2348\ C_{Lu}$$

$$C_D = C_{Du} + 0.0041\ C_{Lu}^2$$

$$C_M = C_{Mu} + 0.00058\ C_{Lu} \text{ (tail on only)}$$

Results obtained with the engines operating have not been corrected for wind tunnel wall interference effects. However, Ref. 18 indicates that the wall corrections for a model of this disk loading would be small.

All tests were conducted without a fairing on the tail strut. Appropriate tare corrections have been applied to the data to account for the

resulting tail strut drag.

All the data have been corrected to equal thrust levels in cases where all engines were not operating at equal thrust. This was accomplished by adding or subtracting an increment to the forces and moments equal to the direct thrust excess or decrement for each engine. These corrections were usually small.

Interference Factors

Interference factors have been computed for the model and are a part of each figure. These factors represent the difference between measured results and results that would be obtained by summing the direct thrust effects with the power-off force and moment data. These factors represent not only the effect of the jet on the airframe, but also the jet wake effect. Engine and nozzle vector angles were taken into account in these calculations.

RESULTS

Table 1 is an index to the figures presented.

The square root of the free stream to exhaust gas momentum ratio is used as the correlating parameter in the presentation of results. The relationship between thrust coefficient and momentum ratio is shown in figure 3.

Figures 4 through 6 present the variation in power-off longitudinal aerodynamic characteristics with angle of attack. The effects of flap deflection, slat deflection, removal of the lift engines and lift-cruise engine exhaust nozzles are shown.

The power-on longitudinal aerodynamic characteristics at selected exhaust gas momentum ratios are shown in figures 7 through 18 for engine vector angles of 90° through 30°, horizontal tail on and off. Each figure presents basic data along with interference increments.

The interference increments or factors were calculated by subtracting the direct thrust and power-off contributions from the measured data.

The trailing edge flaps were set at 45° and the leading edge slats deflected 25° for all results shown.

Figures 19 through 28 show the variation in the longitudinal aerodynamic characteristics with change in momentum ratio at 0° angle of attack. As with preceeding figures, engine vector angles of 90° to 30° are presented. The effects of running lift engines only, lift-cruise engines only, and all engines simultaneously are included.

The variation in the lateral-directional aerodynamic characteristics as a function of sideslip angle are presented in figures 29 through 33 for angles of attack of 0° and 8°. Interference increments are presented as part of each figure.

The final section of figures is devoted to the effects of horizontal tail deflection on longitudinal characteristics.

Figures 34 through 39 show the effect of horizontal tail incidence on the longitudinal aerodynamic characteristics at 0° and 10° angle of attack. Power-off data as well as power-on data with engine vector angles from 90° to 30° is shown. Results are also presented at 16° angle-of-attack for a 45° engine vector angle.

REFERENCES

1. Otis, James H., Jr.: Induced Interference Effects on a Four-Jet VTOL Configuration with Various Wing Planforms in the Transition Speed Range. NASA TN D-1400, 1962.

2. Vogler, Raymond D.: Interference Effects of Single and Multiple Round or Slotted Jets on a VTOL Model in Transition. NASA TN D-2380. 1964

3. Vogler, Raymond D.; and Kuhn, Richard E.: Longitudinal and Lateral Stability Characteristics of Two Four-Jet VTOL Models in the Transition Speed Range. NASA TM X-1092. 1965.

4. Vogler, Raymond D.: Ground Effects on Single-and Multiple-Jet VTOL Models at Transition Speeds over Stationary and Moving Ground Planes. NASA TN D-3213.

5. Margason, Richard J.: Jet-Induced Effects in Transition Flight Conference on V/STOL and STOL Aircraft, NASA SP-116. Paper No. 13. 1966.

6. Margason, Richard J.; and Gentry, Garl L., Jr.: Aerodynamic Characteristics of Five-Jet VTOL Configurations in the Transition Speed Range. NASA TN D-4812. 1968.

7. Winston, Matthew M.: Wind-Tunnel Data from a 0.16-Scale V/STOL Model with Direct-Lift and Lift-Cruise Jets. NASA TMX-1758. 1969.

8. Carter, Arthur W.: Effects of Jet-Exhaust Location on the Longitudinal Aerodynamic Characteristics of a Jet V/STOL Model. NASA TN D-5333. 1969.

9. Vogler, Raymond D.: Wind-Tunnel Investigation of a VTOL Jet-Transport Model with Powered-Lift Engines in Pods at Midspan or Inboard. NASA TN D-5770.

10. Tolhurst, William H.; and Kelly, Mark W.: Characteristics of Two Large-Scale Jet-Lift Propulsion Systems. NASA SP-116 - Paper number 15. 1966.

11. Lavi, Rahim: An Experimental Investigation of VTOL Lift-Engine Inlets. AIAA Journal of Aircraft, March - April 1967.

12. Hammond, Alexander D.; and McLemore, H. Clyde: Hot-Gas Ingestion and Jet-Interference Effects for Jet V/STOL Aircraft. NASA TM-X-60449. 1967.

13. Barrack, Jerry P.; and Kirk, Jerry V.: Low-Speed Characteristics of High Performance Lift-Engine V/STOL Aircraft. SAE Paper 680644, 1968.

14. Lavi, Rahim; Hall, Gordon R.; and Stark, Wilbur W.: Full-Scale Ground Proximity Investigation of a VTOL Fighter Model Aircraft. NASA CR-1098, 1968.

15. McLemore, H. Clyde, and Smith, Charles C., Jr.: Hot-Gas Ingestion Investigation of Large-Scale Jet VTOL Fighter Type Models. NASA TN D-4609. 1968.

16. McLemore, H. Clyde; Smith, Charles C., Jr.; and Hemeter, Patricia G.: Generalyzed Hot-Gas Ingestion of Large-Scale Jet VTOL Fighter-Type Models. NASA TN D-5581. 1970.

17. Kirk, Jerry V.; and Barrack, Jerry P.: Reingestion Characteristics and Inlet Flow Distortion of V/STOL Lift-Engine Fighter Configurations. NASA TN D-7014. 1970.

18. Cook, Woodrow L.; and Hickey, David H.: Comparison of Wind Tunnel and Flight Test Aerodynamic Data in the Transition Speed Range for Five V/STOL Aircraft. NASA SP-116 Paper Number 26, 1966.

TABLE I

FIGURE	C_T	$\sqrt{\frac{\rho_o V_o^2}{\rho_j V_j^2}}$	ENGINES OPERATING	σ DEG	i_t DEG	δ_f DEG	δ_s DEG	α DEG	β DEG
POWER OFF LONGITUDINAL CHARACTERISTICS									
4	0	—	NONE	REMOVED	OFF	0,45	0,25	-4 TO 22	0
5	0	—	NONE	REMOVED	0	0,45	0,25	-4 TO 22	0
6	0	—	NONE	REMOVED	OFF	45	25	-4 TO 22	0
POWER ON LONGITUDINAL CHARACTERISTICS									
7	0, 6.03 14.1, 19.9	∞, .131 .086, .072	ALL	90	OFF	45	25	-4 TO 20	0
8	0, 3.0, 6.0 13.9, 24.2	∞, .187, .131 .086, .065	ALL	90	0	45	25	-4 TO 22	0
9	0, 3.4, 6.0 25.5	∞, .17, .13 .064	ALL	75	OFF	45	25	-4 TO 22 -4 TO 20	0
10	0, .9, 1.7 3.4, 6.1	∞, .34, .25 .18, .13	ALL	75	0	45	25	-4 TO 22	0
11	0, 3.4, 6.0	∞, .17, .13	ALL	60	OFF	45	25	-4 TO 22	0
12	0, .92 1.8, 3.4	∞, .34 .24, .18	ALL	60	0	45	25	-4 TO 22	0
13	0, 2.2 3.4, 6.0	∞, .22 .18, .13	ALL	45	OFF	45	25	-4 TO 22	0
14	0, .7, 1.5 2.2, 3.4	∞, .37, .26 .22, .18	ALL	45	0	45	25	-4 TO 22	0
15	0, .6, .7 .9	∞, .41 .37, .34	ALL	30	OFF	45	25	-4 TO 22	0
16	0, .6, .7 .9	∞, .41 .37, .34	ALL	30	0	45	25	-4 TO 22	0
17	0 2.2 1.1 3.4	∞ .18 .18 .18	NONE LIFT LIFT/CRUISE ALL	60	0	45	25	-4 TO 22	0

TABLE I, CONTINUED

FIGURE	C_T	$\sqrt{\frac{\rho_o V_o^2}{\rho_j V_j^2}}$	ENGINES OPERATING	σ DEG	ι_t DEG	δ_f DEG	δ_s DEG	α DEG	β DEG
18	0 2.3 3.4	∞ .18 .18	NONE LIFT ALL	45 ↓	OFF ↓	45 ↓	25 ↓	-4 TO 22 ↓	0 ↓
EFFECT OF MOMENTUM RATIO VARIATION ON LONGITUDINAL CHARACTERISTICS									
19	VARIABLE	VARIABLE	ALL	90	OFF	45	25	0	0
20	VARIABLE	VARIABLE	ALL	90	0	45	25	0	0
21	VARIABLE ↓	VARIABLE ↓	LIFT LIFT/CRUISE ALL	75 ↓	OFF ↓	45 ↓	25 ↓	0 ↓	0 ↓
22	VARIABLE	VARIABLE	ALL	75	0	45	25	0	0
23	VARIABLE ↓	VARIABLE ↓	LIFT LIFT/CRUISE ALL	60 ↓	OFF ↓	45 ↓	25 ↓	0 ↓	0 ↓
24	VARIABLE ↓	VARIABLE ↓	LIFT LIFT/CRUISE ALL	60 ↓	0 ↓	45 ↓	25 ↓	0 ↓	0 ↓
25	VARIABLE ↓	VARIABLE ↓	LIFT LIFT/CRUISE ALL	45 ↓	OFF ↓	45 ↓	25 ↓	0 ↓	0 ↓
26	VARIABLE ↓	VARIABLE ↓	LIFT LIFT/CRUISE ALL	45 ↓	0 ↓	45 ↓	25 ↓	0 ↓	0 ↓
27	VARIABLE ↓	VARIABLE ↓	LIFT LIFT/CRUISE ALL	30 ↓	OFF ↓	45 ↓	25 ↓	0 ↓	0 ↓
28	VARIABLE	VARIABLE	ALL	30	0	45	25	0	0
LATERAL - DIRECTIONAL CHARACTERISTICS									
29	0 , 24.3 0 , 24.0	∞ , .07 ∞ , .07	ALL ↓	90 ↓	0 ↓	45 ↓	25 ↓	0 8	-16 TO+12 ↓

TABLE I , CONCLUDED

FIGURE	C_T	$\sqrt{\frac{\rho_o V_o^2}{\rho_i V_i^2}}$	ENGINES OPERATING	σ DEG	i_t DEG	δ_f DEG	δ_s DEG	α DEG	β DEG
30	0 , 3.4 0 , 3.4	∞ , .18 ∞ , .18	ALL	75	0	45	25	0 8	-16 TO+12
31	0 , 1.8 0 , 1.9	∞ , .24 ∞ , .24	ALL	60	0	45	25	0 8	-16 TO+12
32	0 , .74 0 , .74	∞ , .37 ∞ , .37	ALL	45	0	45	25	0 8	-16 TO+12
33	0 , .74 0 , .74	∞ , .37 ∞ , .37	ALL	30	0	45	25	0 8	-16 TO+12
EFFECT OF HORIZONTAL TAIL DEFLECTION ON LONGITUDINAL CHARACTERISTICS									
34	0 0	∞ ∞	NONE	ENGINES REMOVED	-30 TO+25	45, 0	25, 0	0 10	0
35	0,3.0,6.0 0, 5.9	∞,.19,.13 ∞, .13	ALL	90	-30 TO+25	45	25	0 10	0
36	0,3.4,6.1 0,3.4,6.1	∞,.18,.13 ∞,.18,.13	ALL	75	-30 TO+25	45	25	0 10	0
37	0,1.8,3.4 0,1.8,3.4	∞,.24,.18 ∞,.24,.18	ALL	60	-30 TO+25	45	25	0 10	0
38	0, 1.5, 2.2 3.4 0, 1.5, 2.2 3.4 0, 3.4	∞,.27,.22 .18 ∞,.26,.22 .18 ∞, .18	ALL ↓	45 ↓	-30 TO+25 ↓	45 ↓	25 ↓	0 0 10 10 16	0 ↓
39	0 , .74	∞ , .37	ALL	30	-30 TO+25	45	25	0 , 10	0

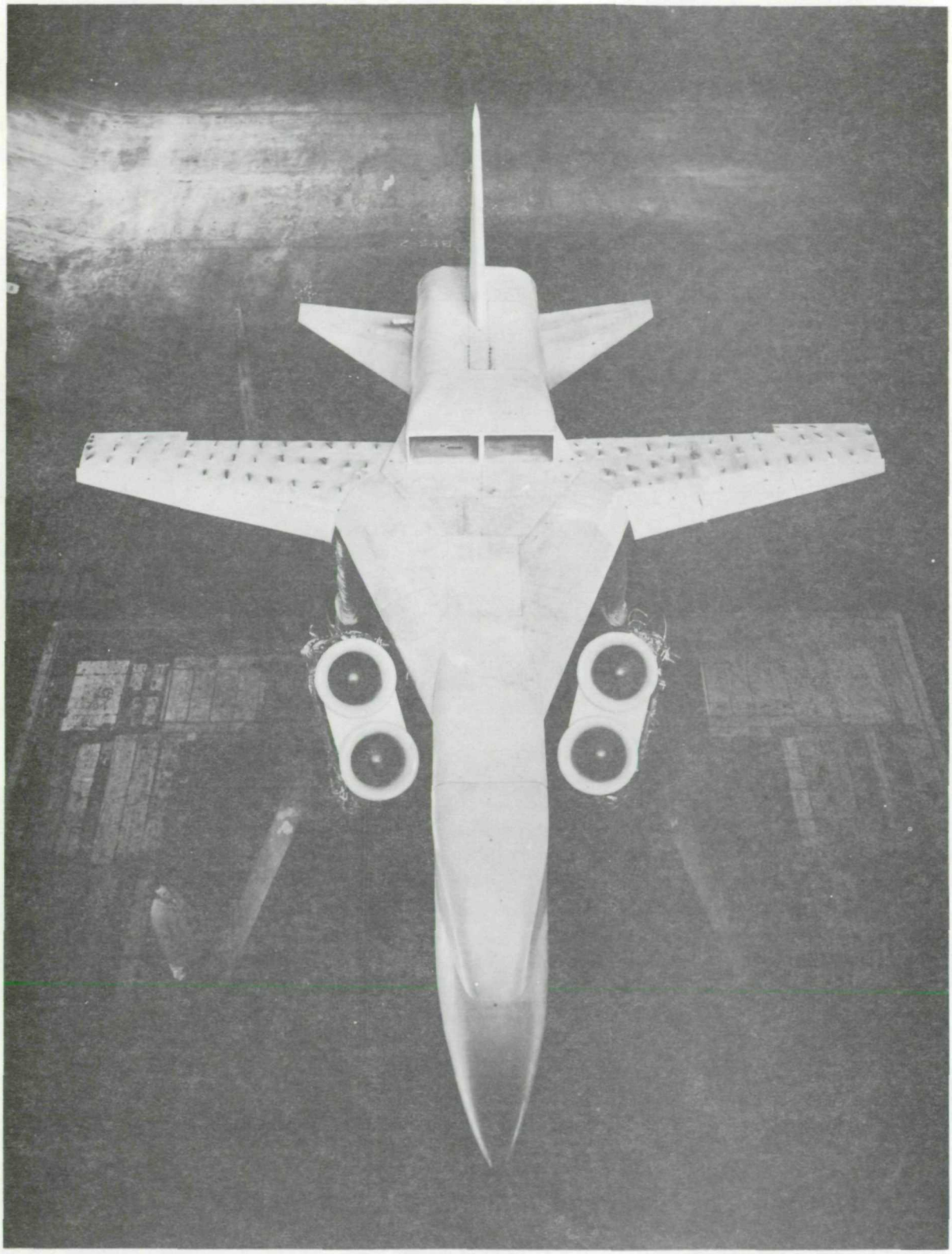

Figure 1.- Model mounted in 40- by 80-foot wind tunnel

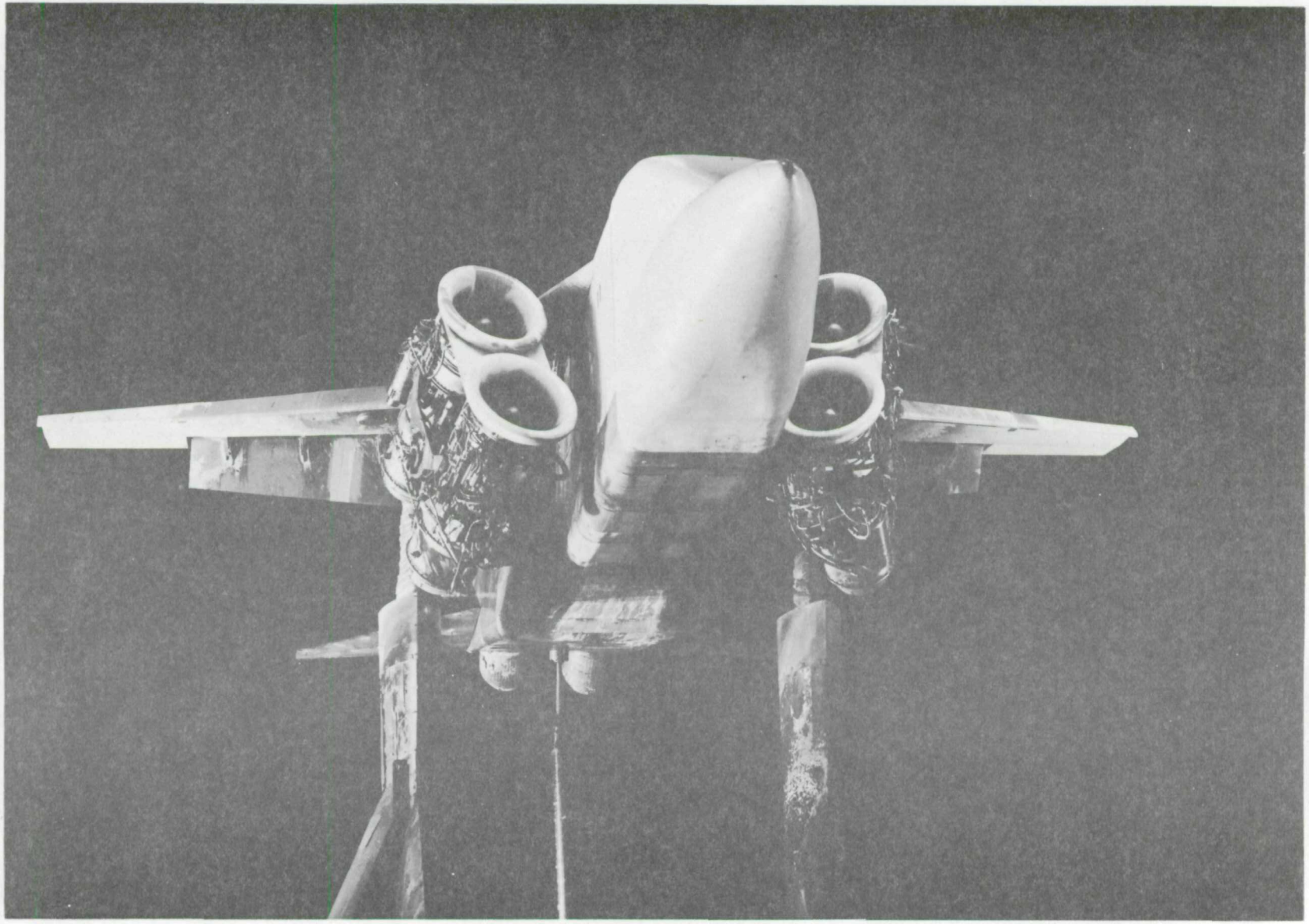

Figure 1.- Concluded.

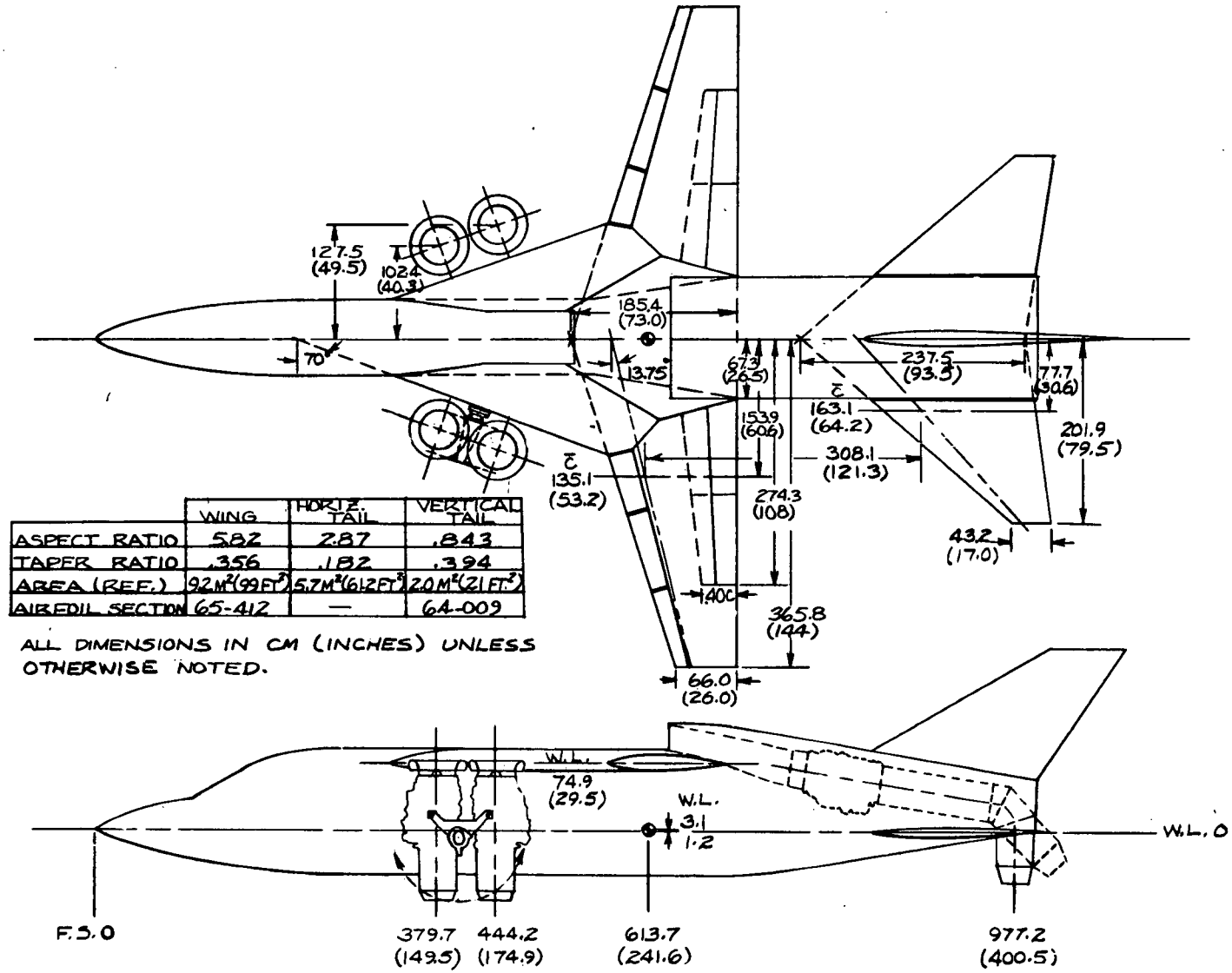

	WING	HORIZ. TAIL	VERTICAL TAIL
ASPECT RATIO	5.82	2.87	.843
TAPER RATIO	.356	.182	.394
AREA (REF.)	92 M² (99 FT²)	5.7 M² (61.2 FT²)	2.0 M² (21 FT²)
AIRFOIL SECTION	65-412	—	64-009

ALL DIMENSIONS IN CM (INCHES) UNLESS OTHERWISE NOTED.

(a) Model geometry

Figure 2.- General arrangement of the model

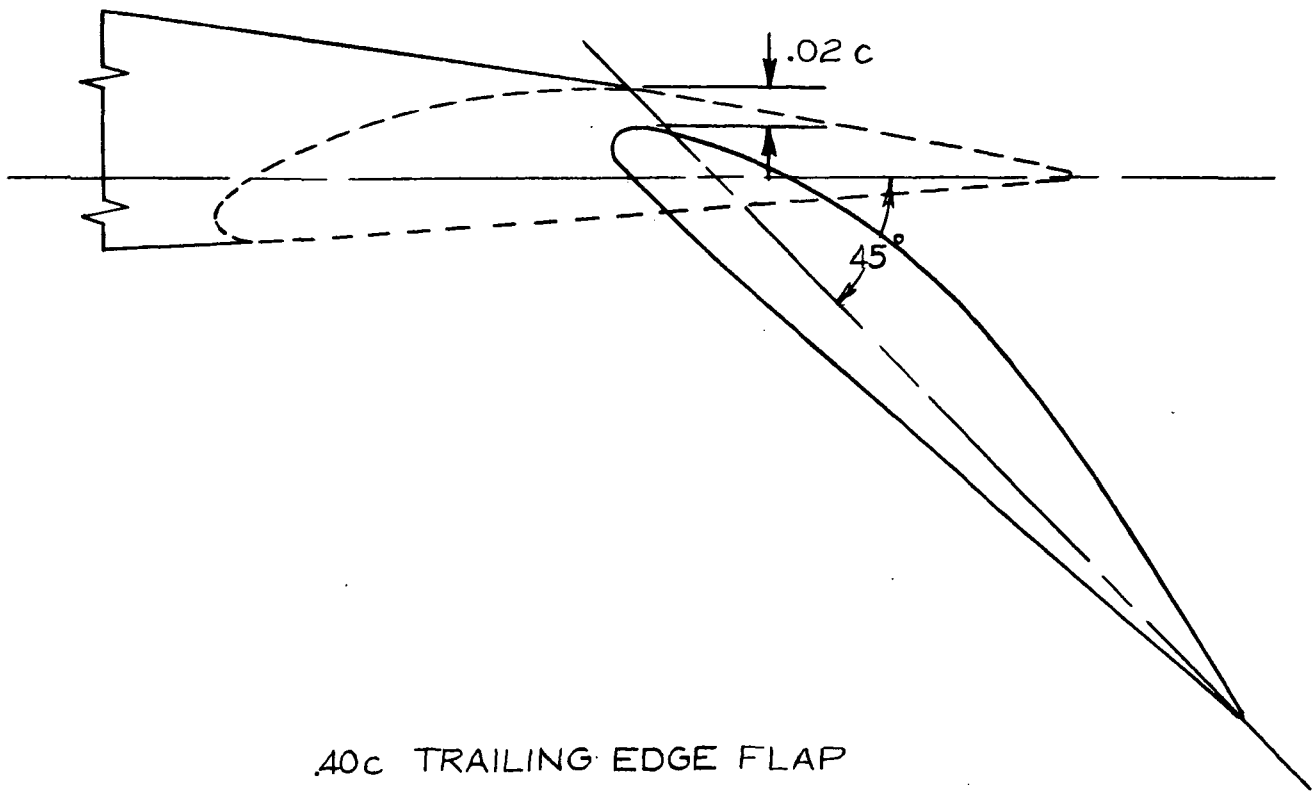

.40c TRAILING EDGE FLAP

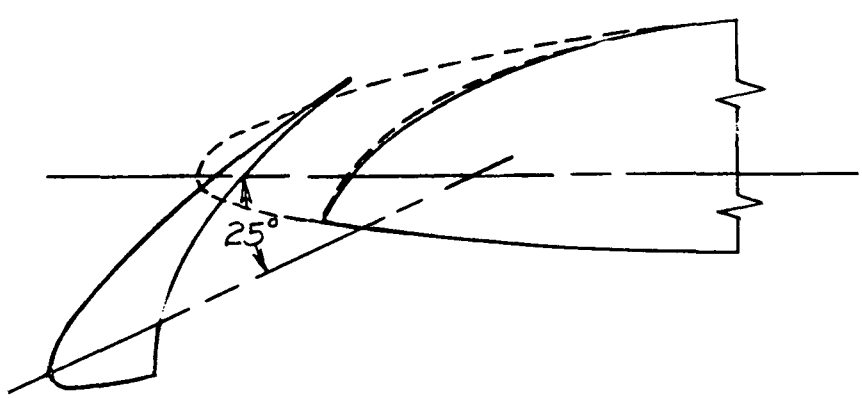

.20c LEADING EDGE SLAT

b- details of the high lift devices

Figure 2.- Concluded.

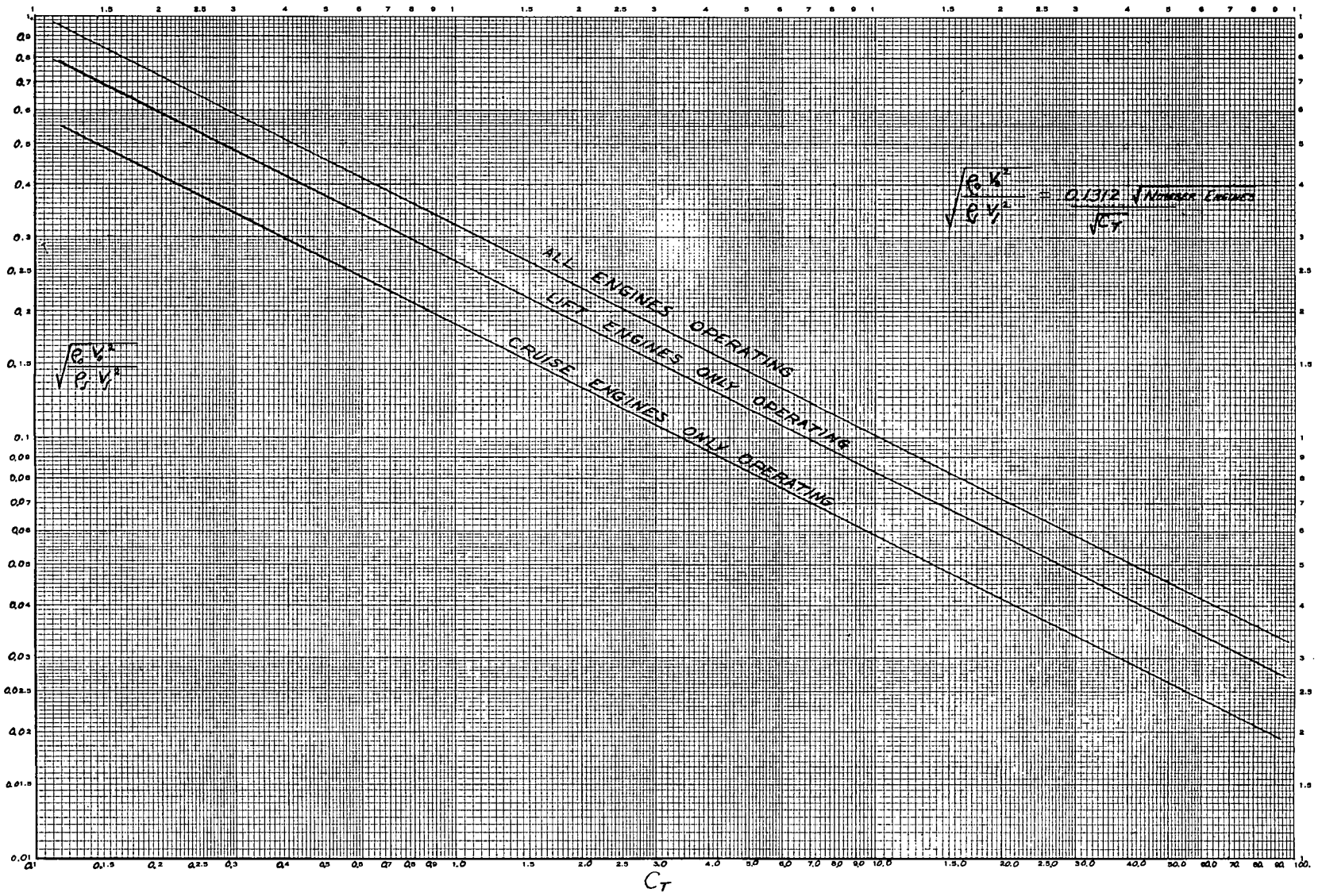

Figure 3.- Relationship between thrust coefficient and exhaust gas momentum ratio.

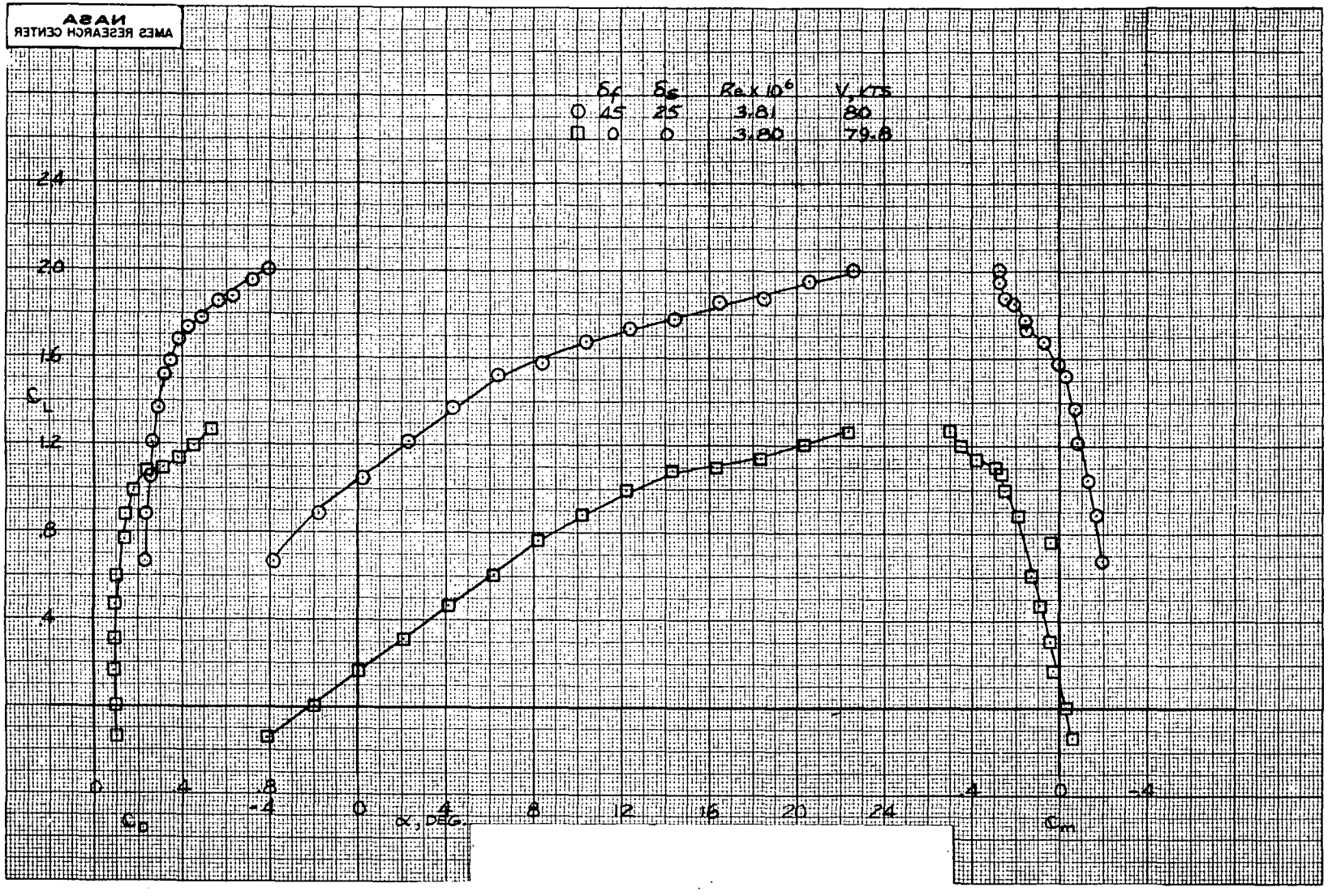

Figure 4.- Effect of slats and flaps on longitudinal aerodynamic characteristics. Power off. Lift engines removed. Cruise engine nozzles removed. Horizontal tail off.

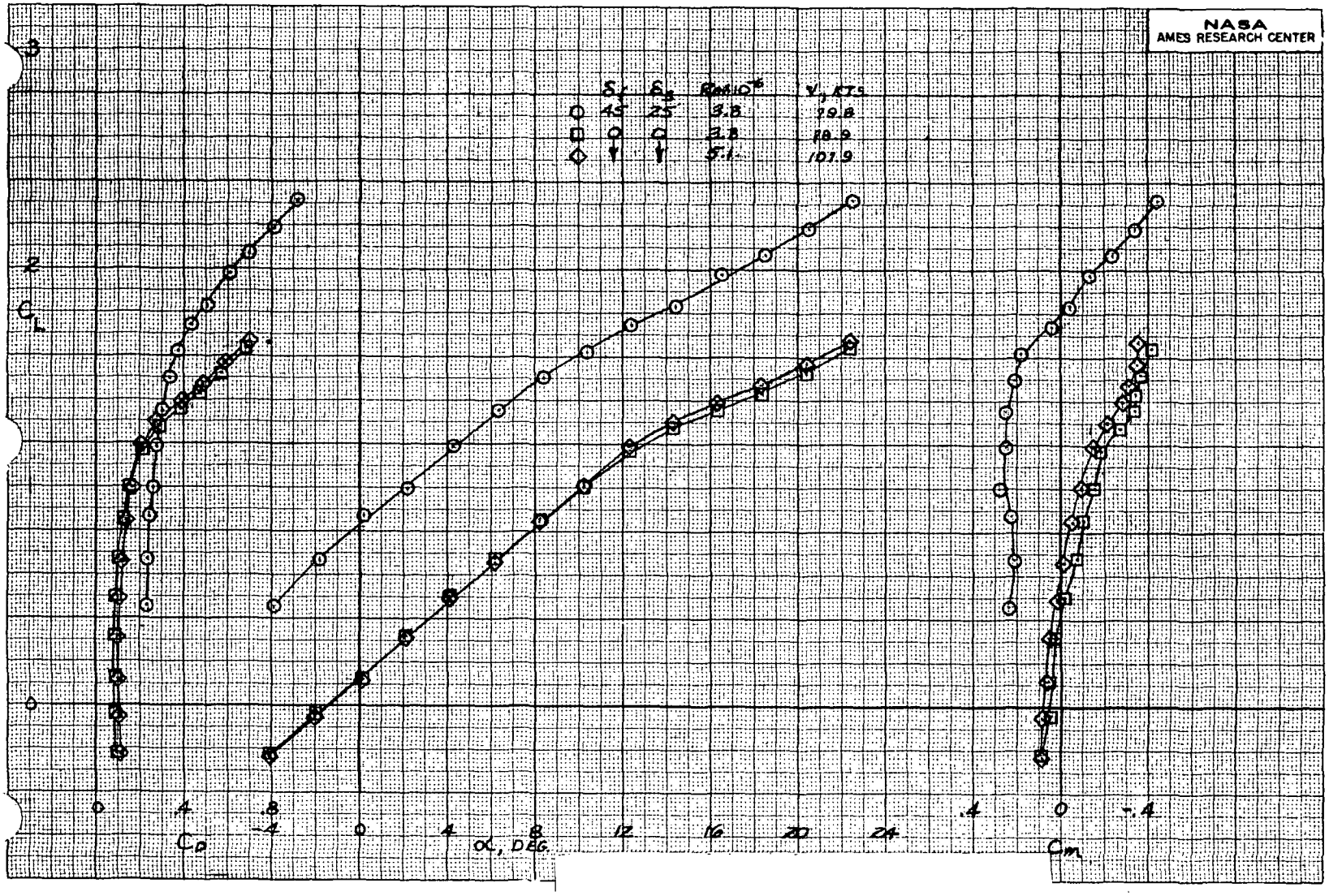

Figure 5.- Effect of slats and flaps on longitudinal aerodynamic characteristics. Power off. Lift engines removed. Cruise engine nozzles removed. $i_t = 0°$. $\beta = 0°$.

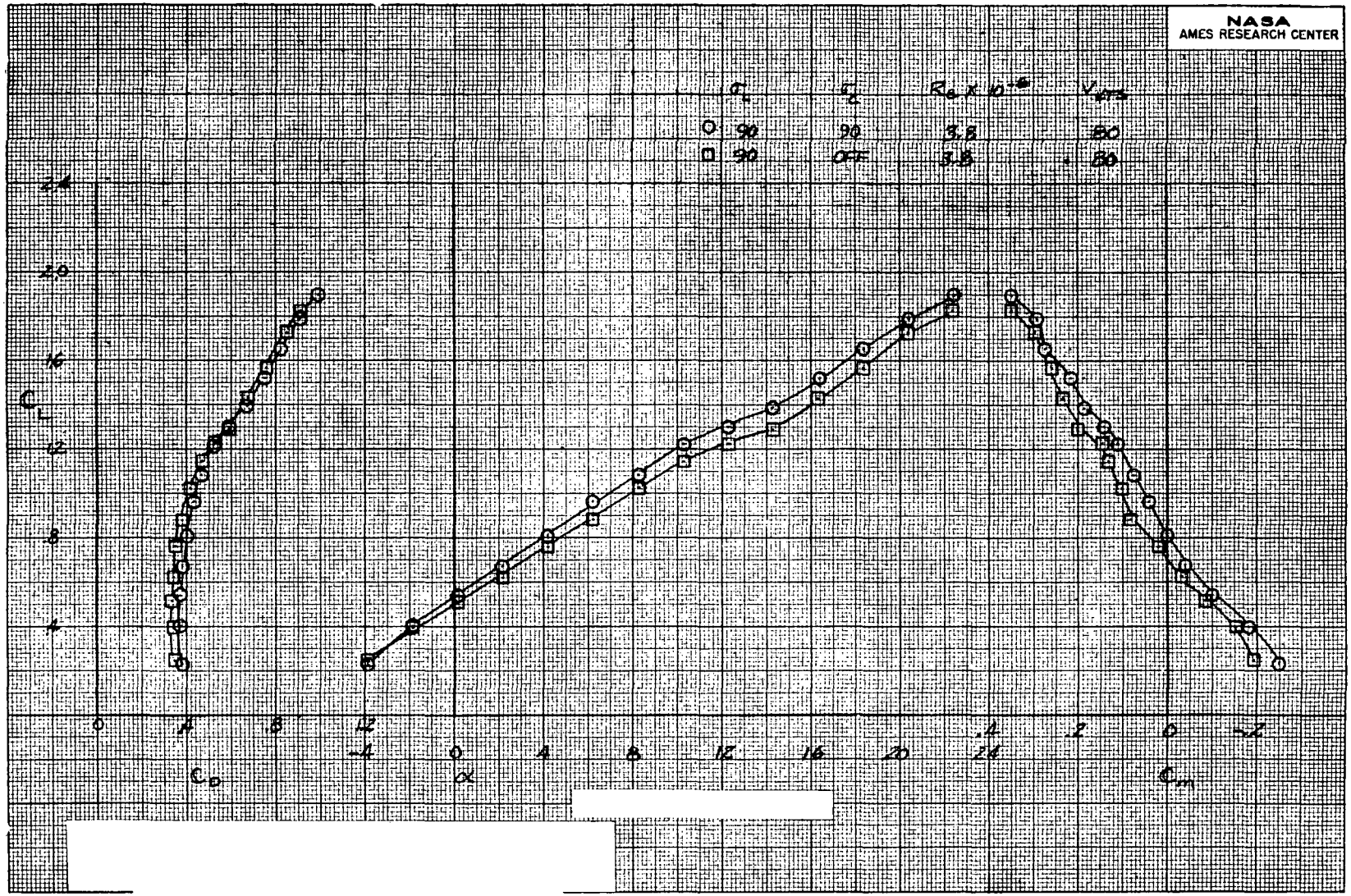

Figure 6.- The effect of removing the lift engines and lift/cruise nozzles on longitudinal aerodynamic characteristics; power off, horizontal tail off, $\beta = 0$, $\delta_f = 45°$, $\delta_s = 25.°$

a- Effect of lift/cruise nozzles

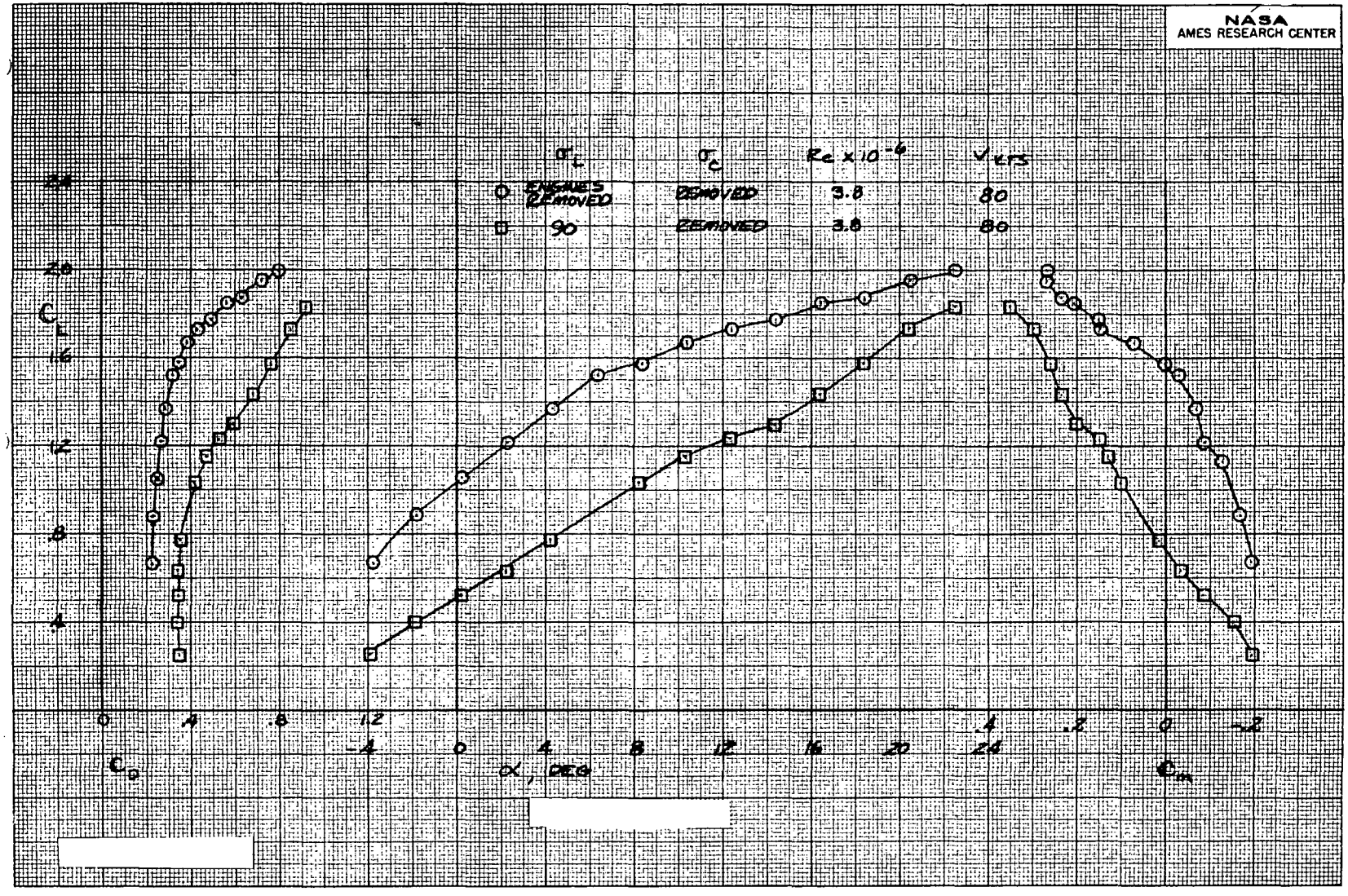

Figure 6.- concluded

b- Effect of lift engines

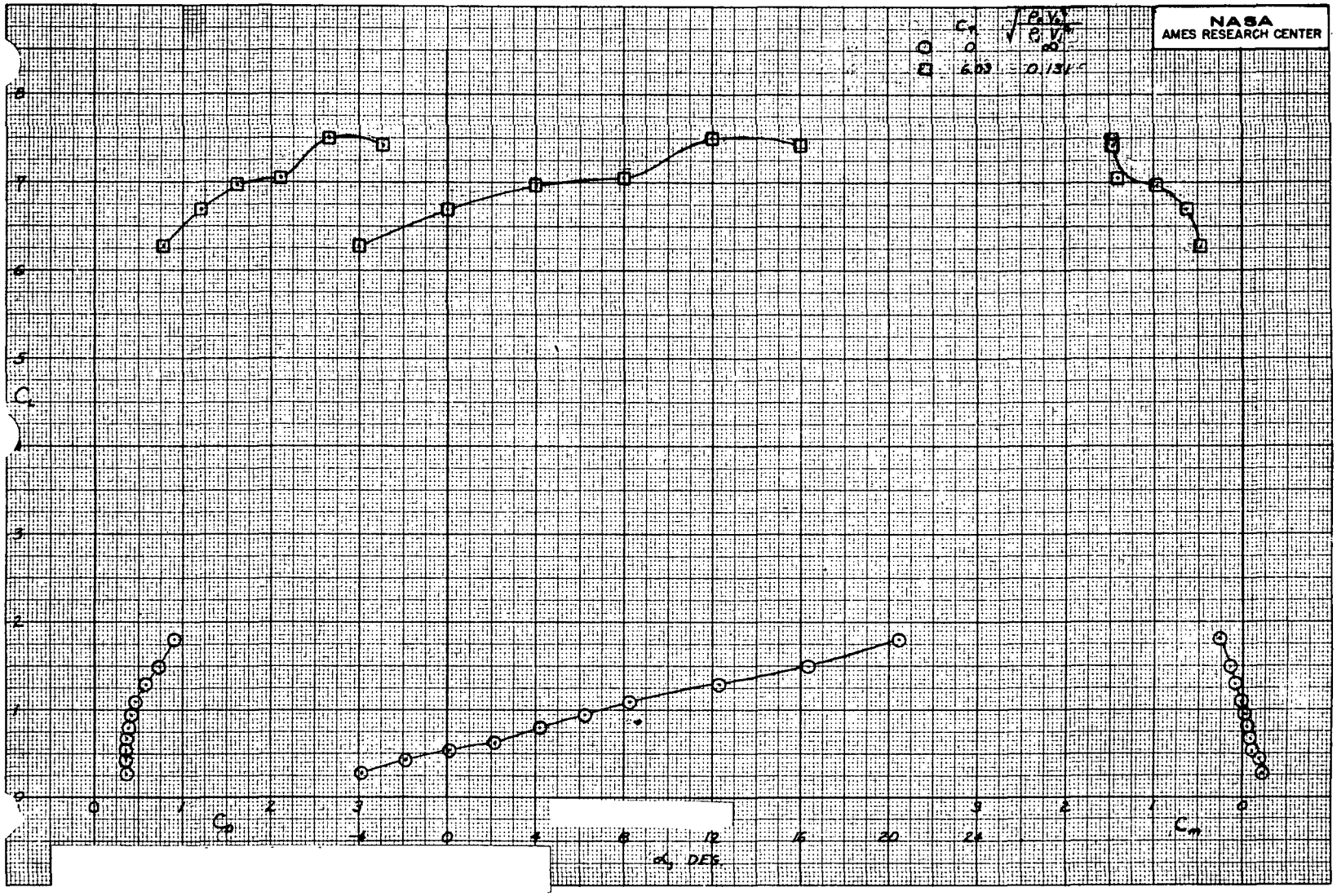

Figure 7.- Effect of angle of attack on longitudinal aerodynamic characteristics; $\alpha = 90°$, All engines at equal thrust, Horizontal tail off, $\beta = 0°$, $\delta_f = 45°$, $\delta_s = 25°$.

a- C_L vs C_D, α, C_M

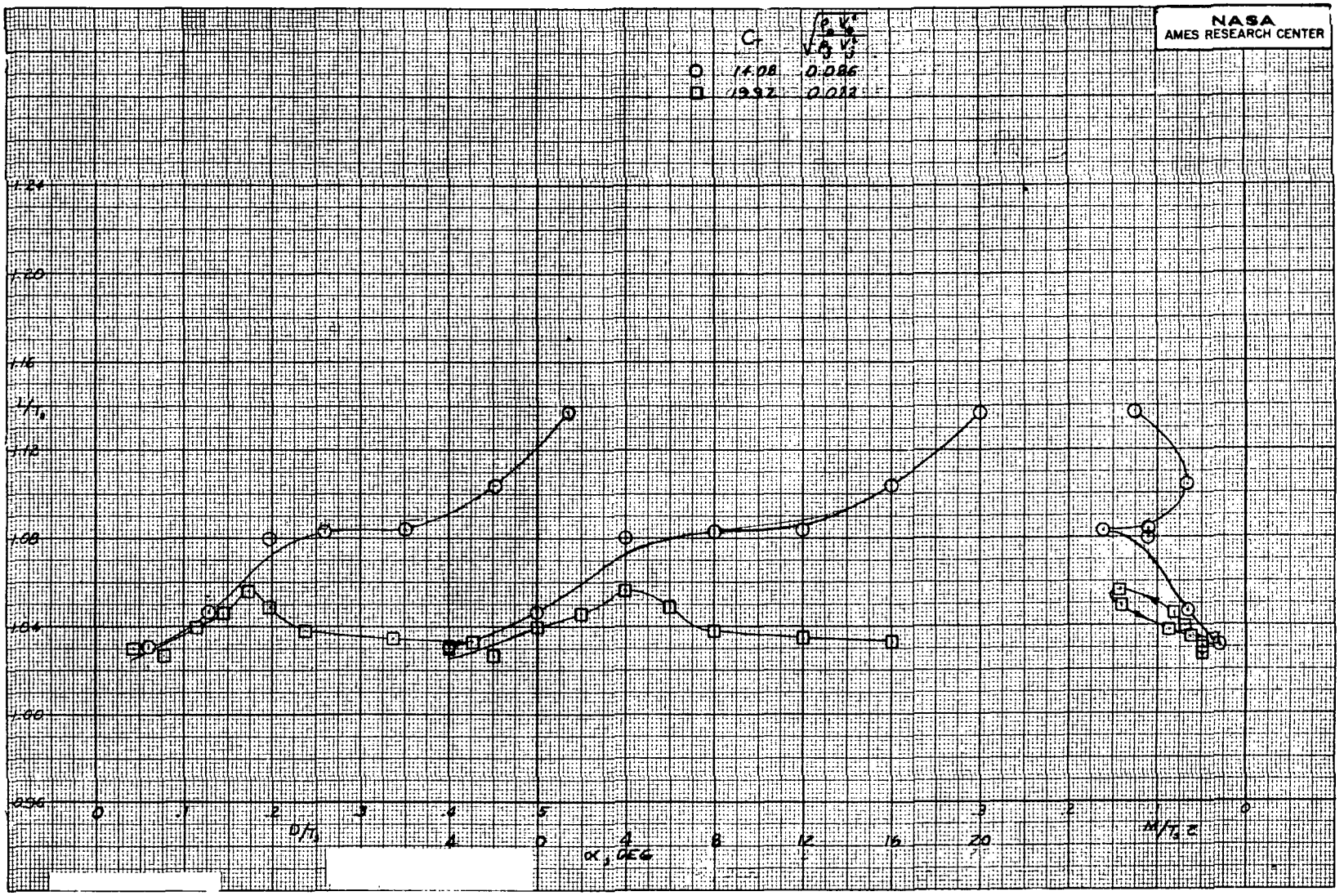

b- $\frac{L}{T_s}$ vs $\frac{D}{T_s}$, α, $\frac{M}{T_s}\bar{c}$

Figure 7.- Continued.

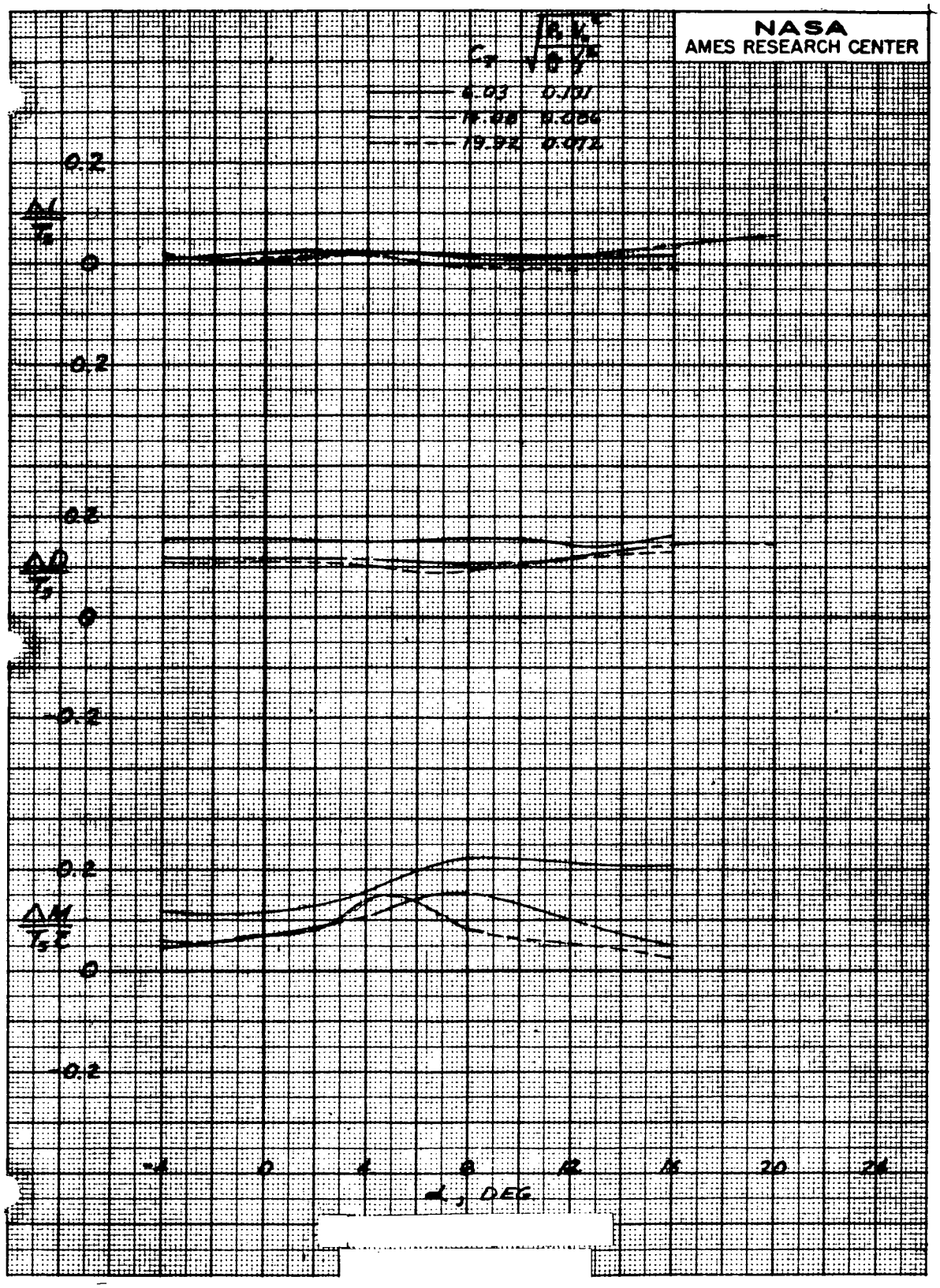

Figure 7.- Concluded.

c- Interference increments.

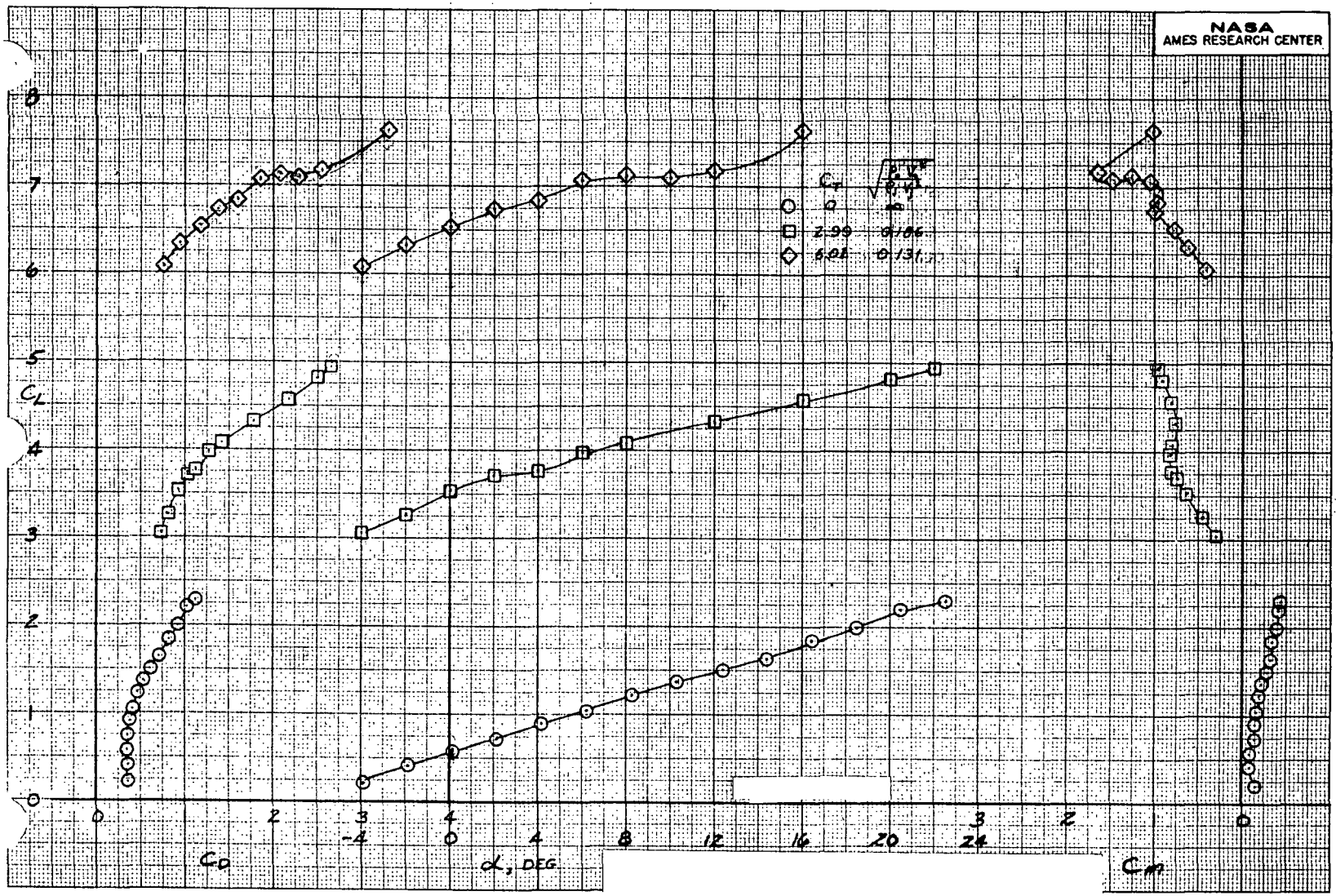

Figure 8.- Effect of angle of attack on longitudinal aerodynamic characteristics; α = 90°, All engines at equal thrust i_t = 0°, β= 0°, δ_f = 45°, δ_s = 25°.

a- C_L vs C_D, α, C_M

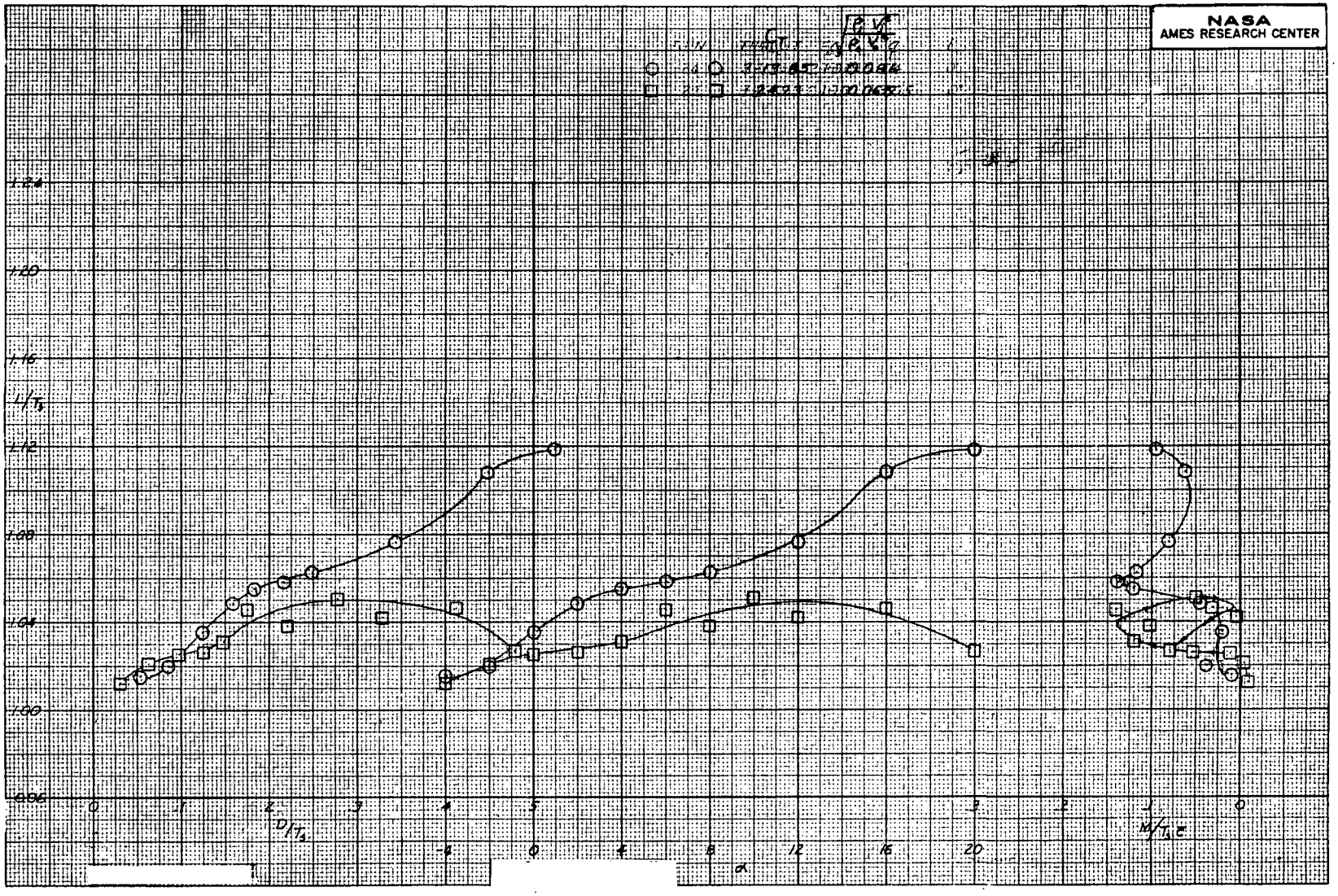

b- $\frac{L}{T_s}$ vs $\frac{D}{T_s}$, α, $\frac{M}{T_s \bar{c}}$

Figure 8.- Continued

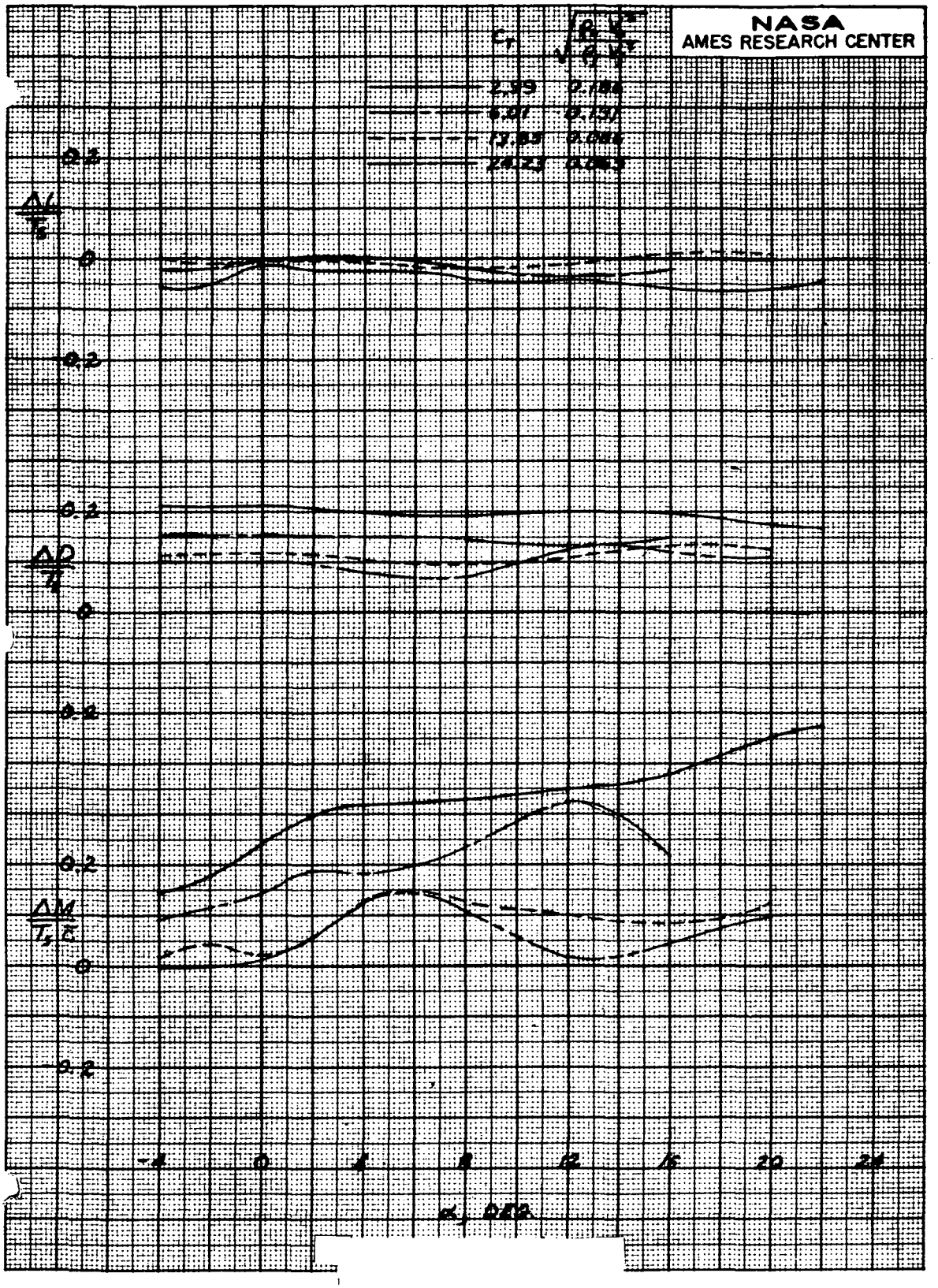

Figure 8.- Concluded

c- Interference increments

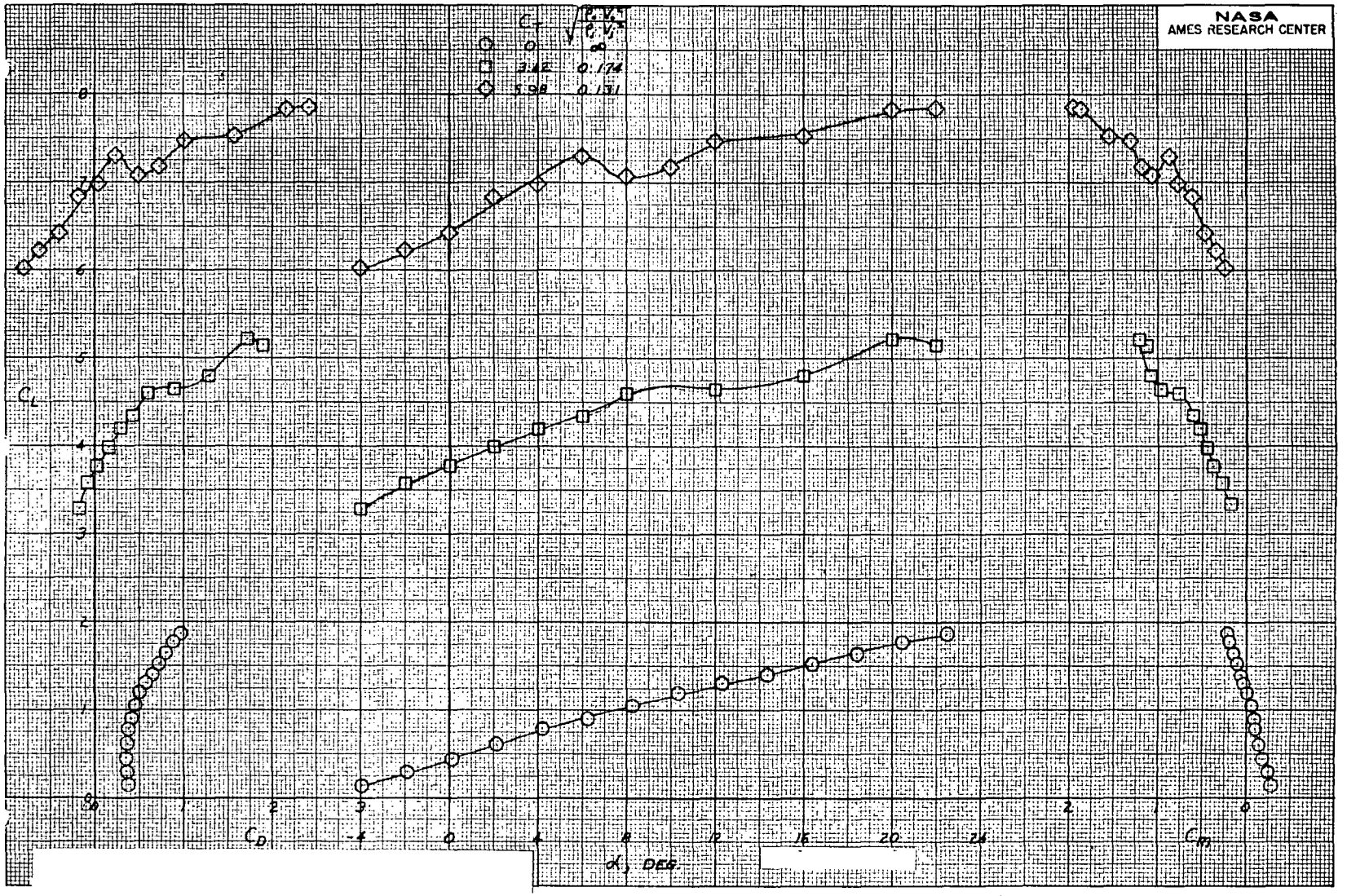

Figure 9.- Effect of angle of attack on longitudinal aerodynamic characteristics; σ = 75°, All engines at equal thrust, Horizontal tail off, β = 0°.

a- C_L vs C_D, α , C_M

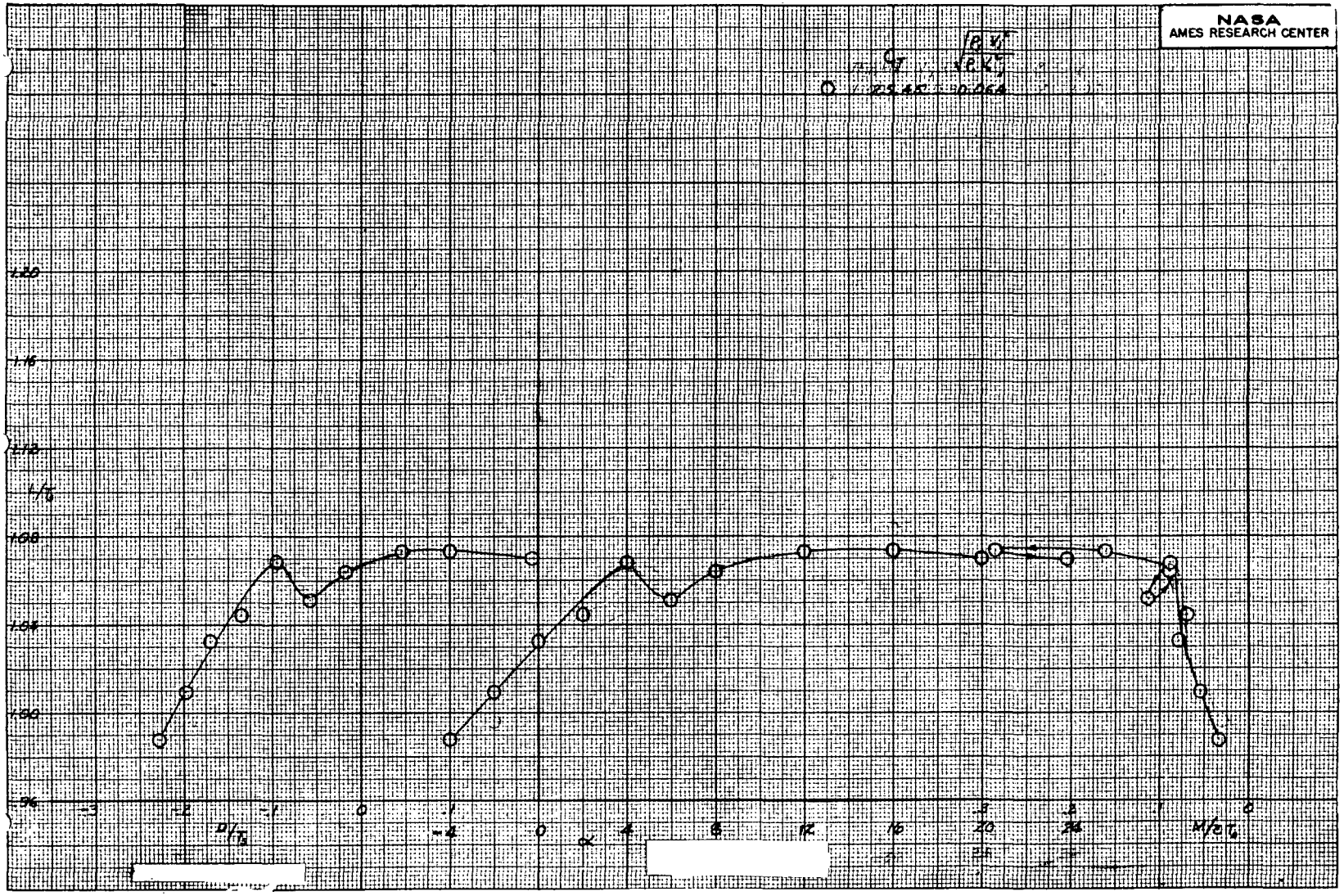

b- $\frac{L}{T_s}$ vs $\frac{D}{T_s}$, α, $\frac{M}{T_s\bar{c}}$

Figure 9.- Continued

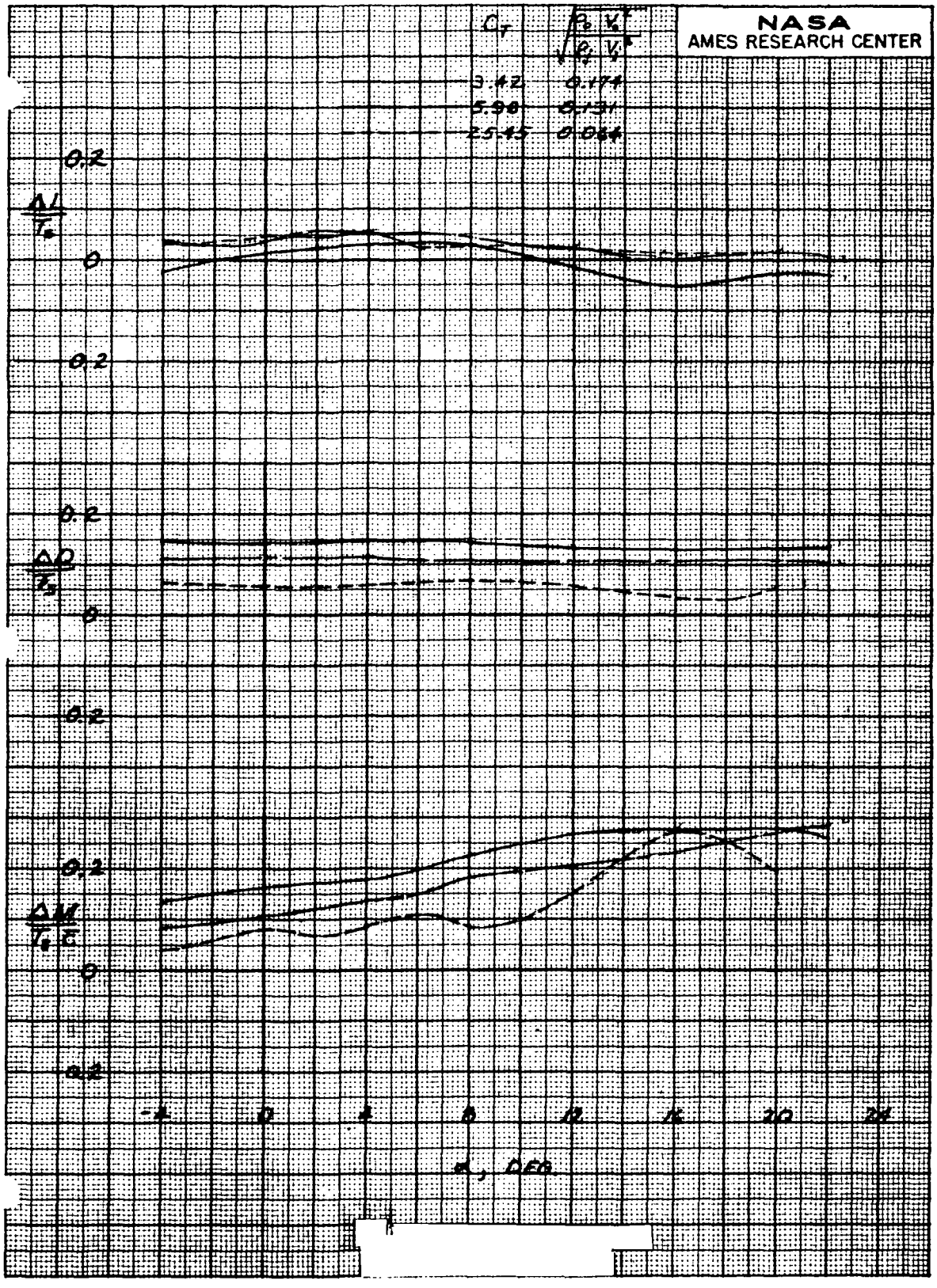

c- Interference increments.

Figure 9.- Concluded.

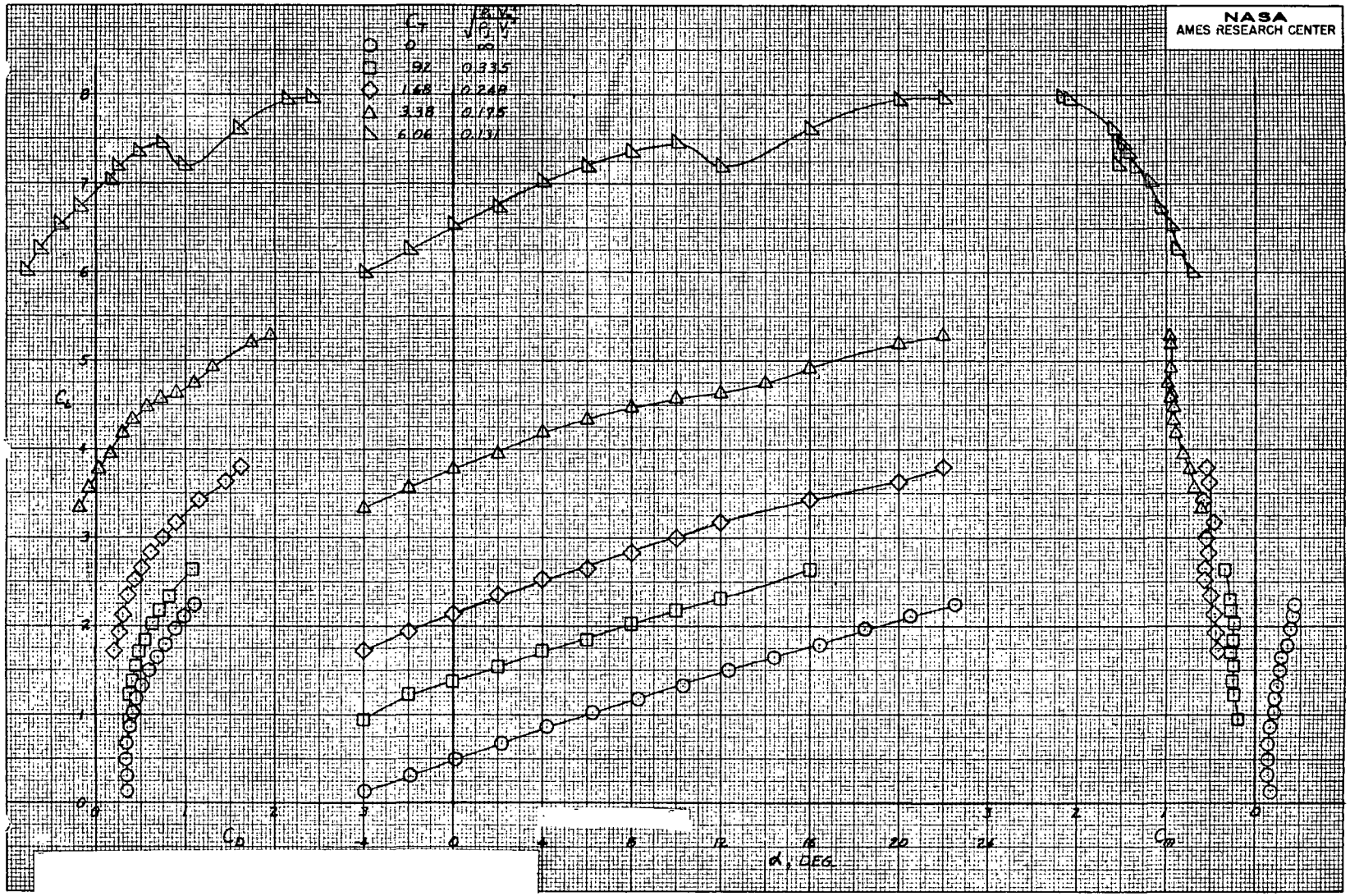

Figure 10.- Effect of angle of attack on longitudinal aerodynamic characteristics; $\sigma = 75°$, All engines at equal thrust, $i_t = 0°$, $\beta = 0°$, $\delta_f = 45°$, $\delta_s = 25°$

a- C_L vs C_D, α , C_M

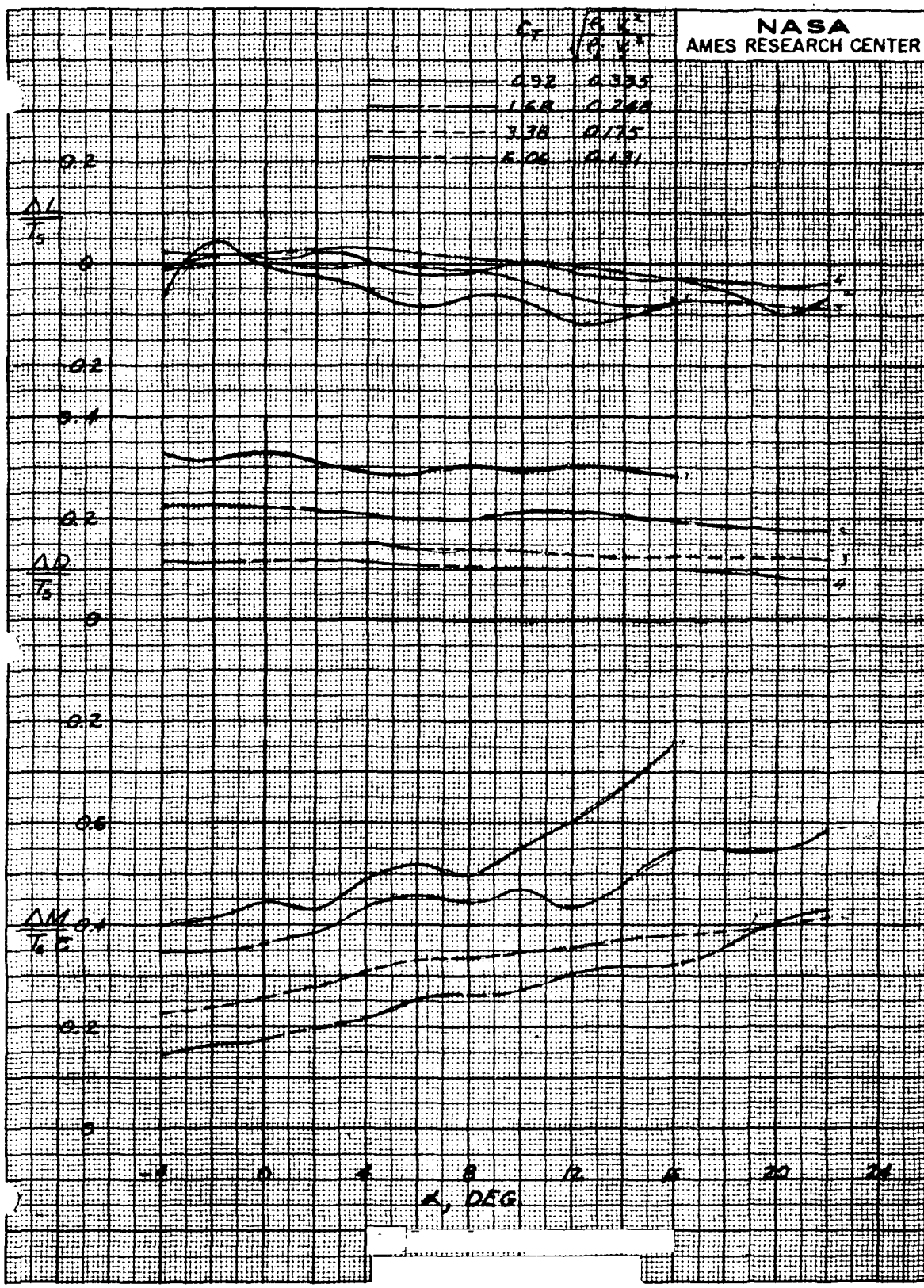

Figure 10.- Concluded.

b- Interference increments.

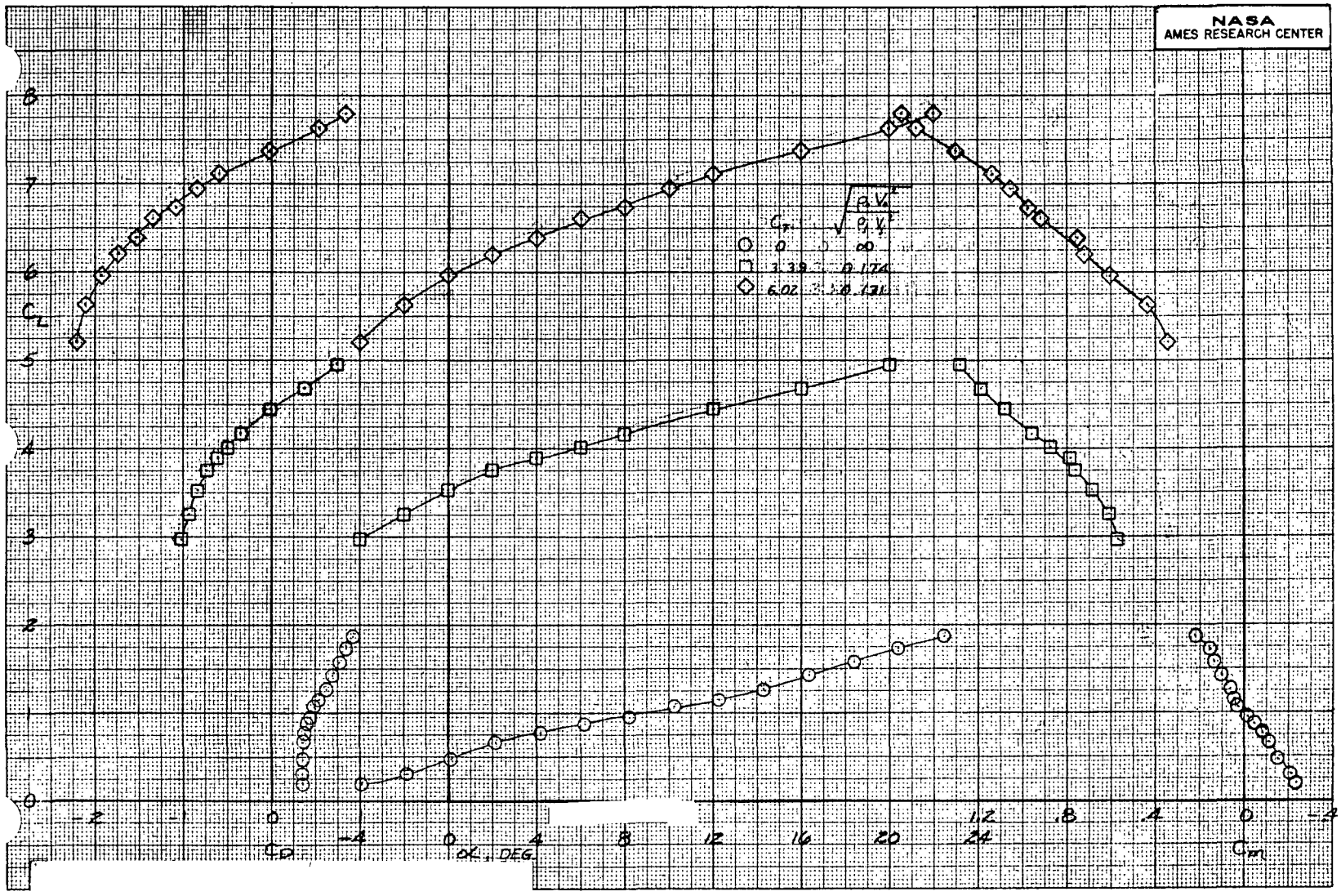

Figure 11.- Effect of angle of attack on longitudinal aerodynamic characteristics; $\sigma = 60°$, All engines at equal thrust, Horizontal tail off, $\beta = 0°$, $\delta_f = 45°$, $\delta_s = 25°$.

a- C_L vs C_D, α , C_M

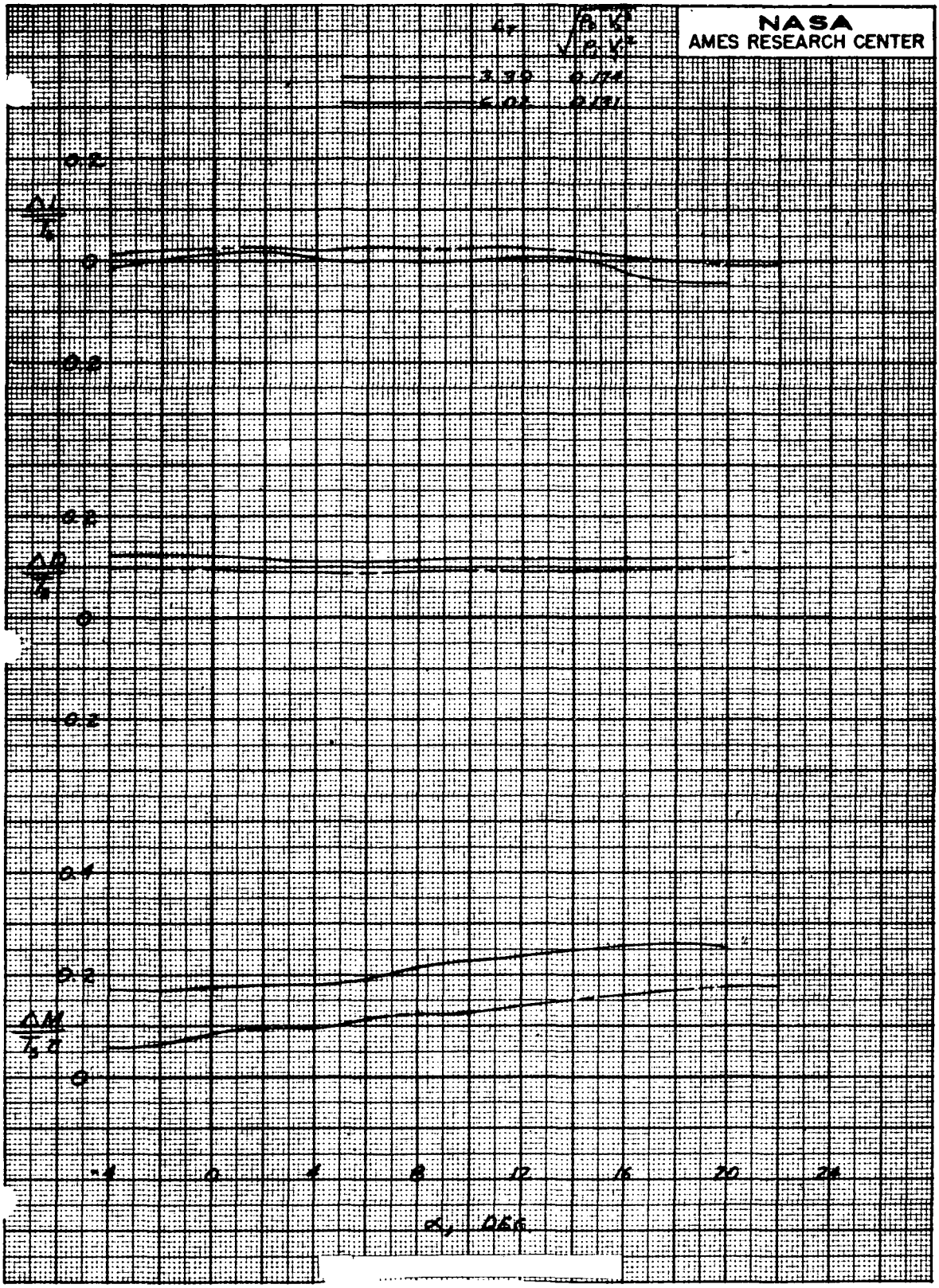

Figure 11.- Concluded.

b- Interference increments.

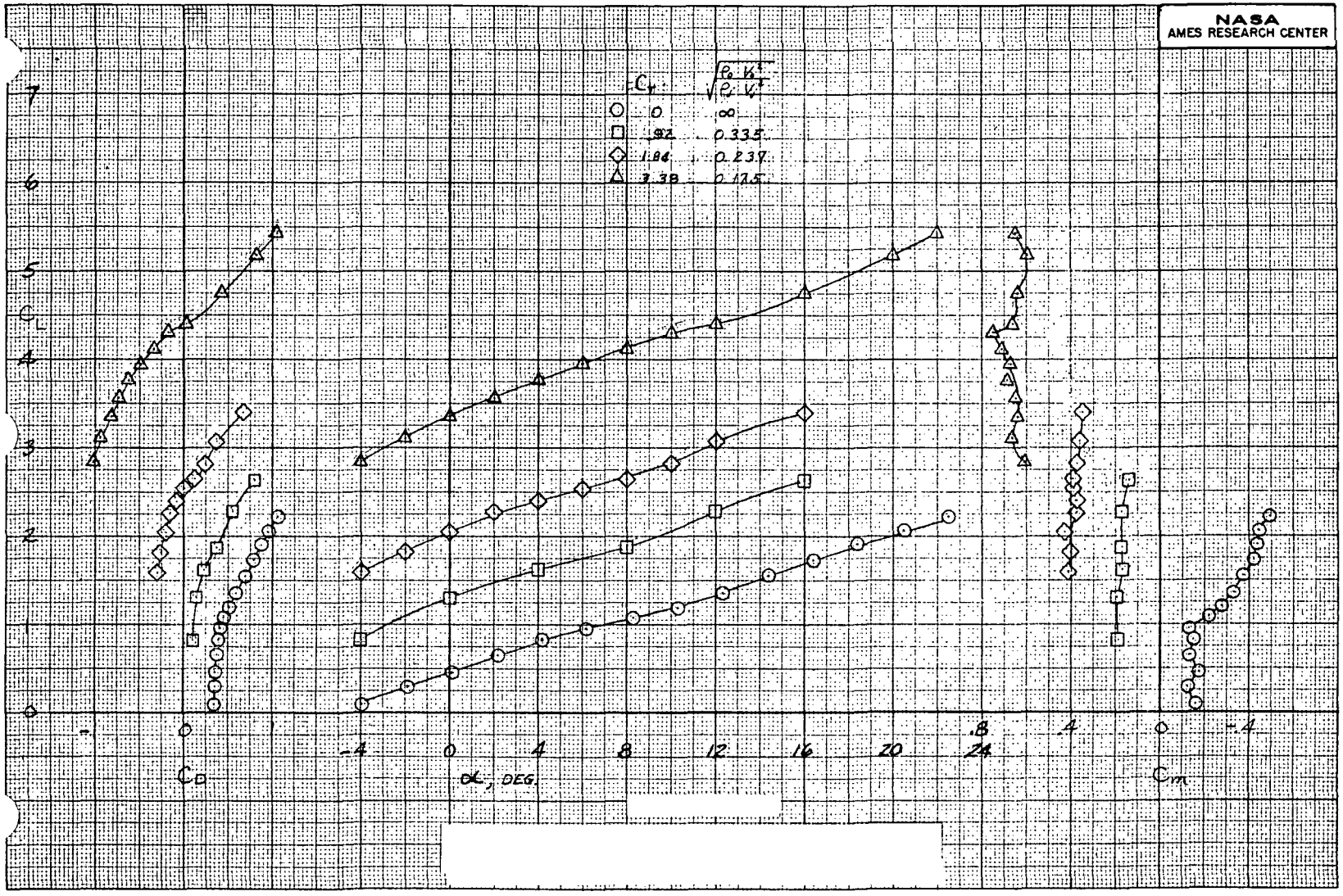

Figure 12.- Effect of angle of attack on longitudinal aerodynamic characteristics; $\sigma = 60°$, All engines at equal thrust, $i_t = 0°$, $\beta = 0°$, $\delta_f = 45°$, $\delta_s = 25°$.

a- C_L vs C_D, α , C_M

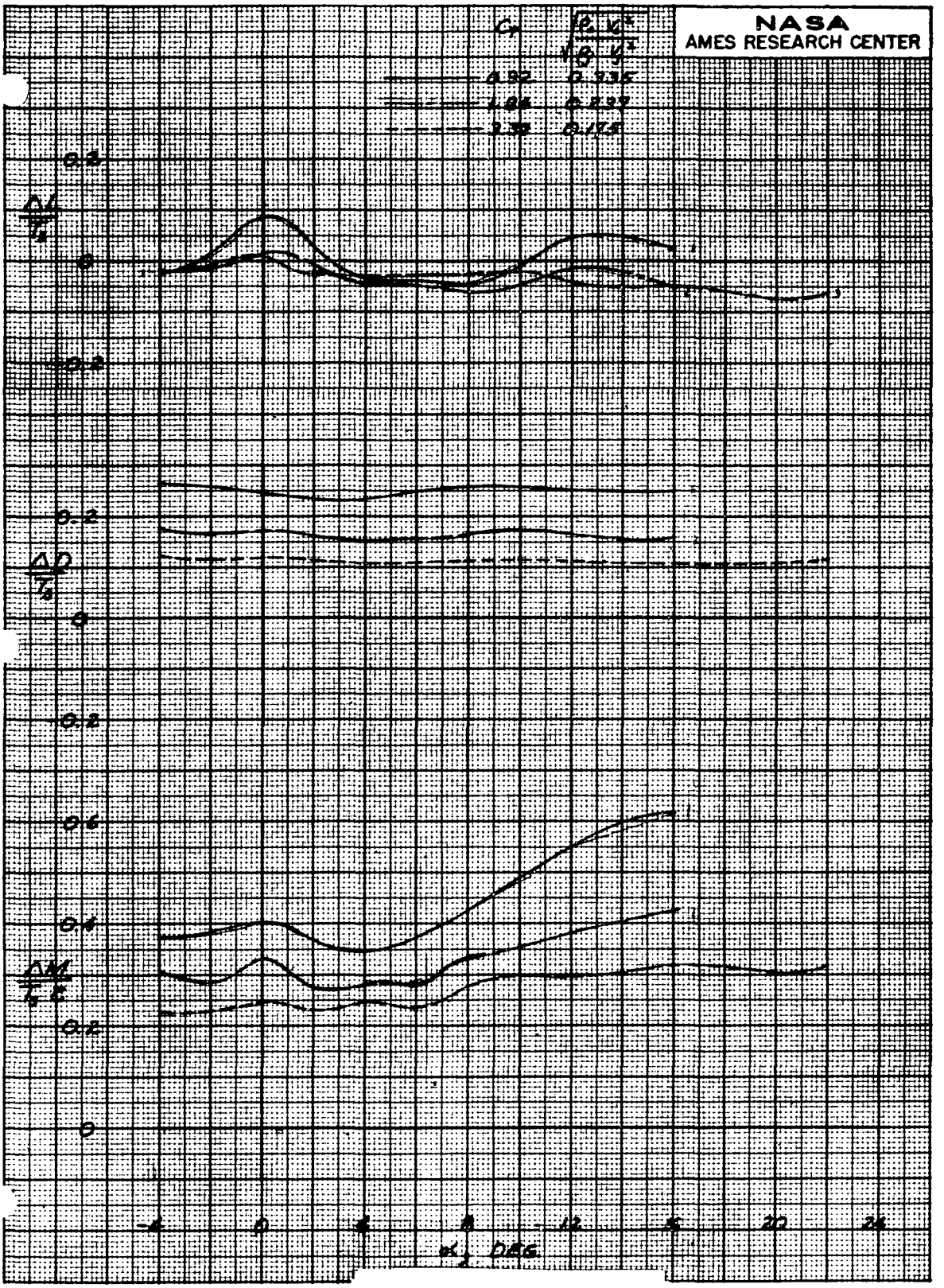

Figure 12.- Concluded.

b- Interference increments.

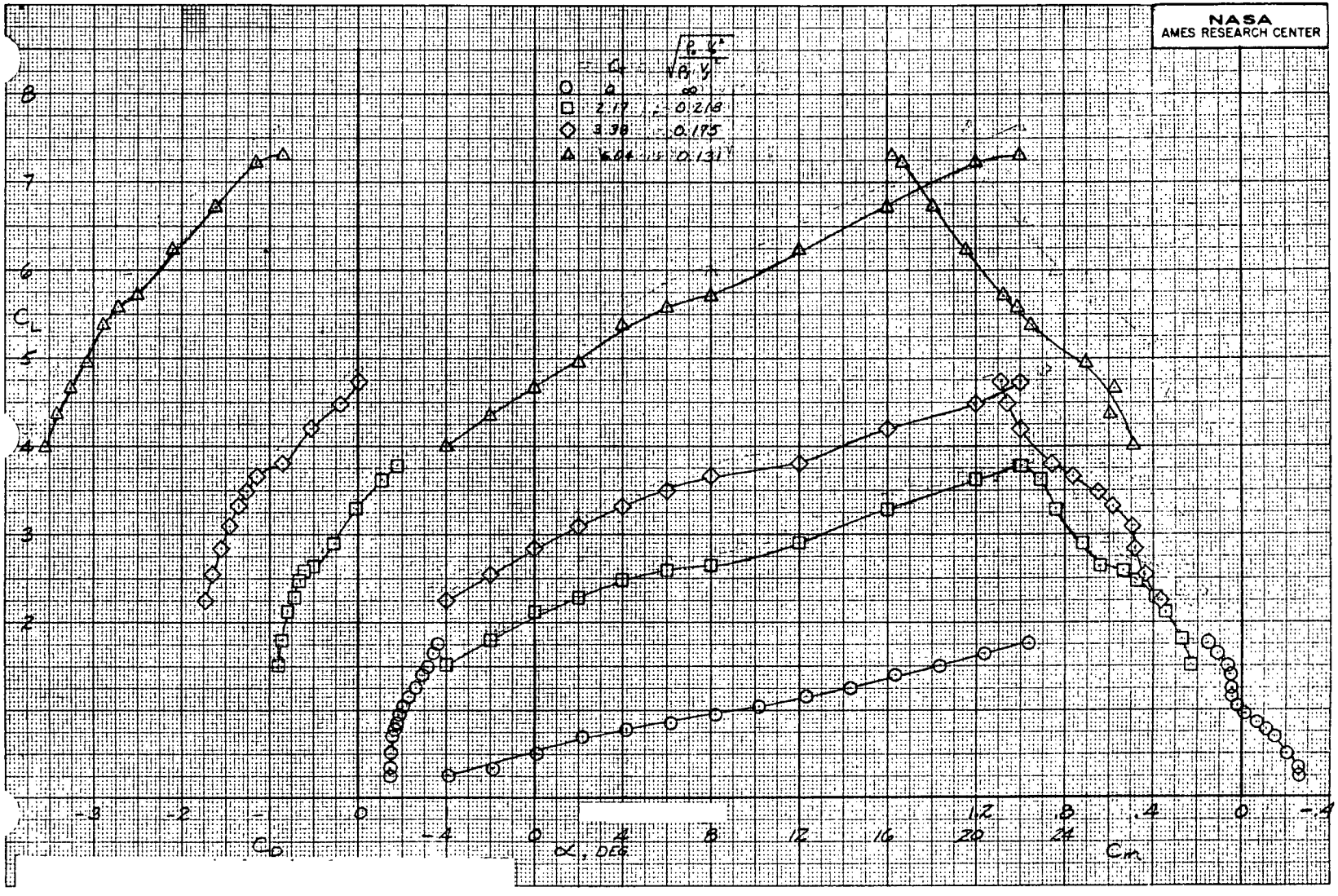

Figure 13.- Effect of angle of attack on longitudinal aerodynamic characteristics; $\sigma = 45°$, All engines at equal thrust, Horizontal tail off, $\beta = 0°$, $\delta_f = 45°$, $\delta_s = 25°$.

a- C_L v s C_D, α, C_M

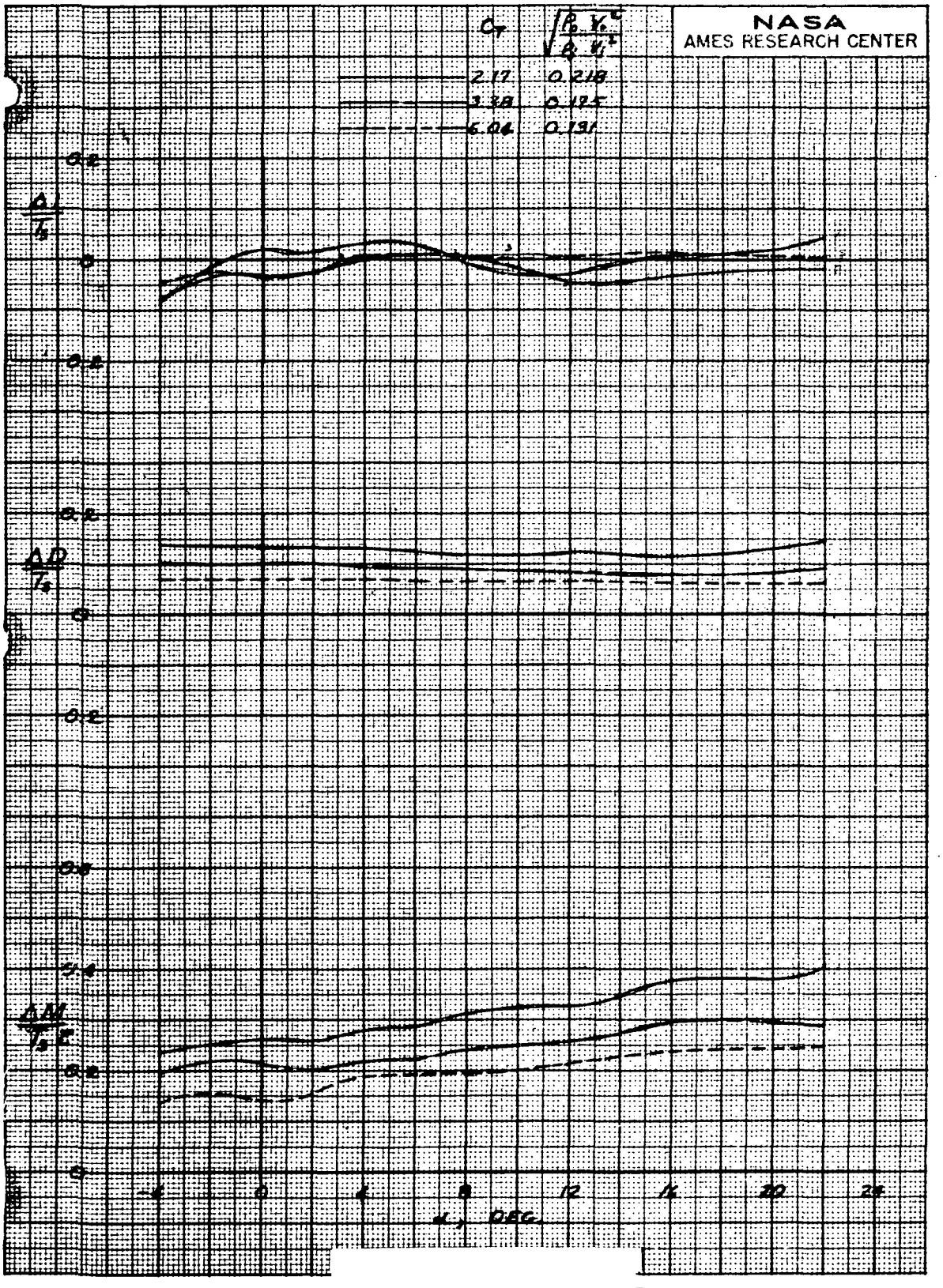

Figure 13.- Concluded.

b- Interference increments.

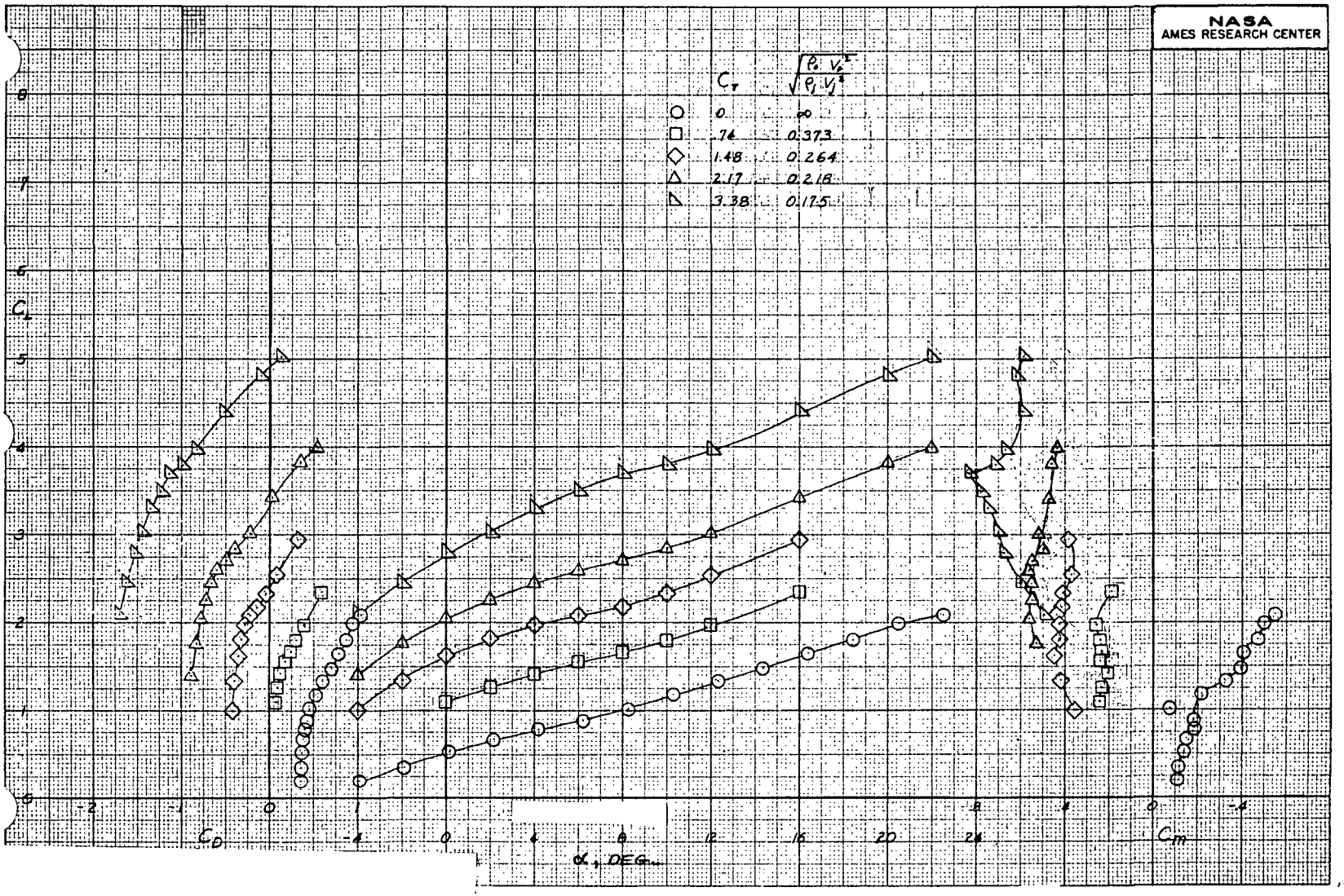

Figure 14.- Effect of angle of attack on longitudinal aerodynamic characteristics; $\sigma = 45°$, All engines at equal thrust, $i_t = 0°$, $\beta = 0°$, $\delta_f = 45°$, $\delta_s = 25°$.

a- C_L vs C_D, α , C_M

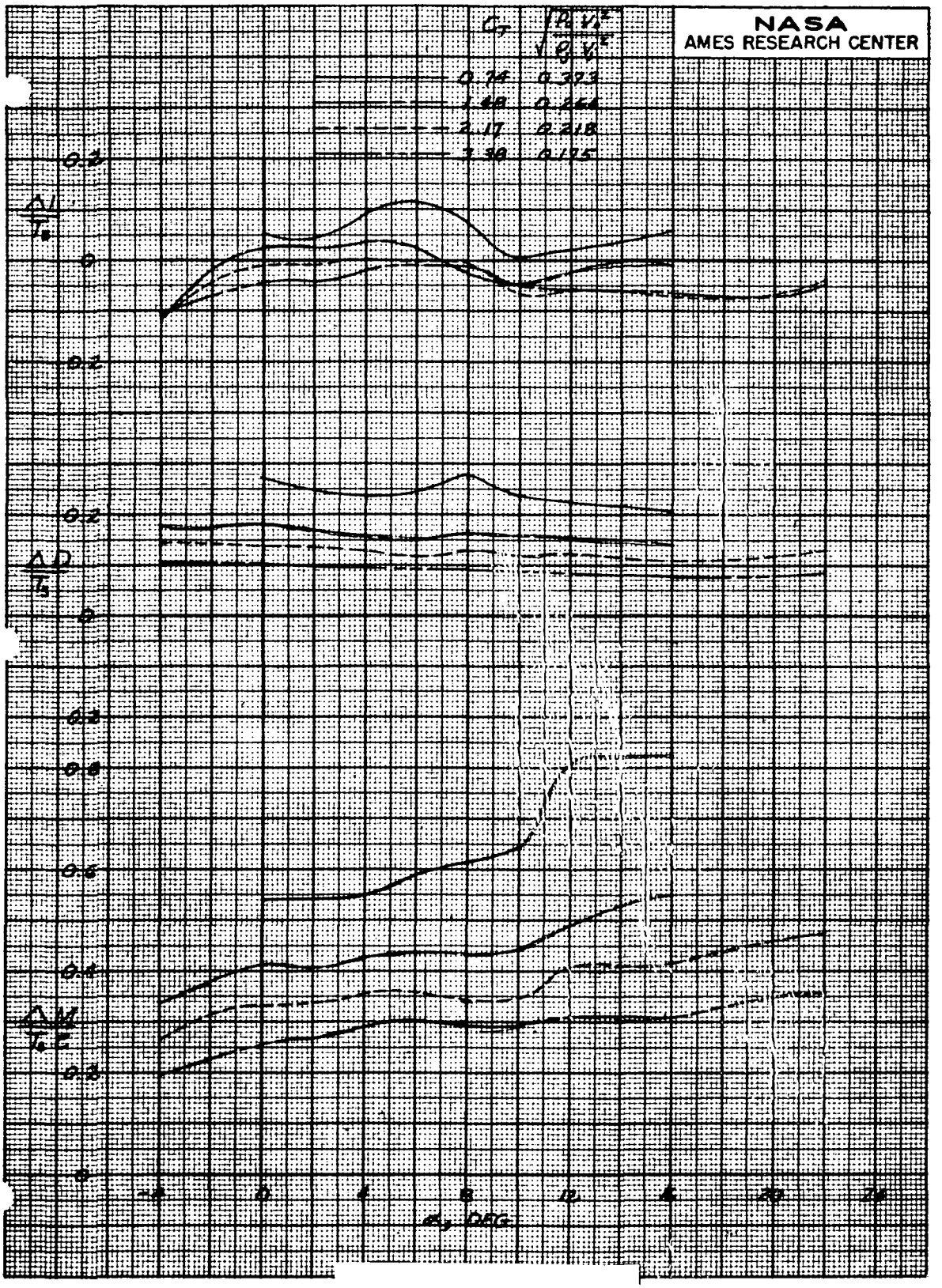

Figure 14.- Concluded.

b- Interference increments.

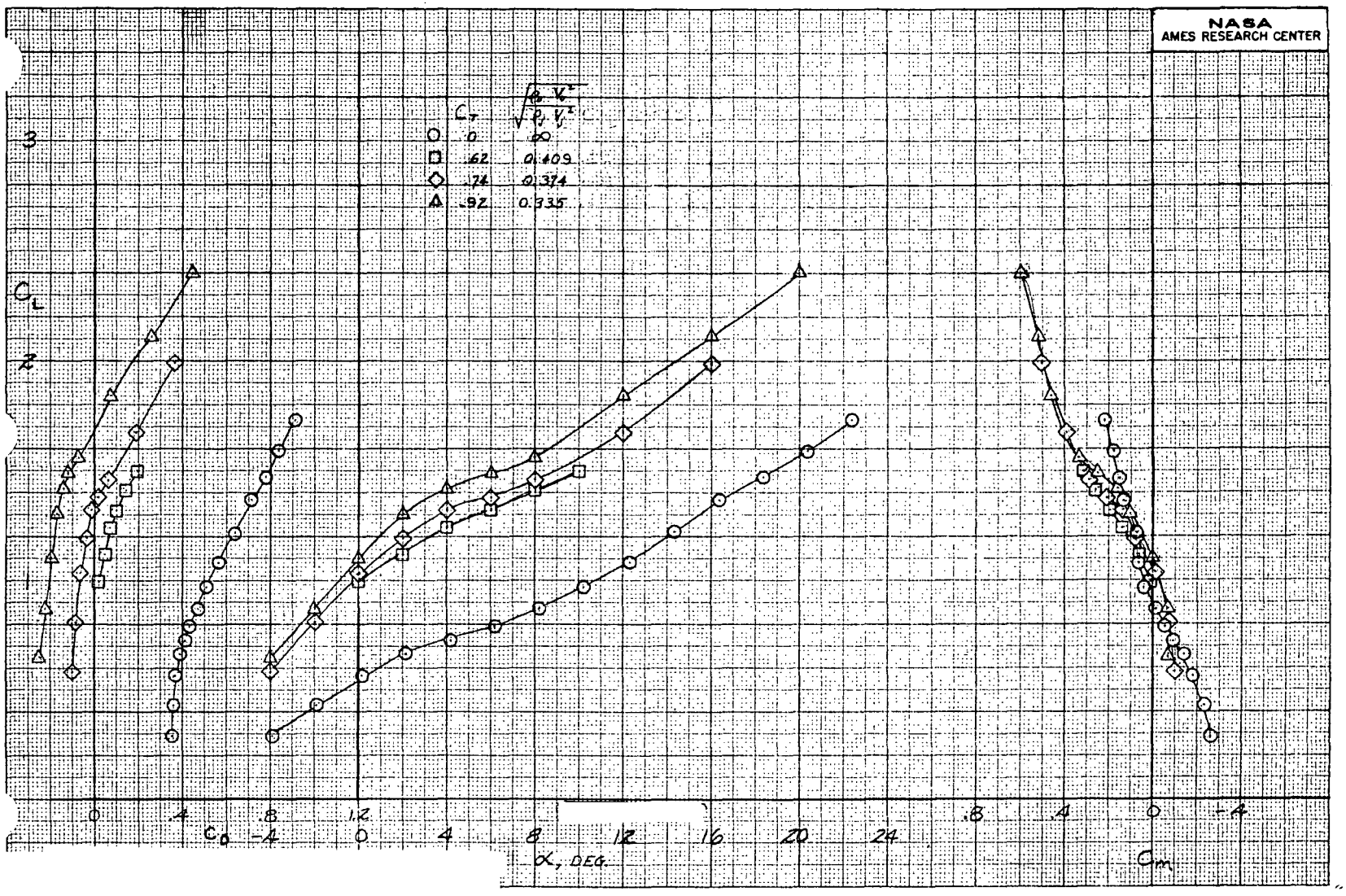

Figure 15.- Effect of angle of attack on longitudinal aerodynamic characteristics; σ = 30°, All engines at equal thrust, Horizontal tail off, β= 0°, δ_f = 45°, δ_s = 25°.

a- C_L vs C_D , α , C_M

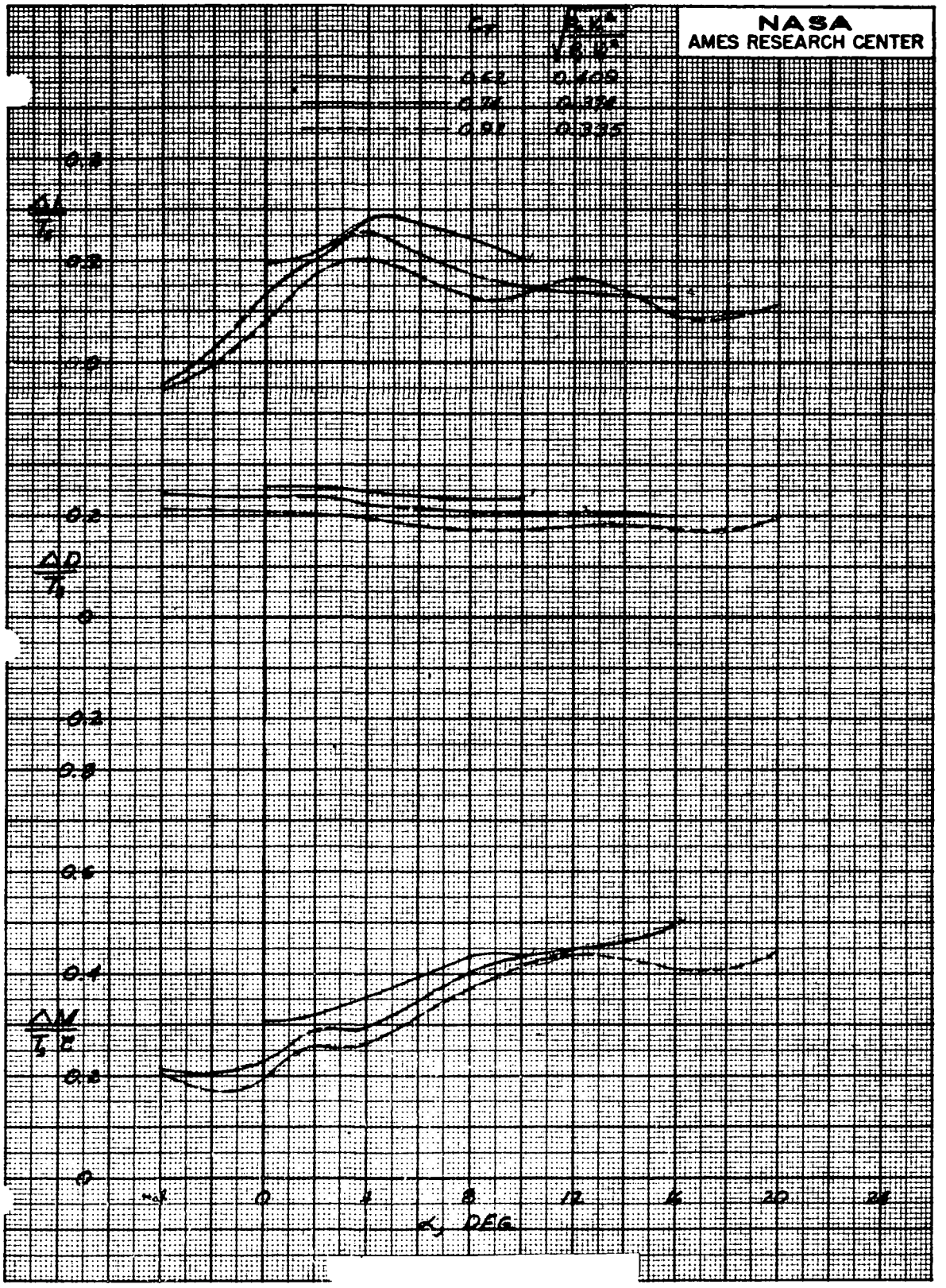

Figure 15.- Concluded.

b- Interference increments.

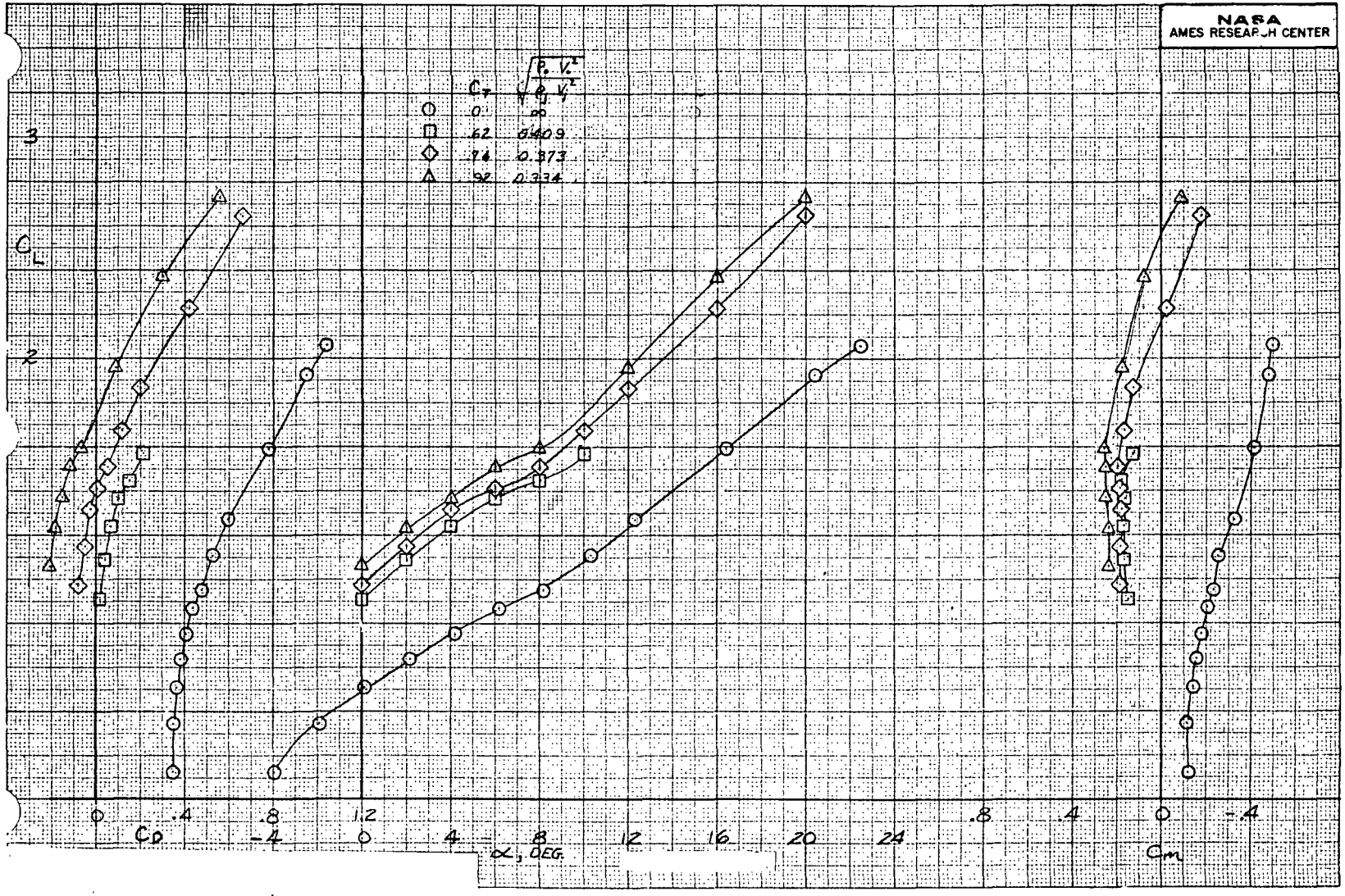

Figure 16.- Effect of angle of attack on longitudinal aerodynamic characteristics; $\sigma = 30°$, All engines at equal thrust, $i_t = 0°$, $\beta = 0°$, $\delta_f = 45°$, $\delta_s = 25°$.

a- C_L vs C_D, α, C_M

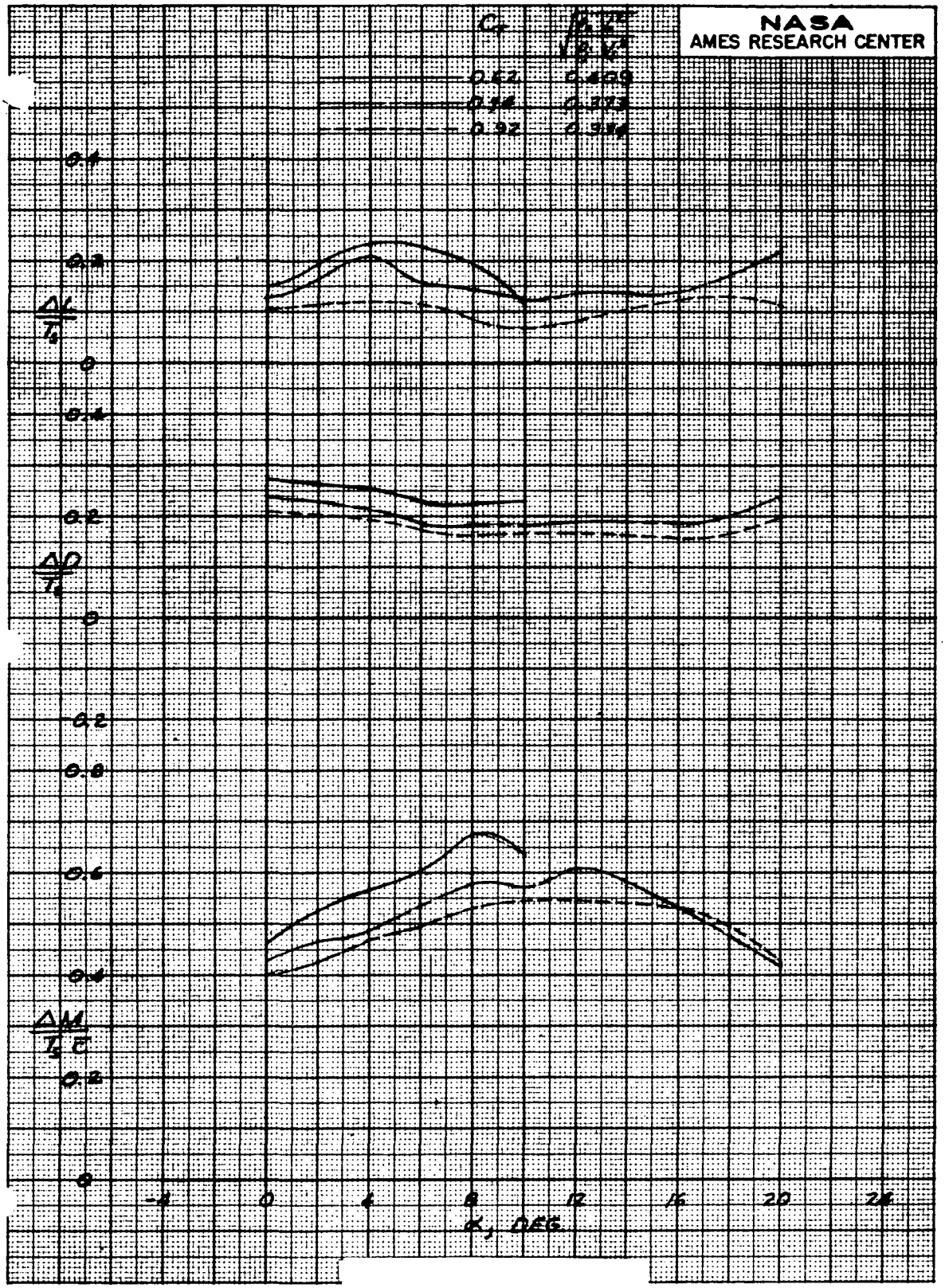

Figure 16.- Concluded.

b- Interference increments.

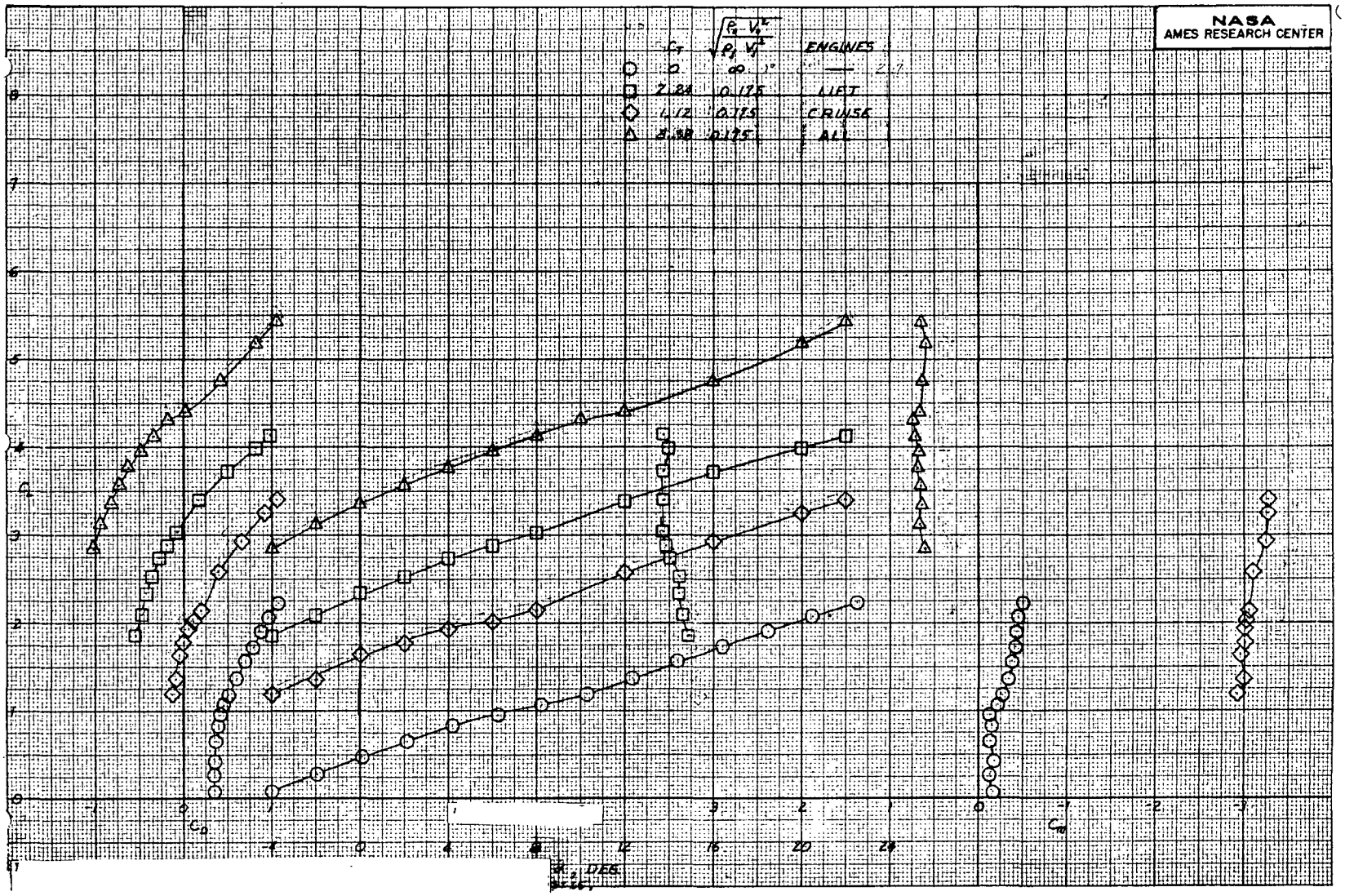

Figure 17.- Effect of lift and cruise engine operation on longitudinal aerodynamic characteristics; $\sigma = 60°$, $i_t = 0°$, $\beta = 0°$, $\delta_f = 45°$, $\delta_s = 25°$.

a- C_L vs C_D, α, C_m

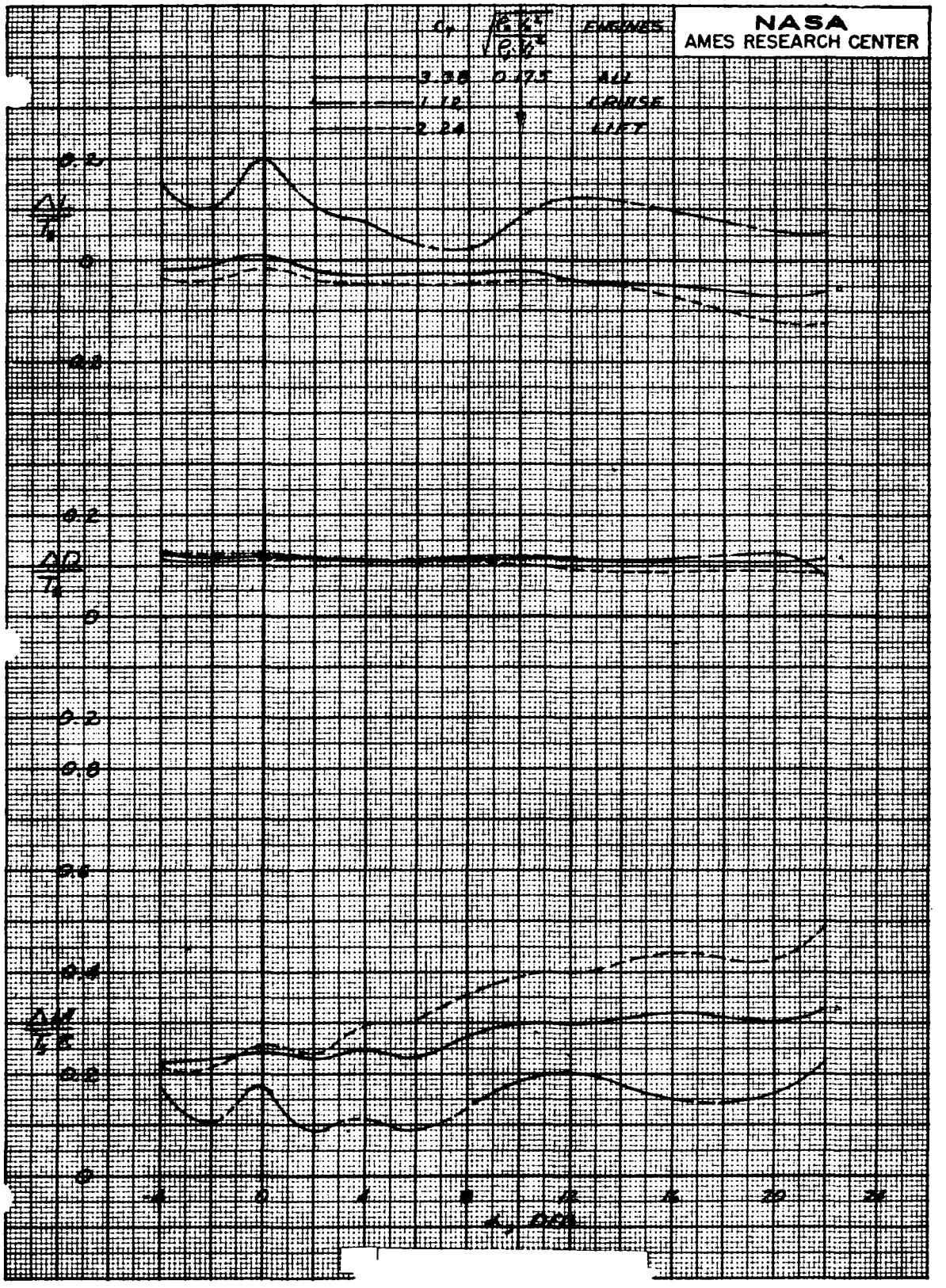

Figure 17.- Concluded.

b- Interference increments.

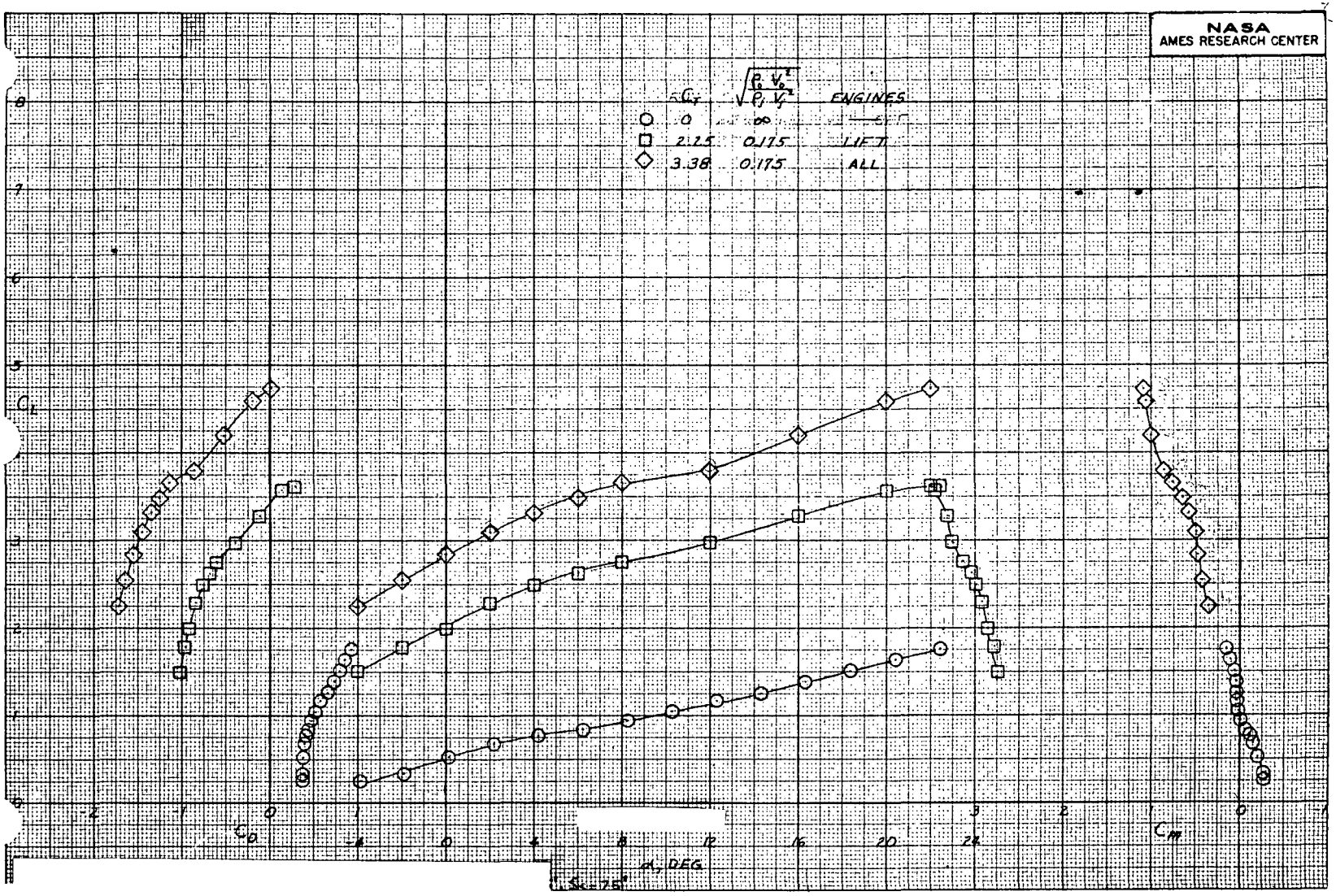

Figure 18.- Effect of lift engine operation on longitudinal aerodynamic characteristics; $\sigma = 45°$, Horizontal tail off, $\beta = 0°$, $\delta_f = 45°$, $\delta_s = 25°$.

a- C_L vs C_D, α, C_m

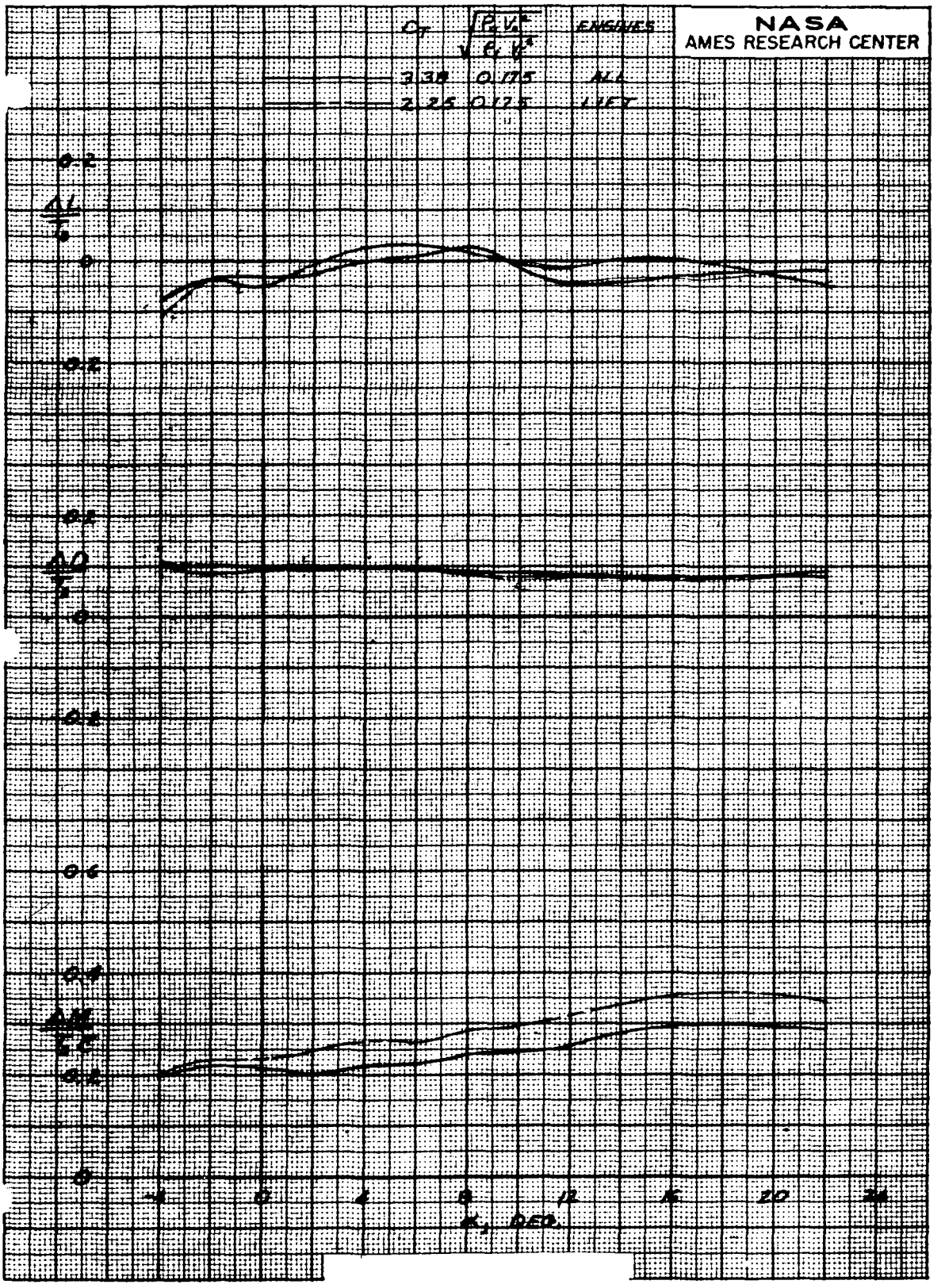

Figure 18.- Concluded.

b- Interference increments.

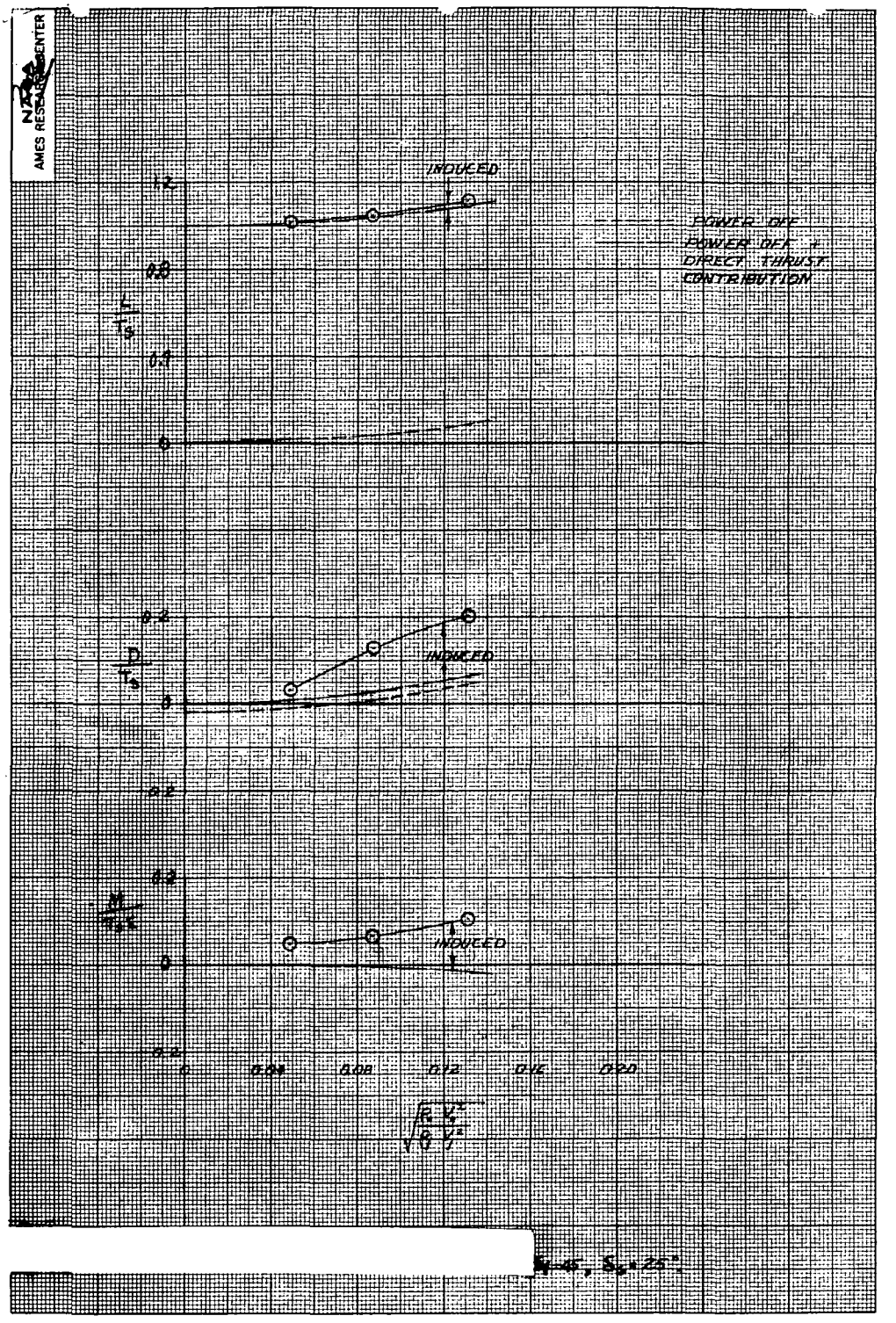

Figure 19.- Effect of momentum ratio variation on the longitudinal aerodynamic characteristics of the model; $\sigma = 90°$, All engines operating, Horizontal tail off, $\quad = 0°$, $\beta = 0°$, $\delta_f = 45°$; $\delta_s = 25°$.

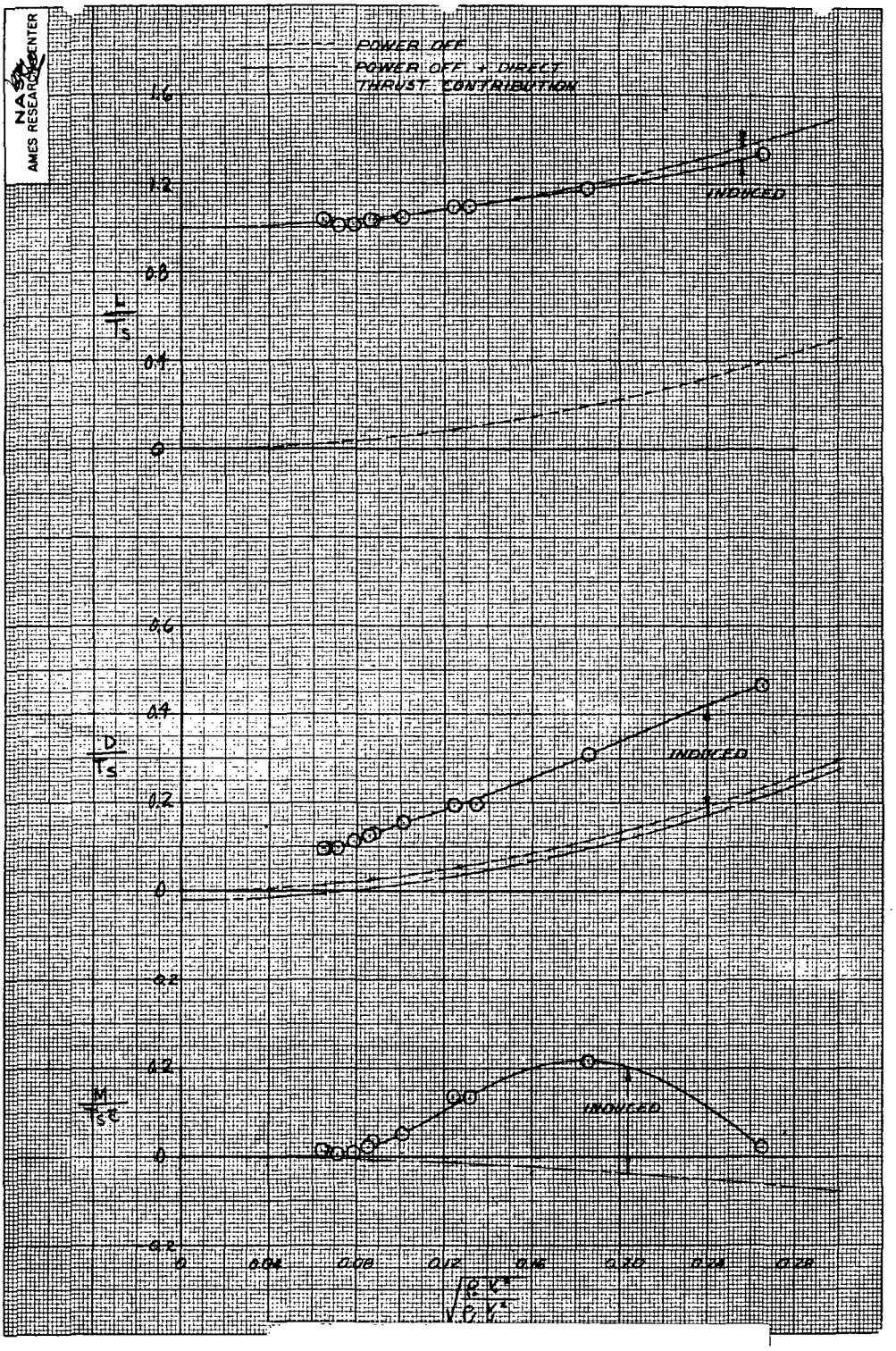

Figure 20.- Effect of momentum ratio variation on the longitudinal aerodynamic characteristics of the model; $\sigma = 90°$, All engines operating, $i_t = 0°$, $\alpha = 0°$, $\beta = 0°$, $\delta_f = 45°$, $\delta_s = 25°$.

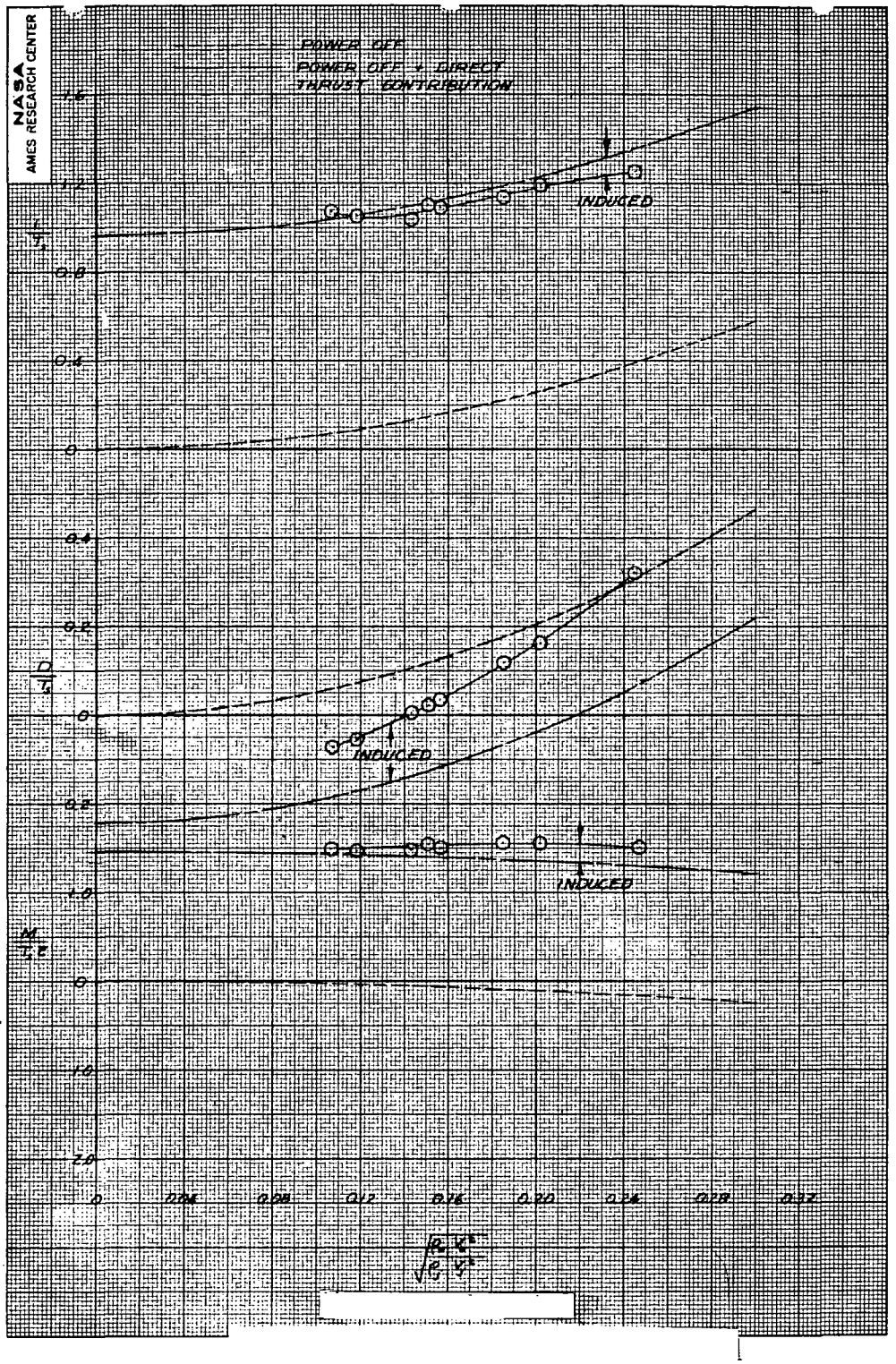

Figure 21.- Effect of momentum ratio variation on the longitudinal aerodynamic characteristics of the model; $\alpha = 75°$, Horizontal tail off, $\alpha = 0°$, $\beta = 0°$, $\delta_f = 45°$, $\delta_s = 25°$.

(a) Lift engines only operating

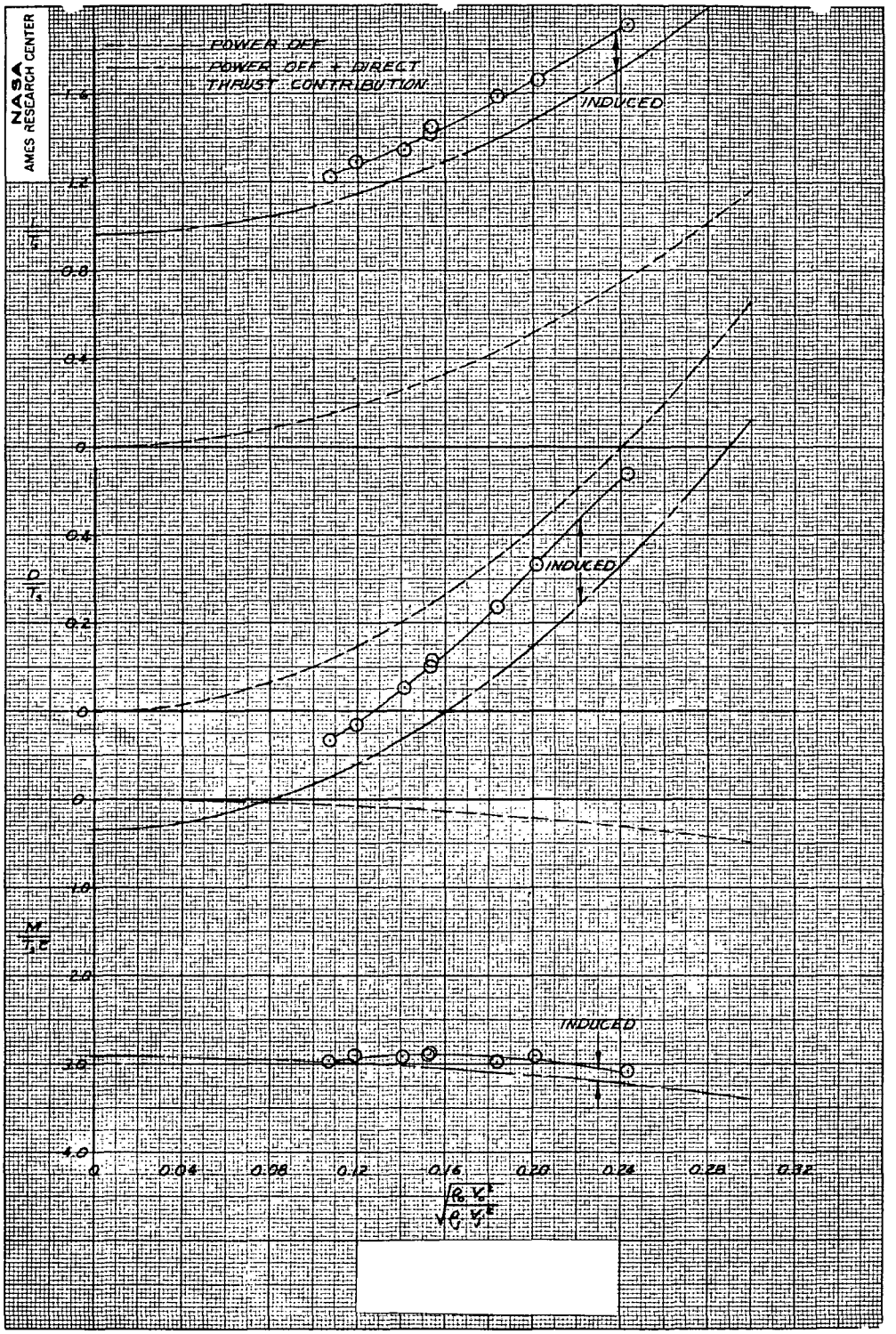

Figure 21.- Continued.

(b) Cruise engines only operating

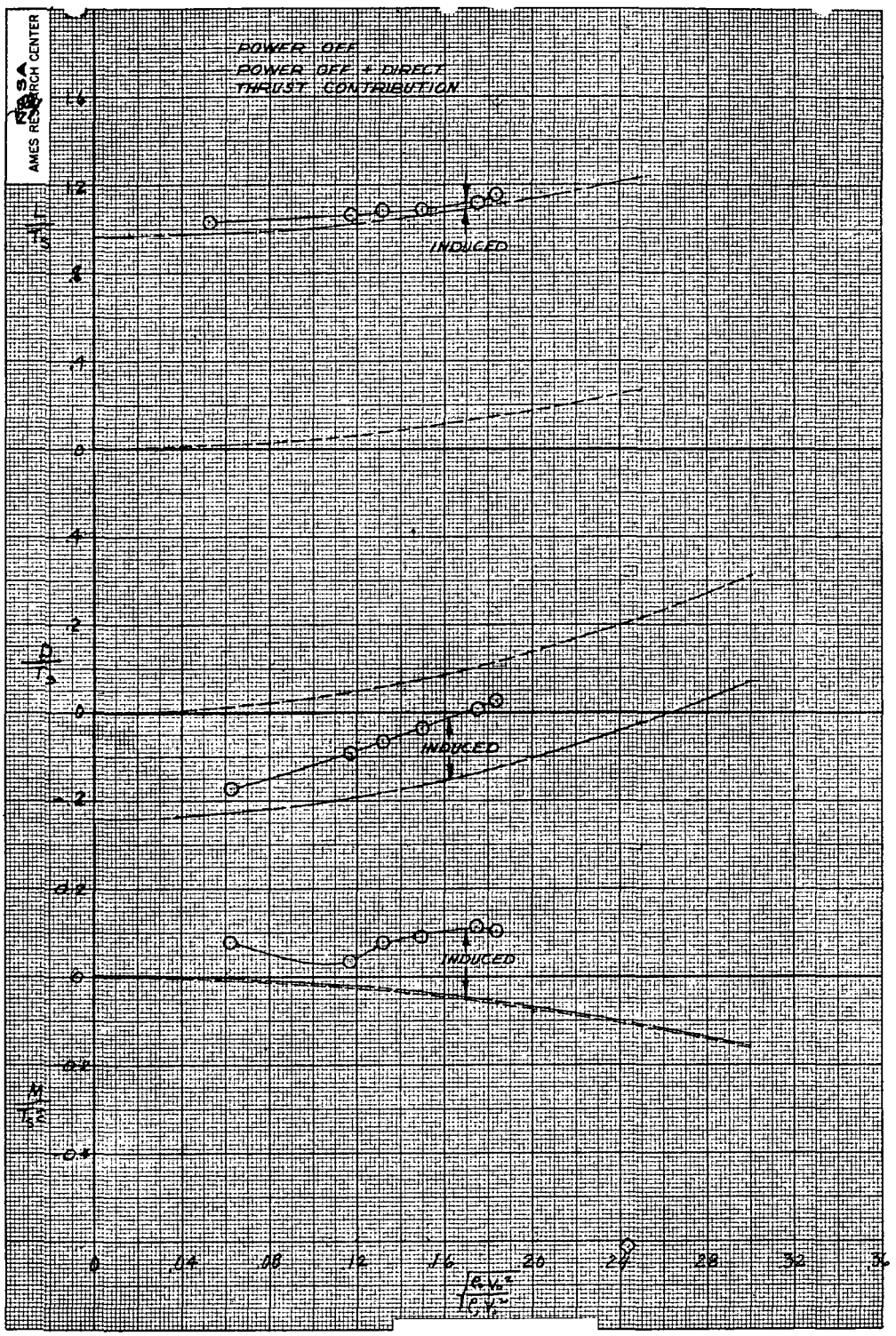

Figure 21.- Concluded.

(c) All engines operating

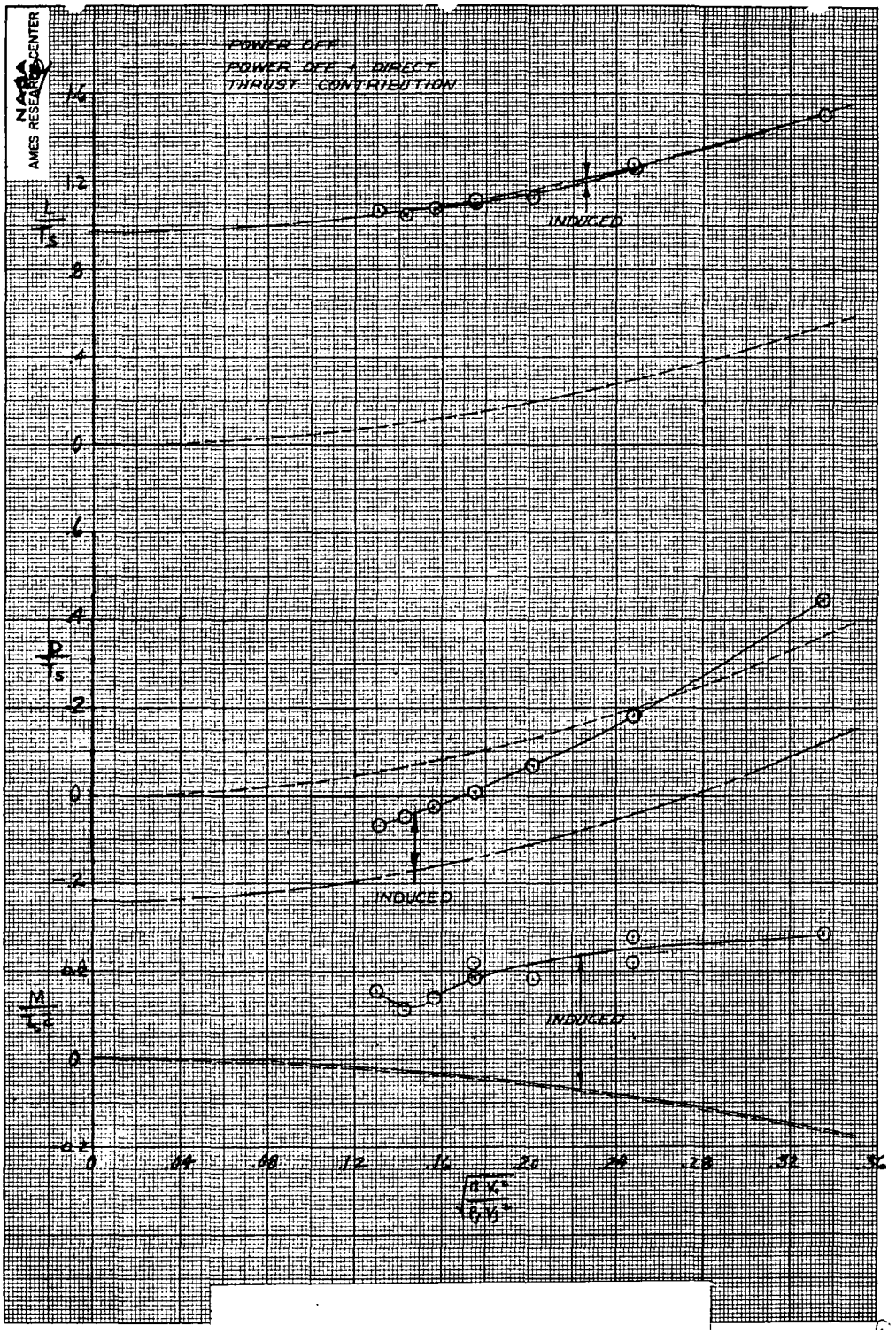

Figure 22.- Effect of momentum ratio variation on the longitudinal aerodynamic characteristics of the model; $\alpha = 75°$, All engines operating, $i_t = 0°$, $\alpha = 0°$, $\beta = 0°$.

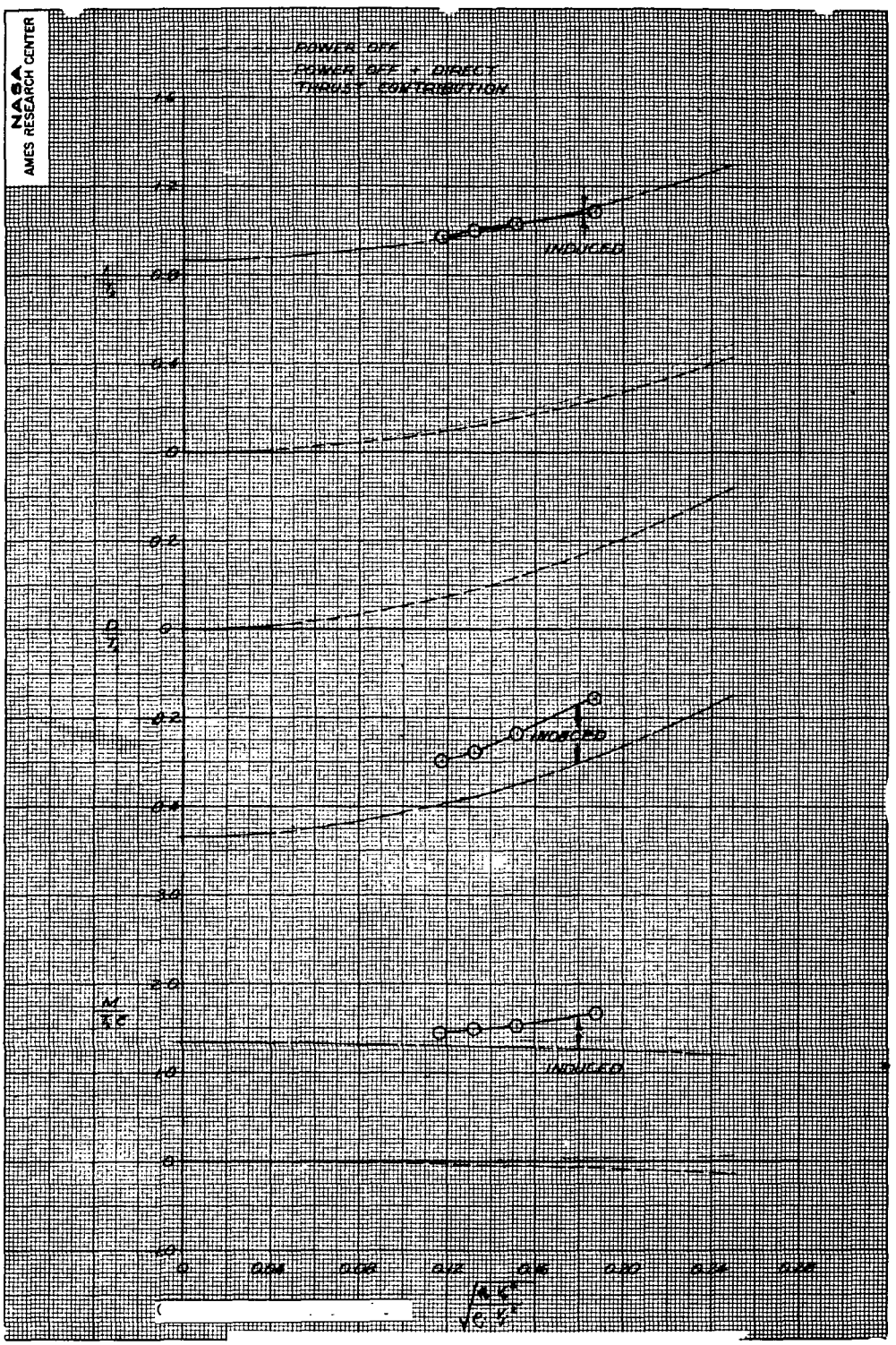

Figure 23.- Effect of momentum ratio variation on the longitudinal aerodynamic characteristics of the model; $\sigma = 60°$, Horizontal tail off, $\alpha = 0°$, $\beta = 0°$, $\delta_f = 45°$, $\delta_s = 25°$.

(a) Lift engines only operating

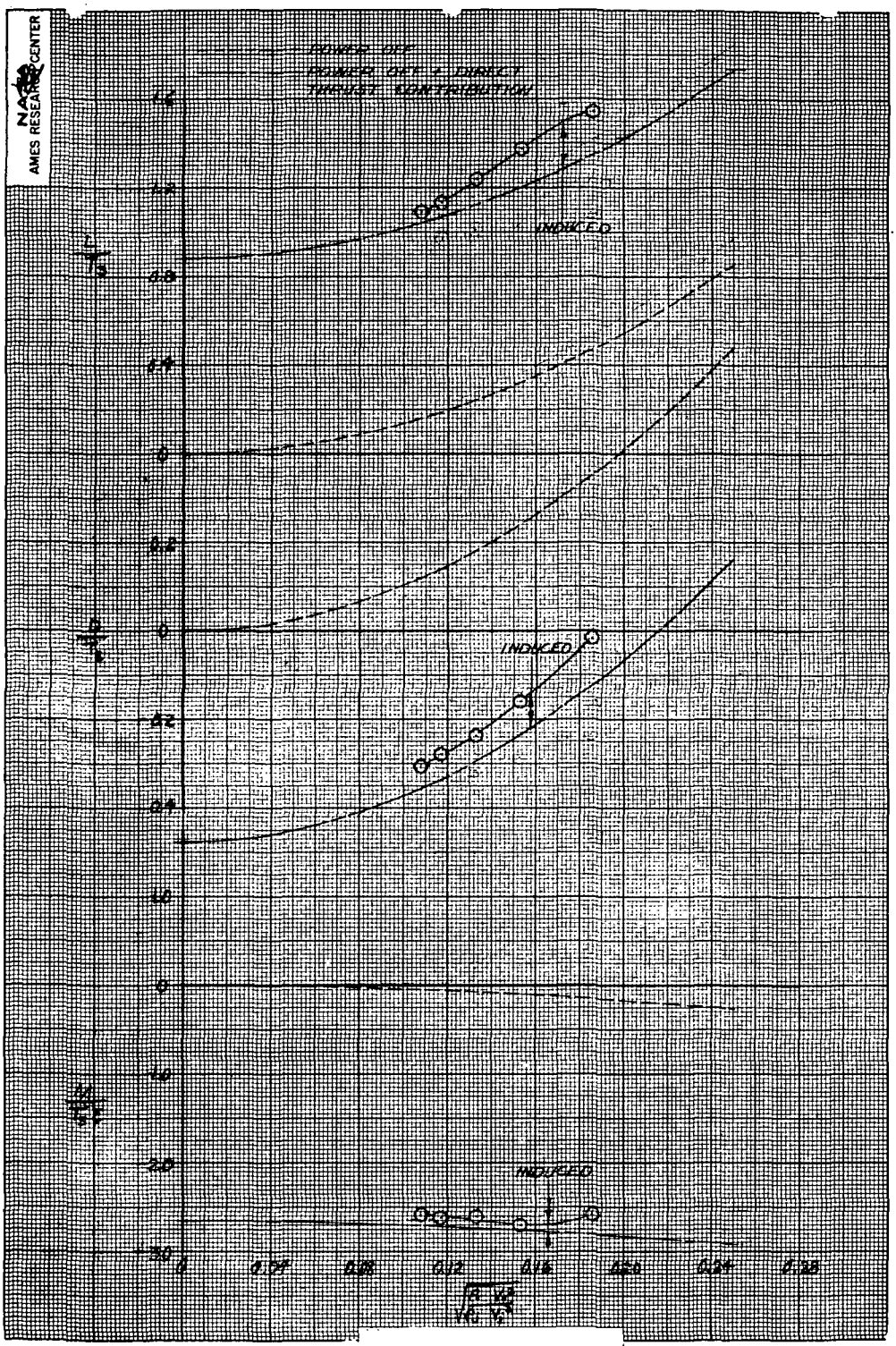

Figure 23.- Continued.

(b) Cruise engines only operating.

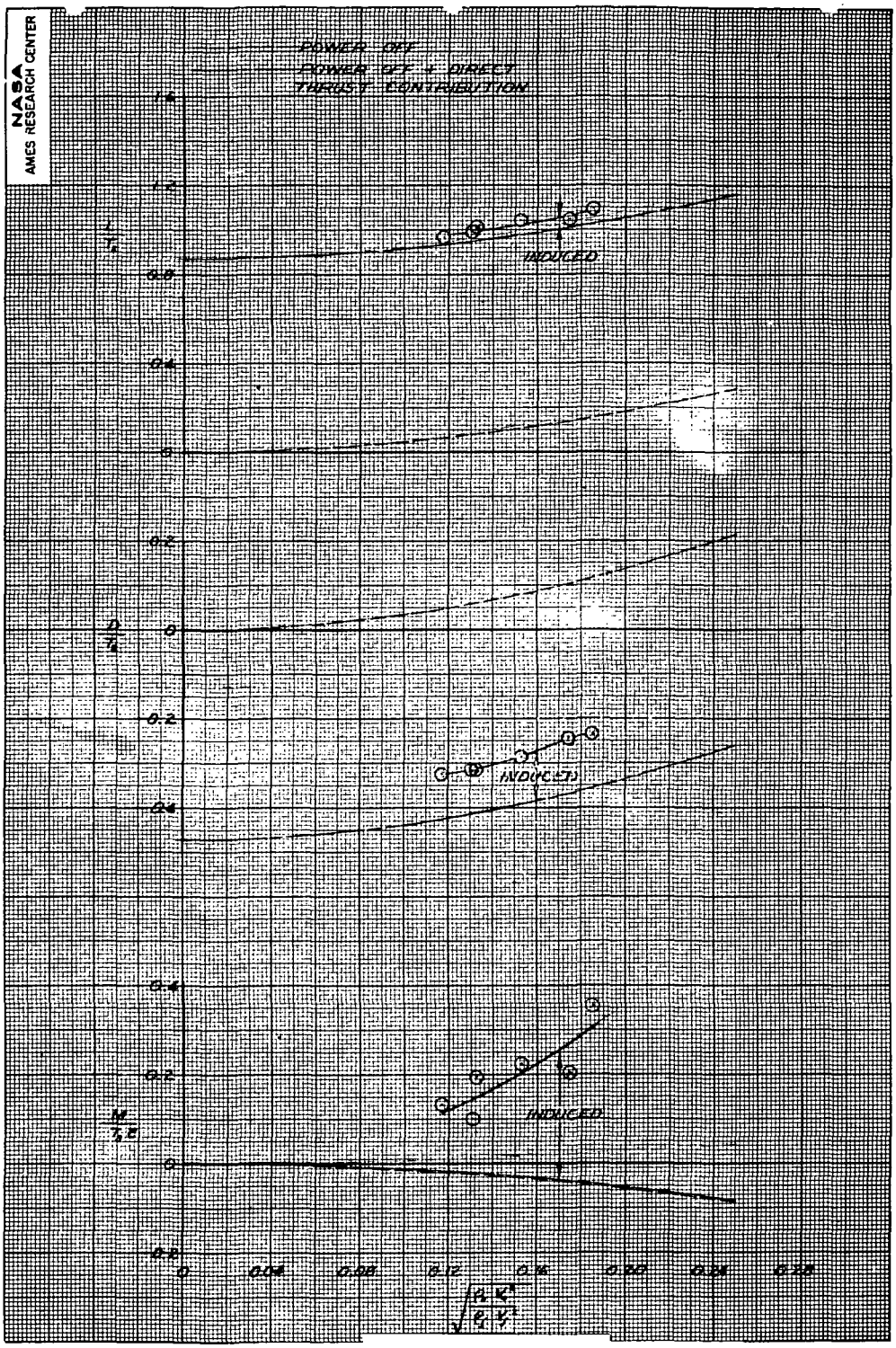

Figure 23.- Concluded.

(c) All engines operating.

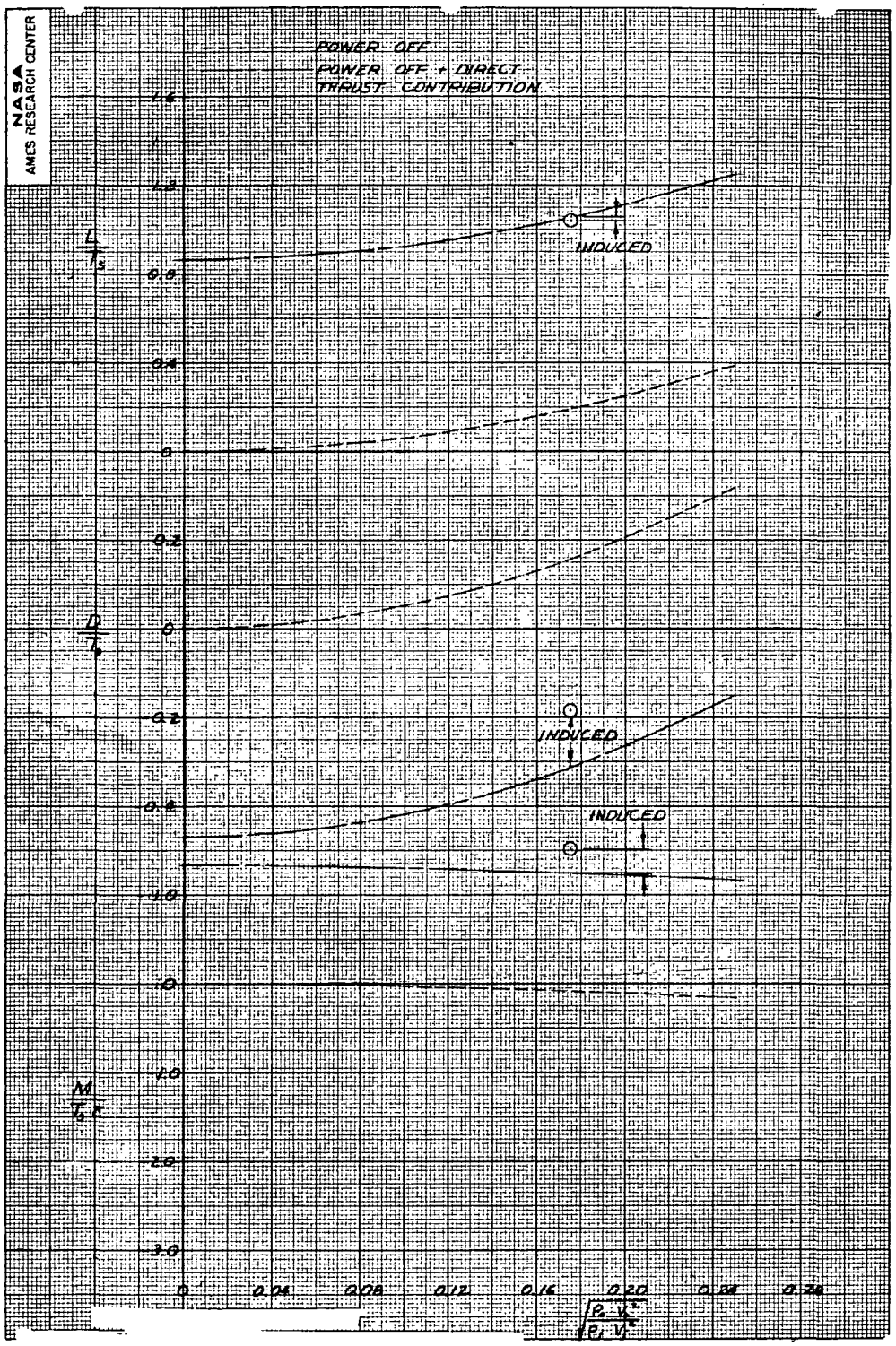

Figure 24.- Effect of momentum ratio variation on the longitudinal aerodynamic characteristics of the model; $\sigma = 60°$, $i_t = 0°$, $\alpha = 0°$, $\beta = 0°$, $\delta_f = 45°$, $\delta_s = 25°$.

(a) Lift engines only operating

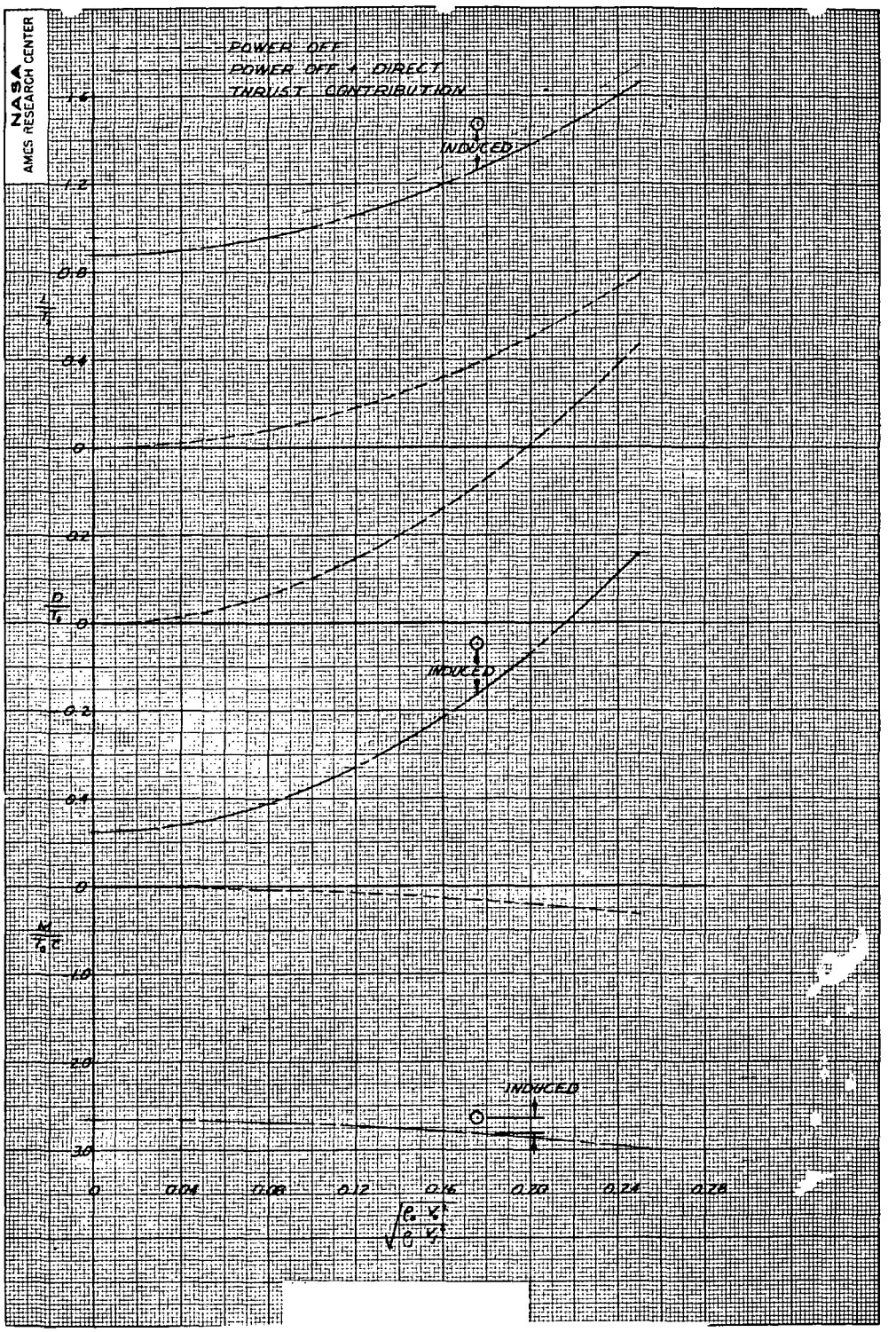

Figure 24.- Continued.

(b) Cruise engines only operating.

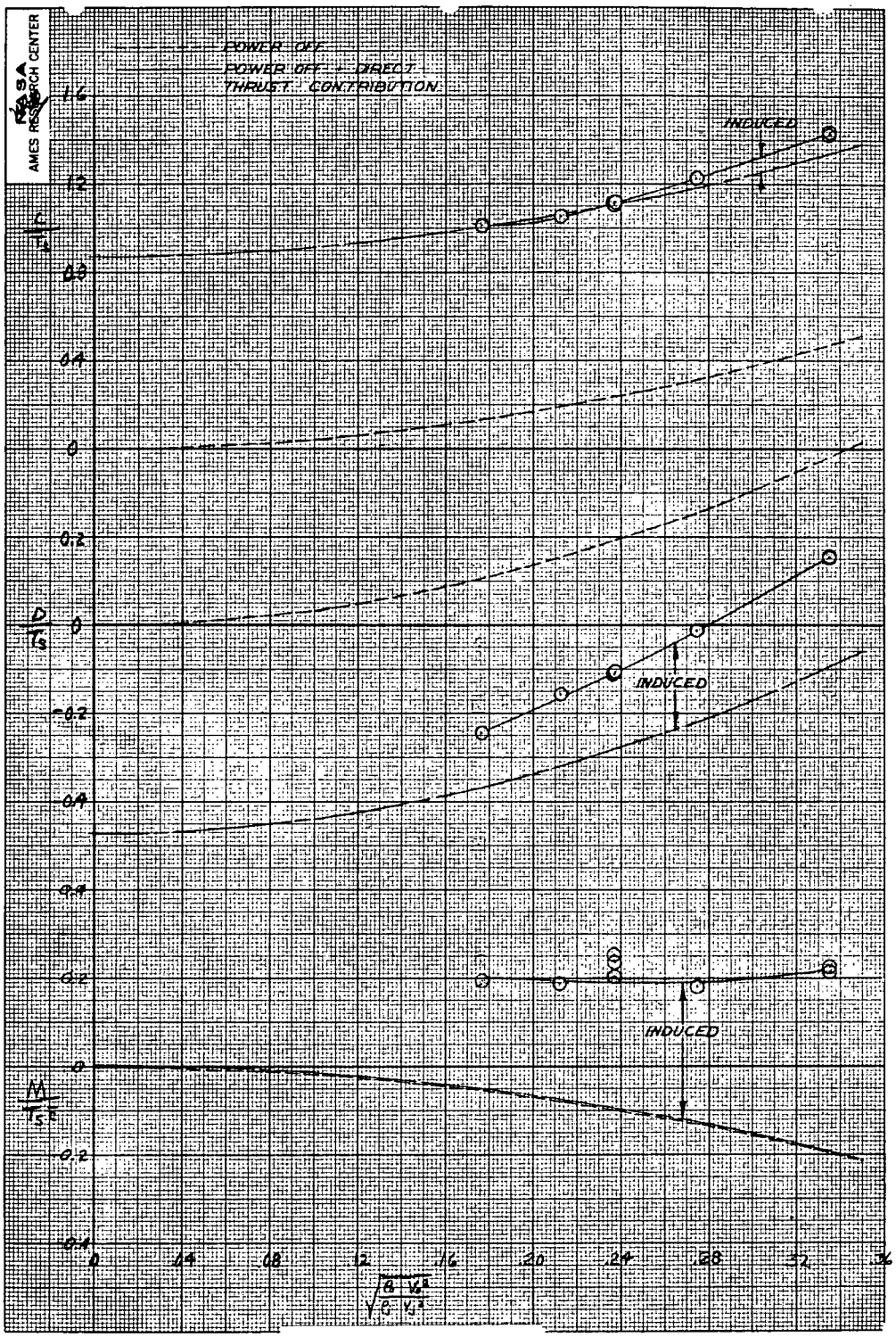

Figure 24.- Concluded.

(c) All engines operating.

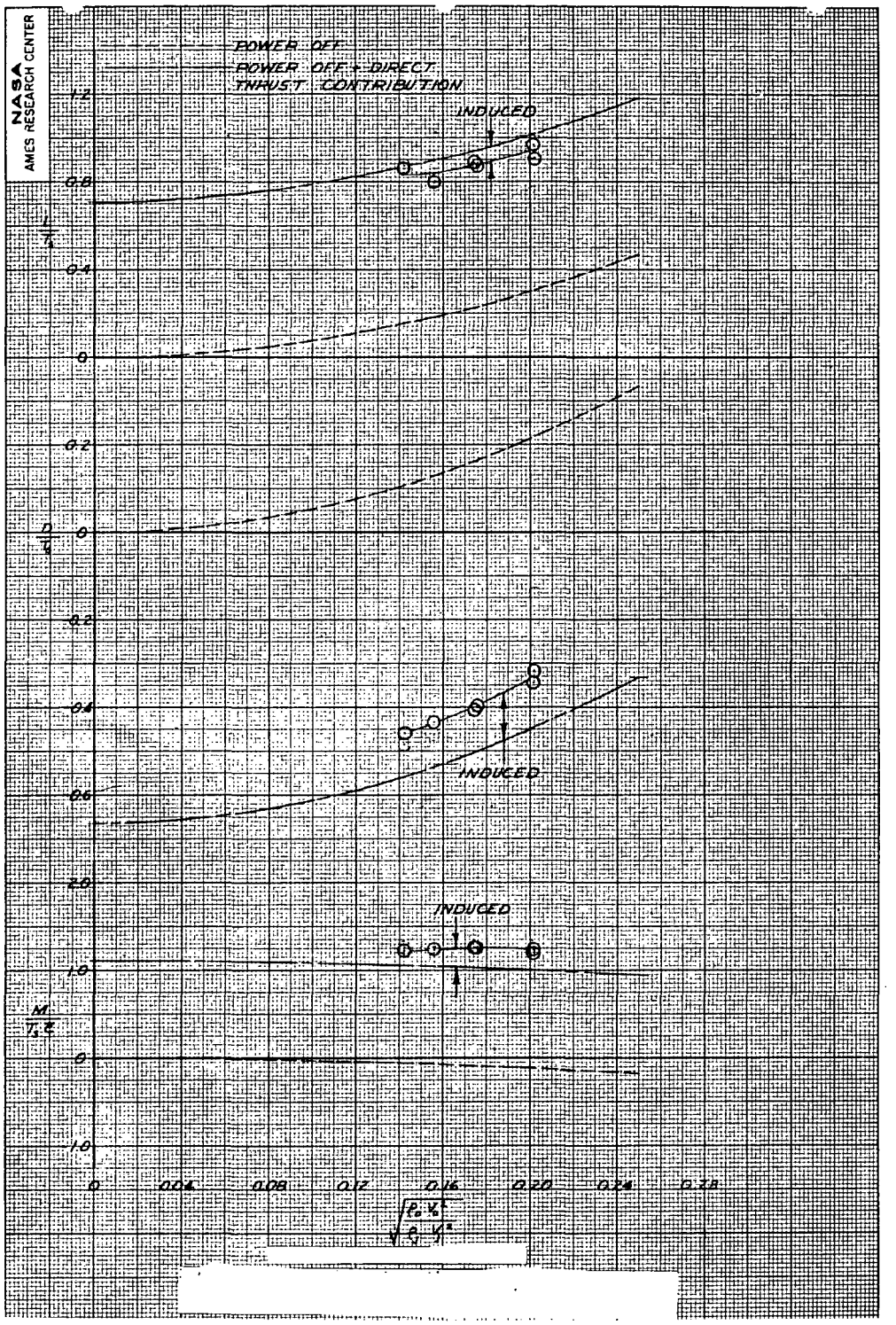

Figure 25.- Effect of momentum ratio variation on the longitudinal aerodynamic characteristics of the model; $\sigma = 45°$, Horizontal tail off, $\alpha = 0°$, $\beta = 0°$, $\delta_f = 45°$, $\delta_s = 25°$.

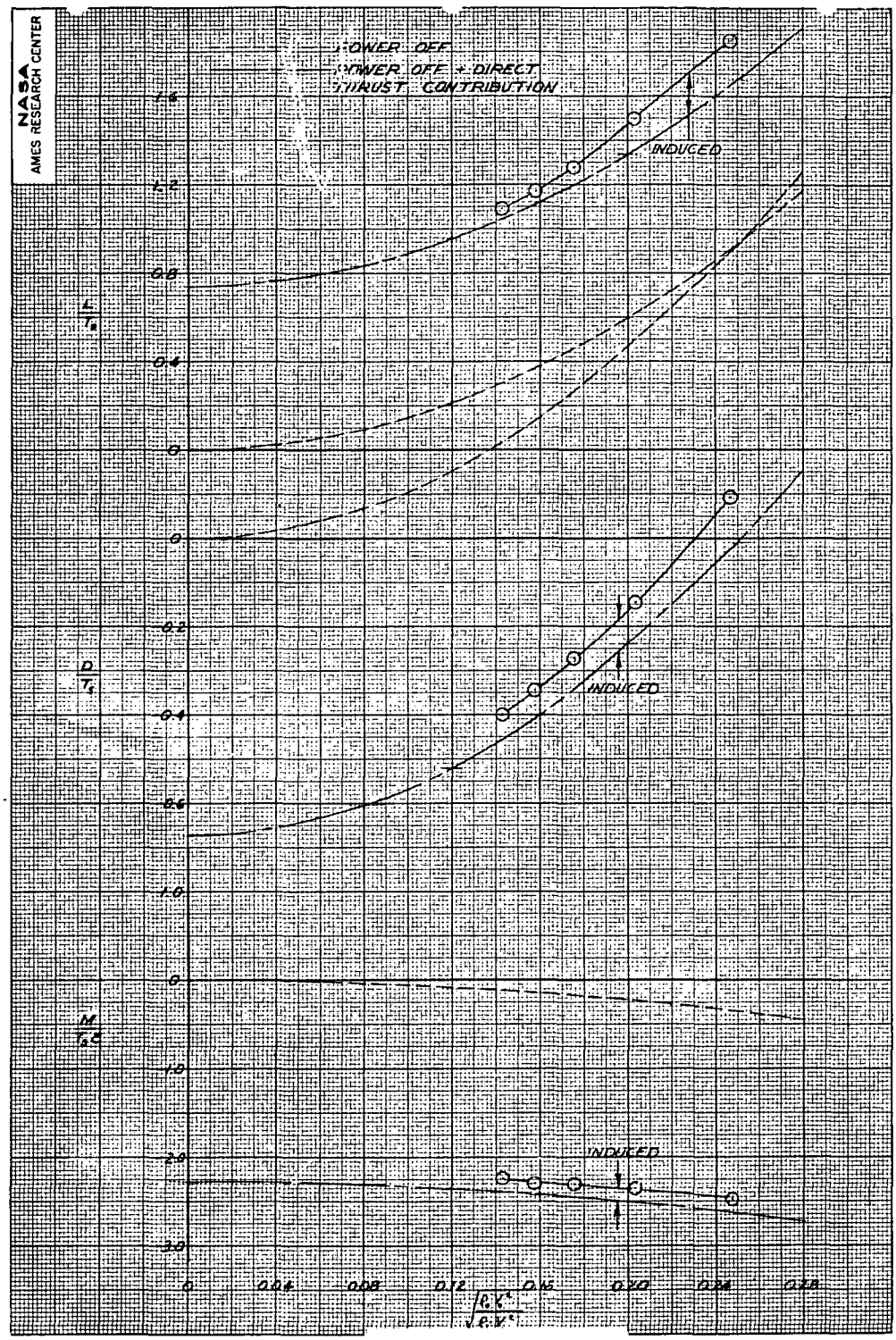

Figure 25.- Continued.

(b) Cruise engines only operating.

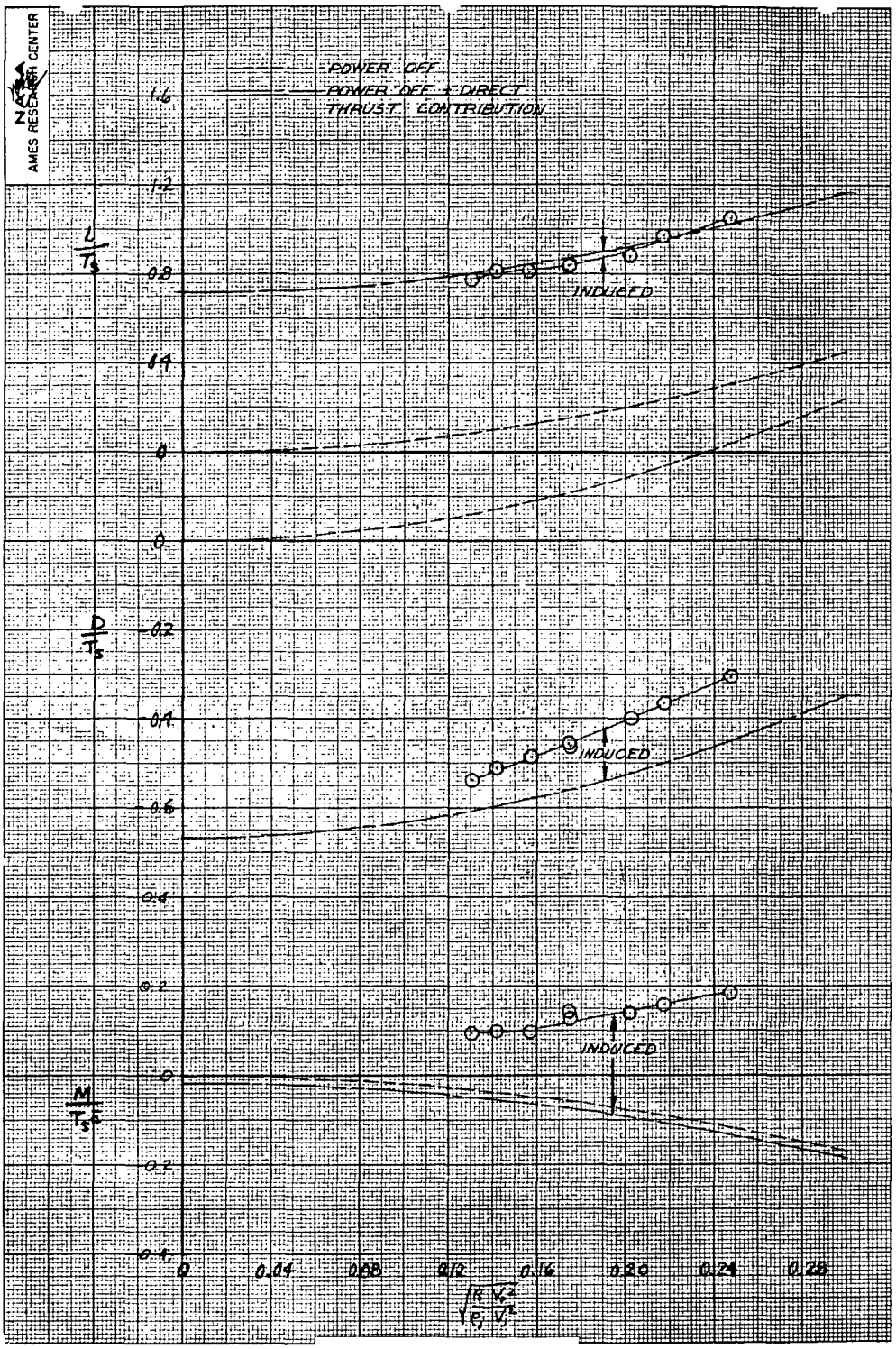

Figure 25.- Concluded.

(c) All engines operating.

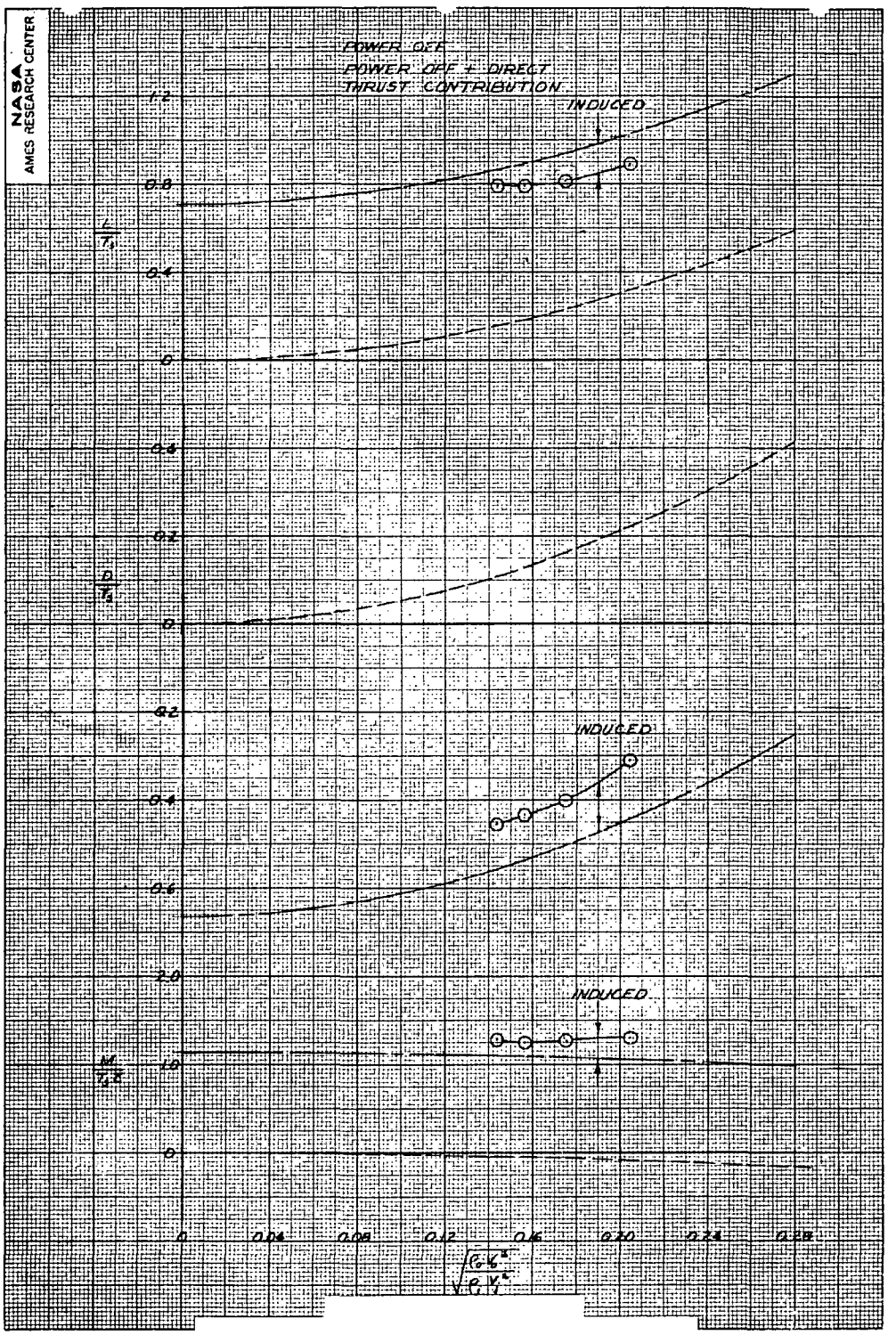

Figure 26.- Effect of momentum ratio variation on the longitudinal aerodynamic characteristics of the model; $\sigma = 45°$, $i_t = 0°$, $\alpha = 0°$, $\beta = 0°$, $\delta_f = 45°$, $\delta_s = 25°$.

(a) Lift engines only operating

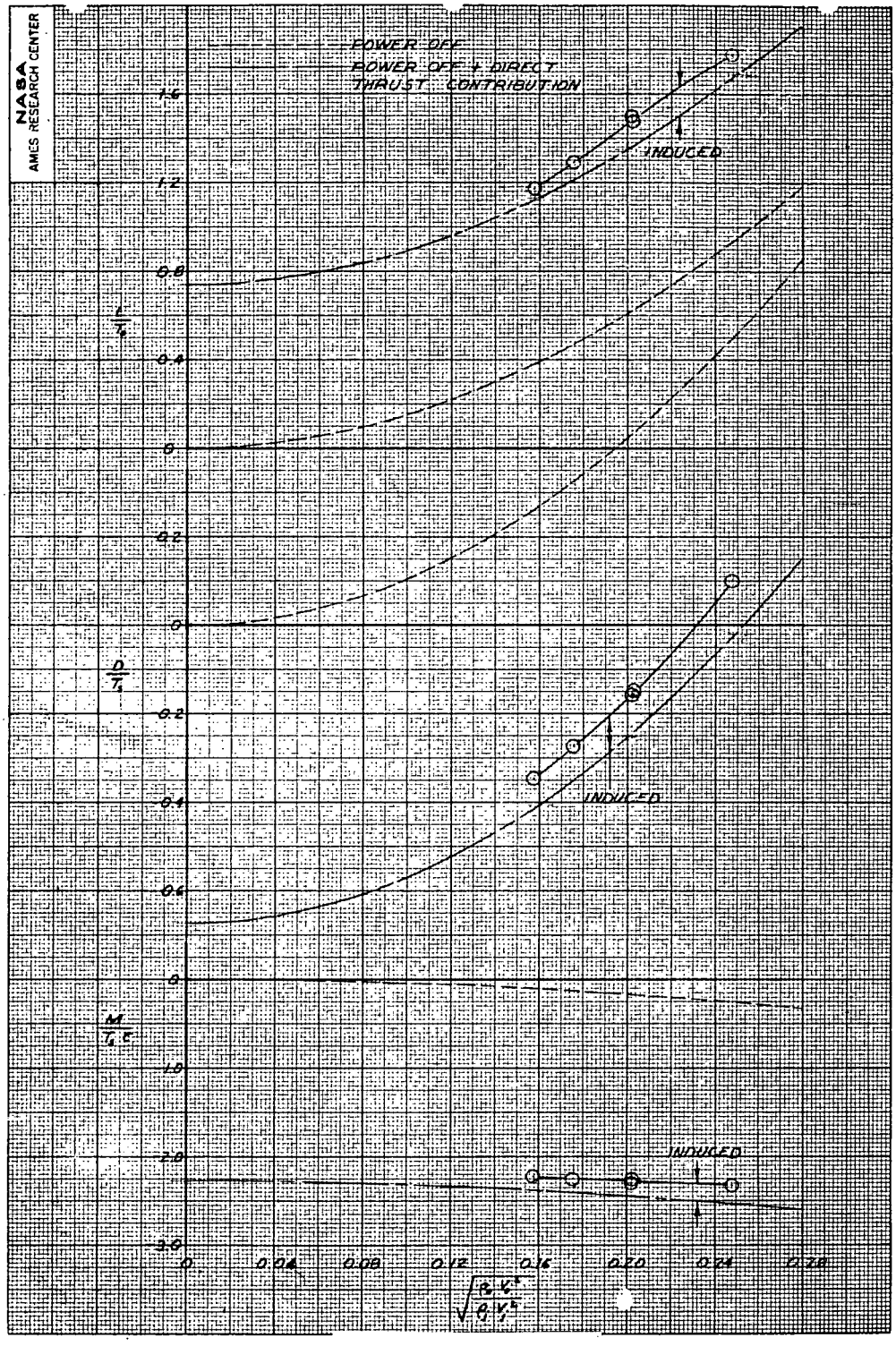

Figure 26.- Continued.

(b) Cruise engines only operating.

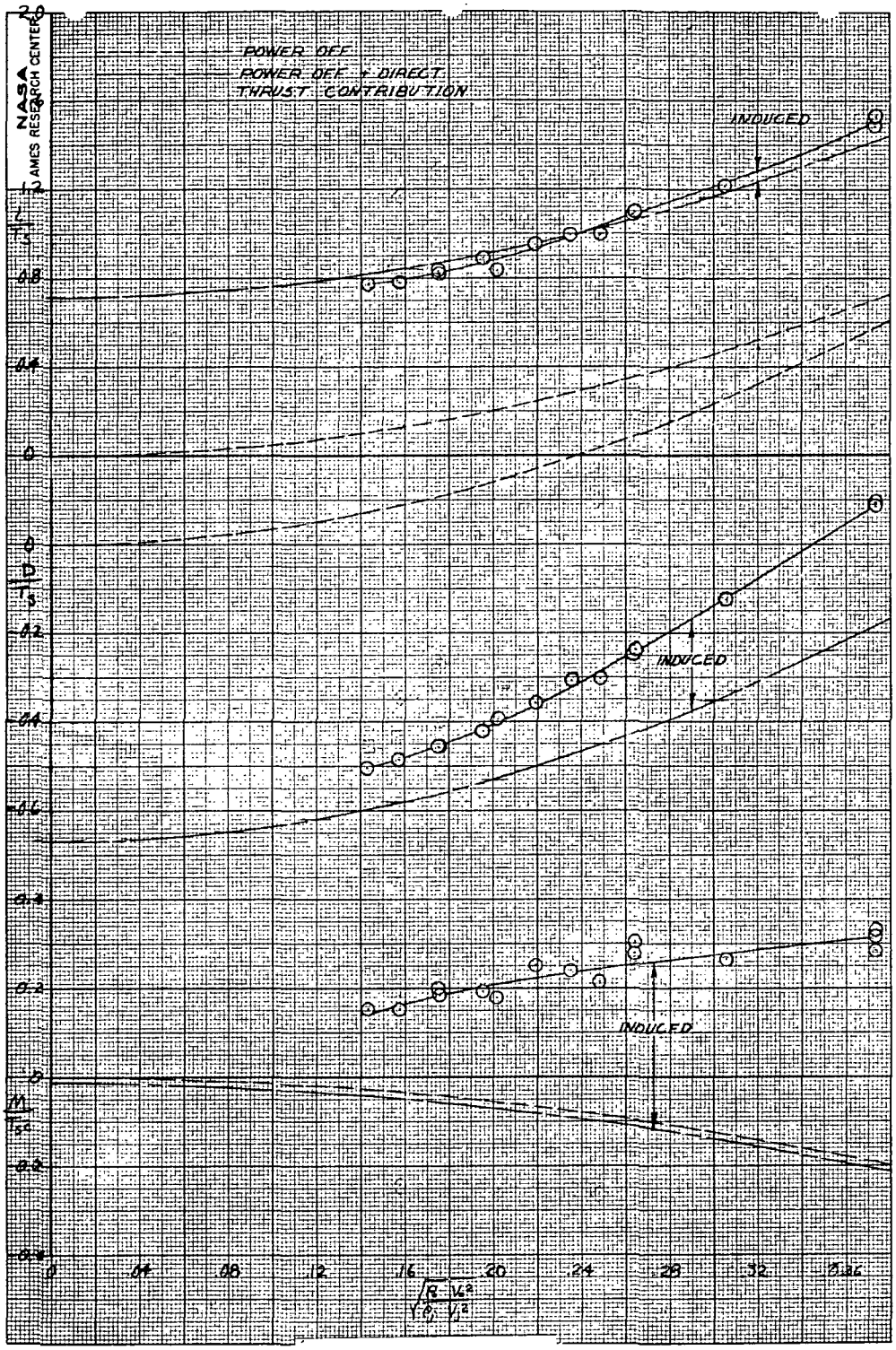

Figure 26.- Concluded.

(c) All engines operating.

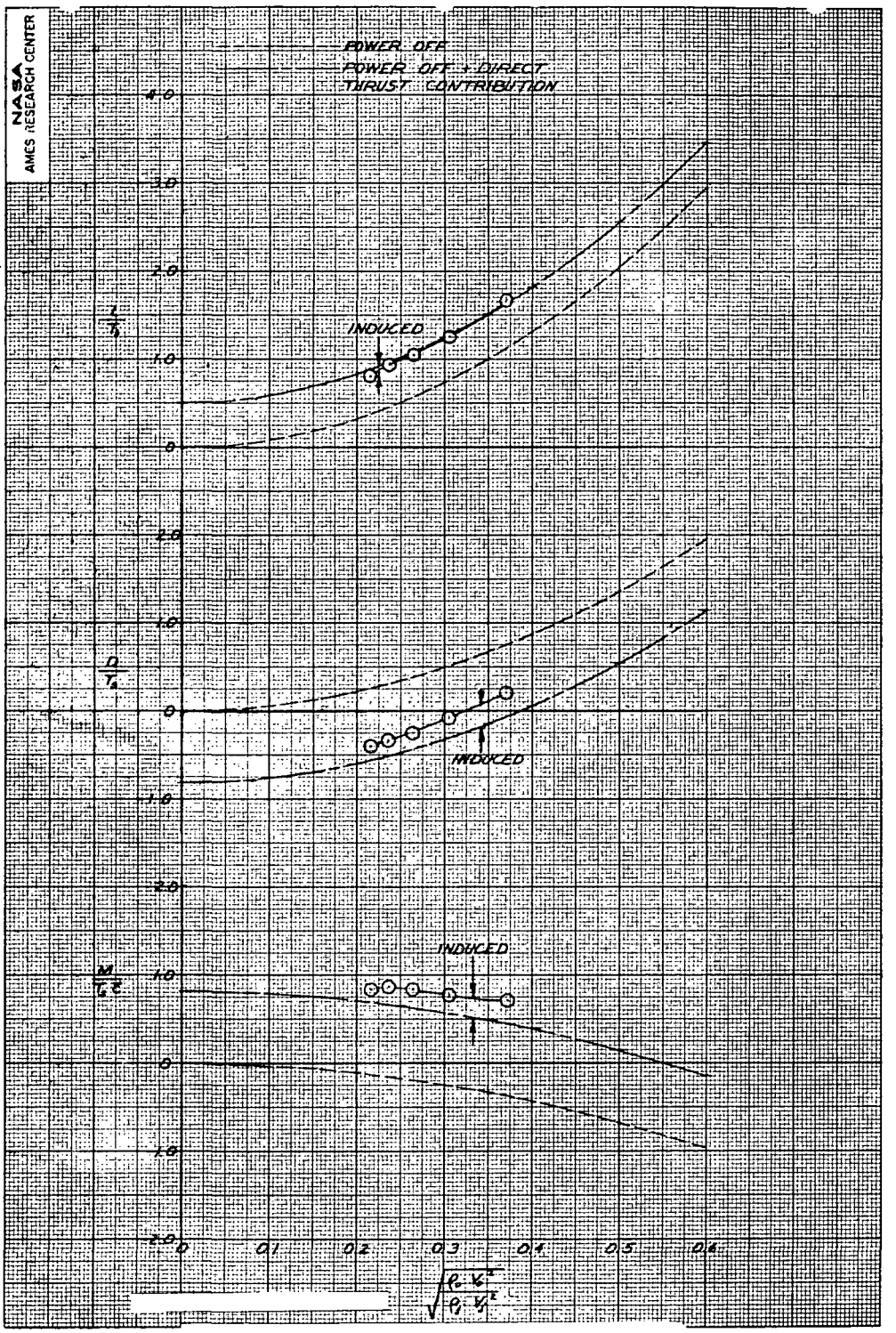

Figure 27.- Effect of momentum ratio variation on the longitudinal aerodynamic characteristics of the model; $\sigma = 30°$, Horizontal tail off, $\alpha = 0°$, $\beta = 0°$, $\delta_f = 45°$, $\delta_s = 25°$.

(a) Lift engines only operating

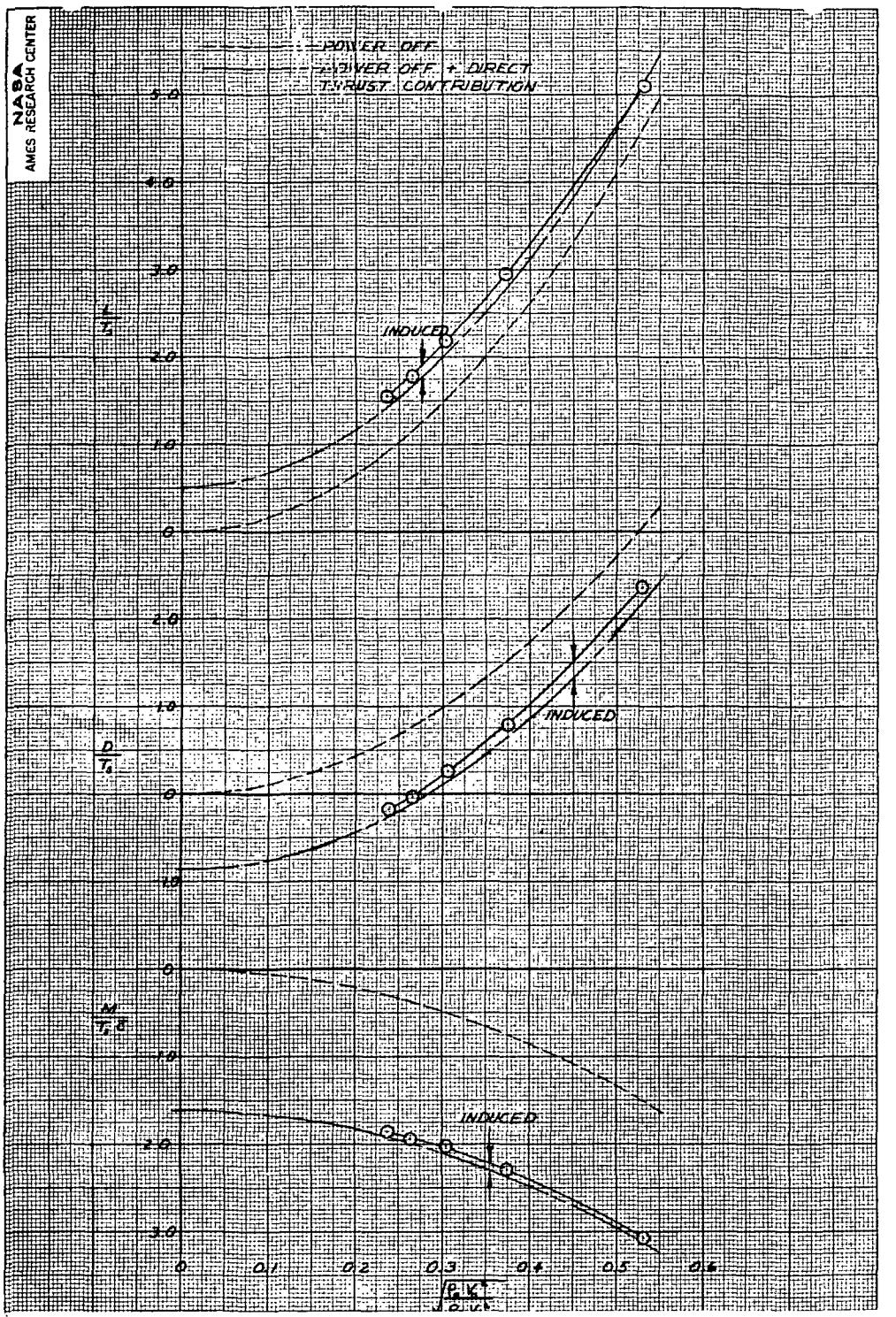

Figure 27.- Continued.

(b) Cruise engines only operating.

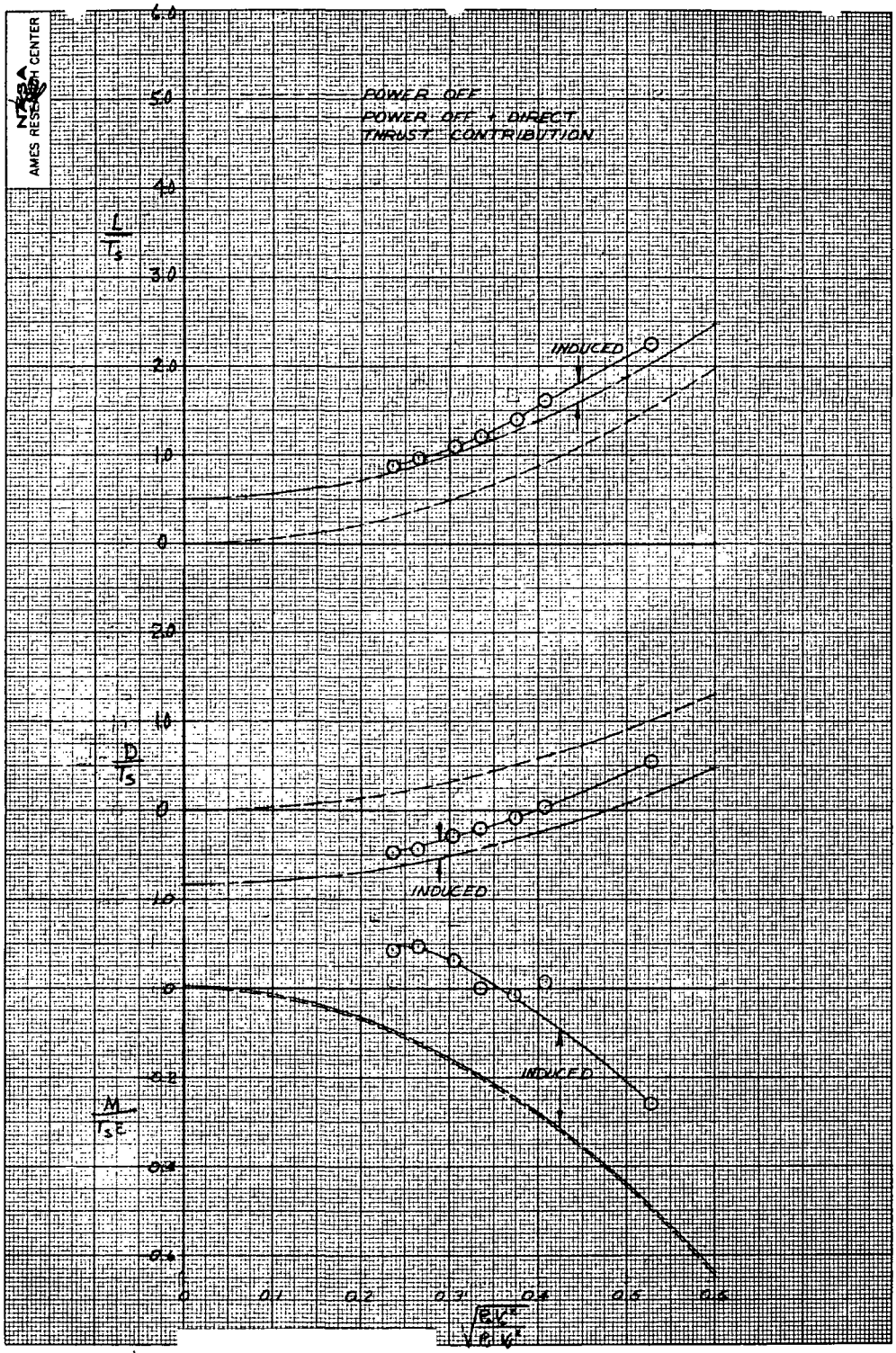

Figure 27.- Concluded.

(c) All engines operating.

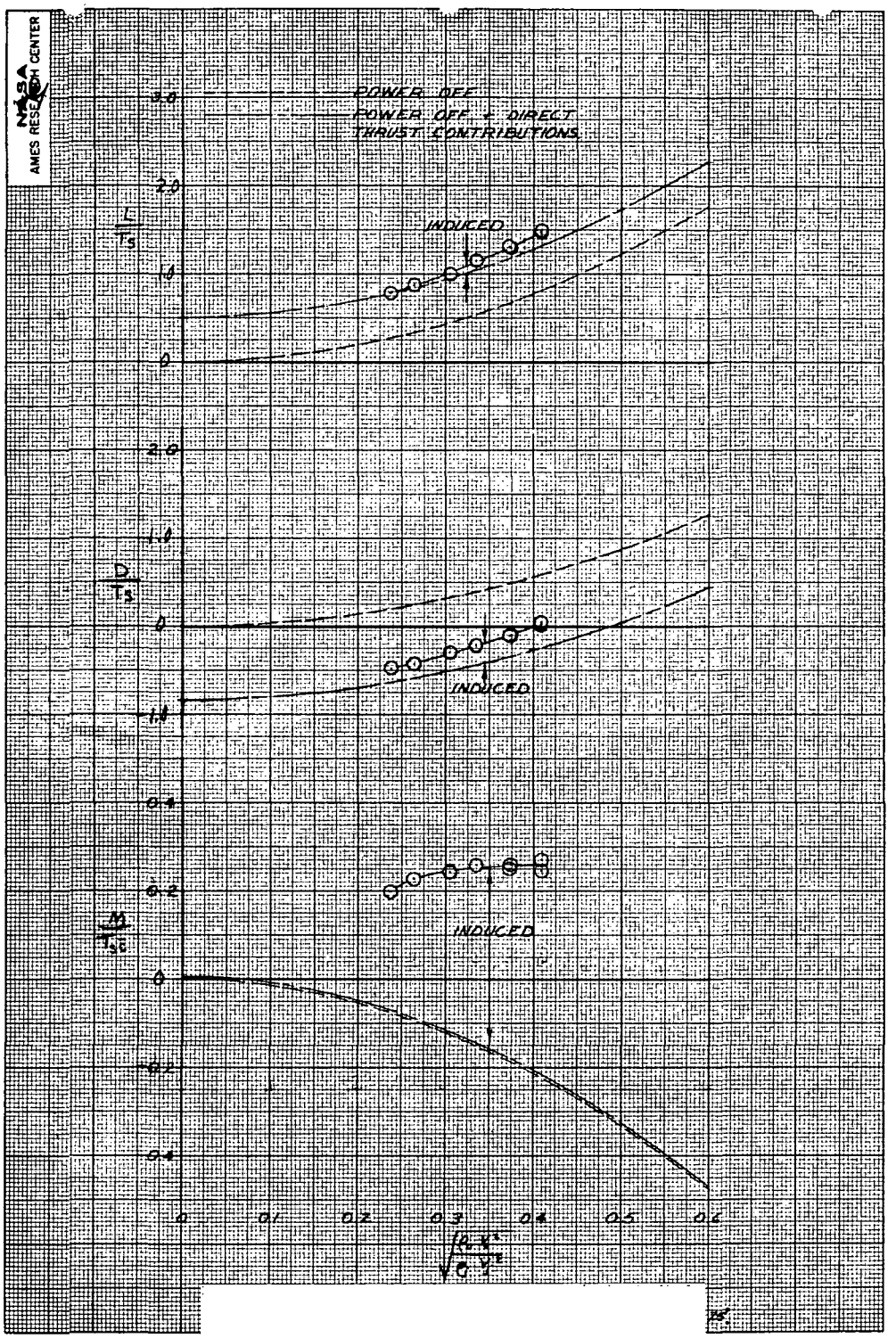

Figure 28.- Effect of momentum ratio variation on the longitudinal aerodynamic characteristics of the model; $\sigma = 30°$, All engines operating, $i_t = 0°$, $\alpha = 0°$, $\beta = 0°$, $\delta_f = 45°$, $\delta_s = 25°$.

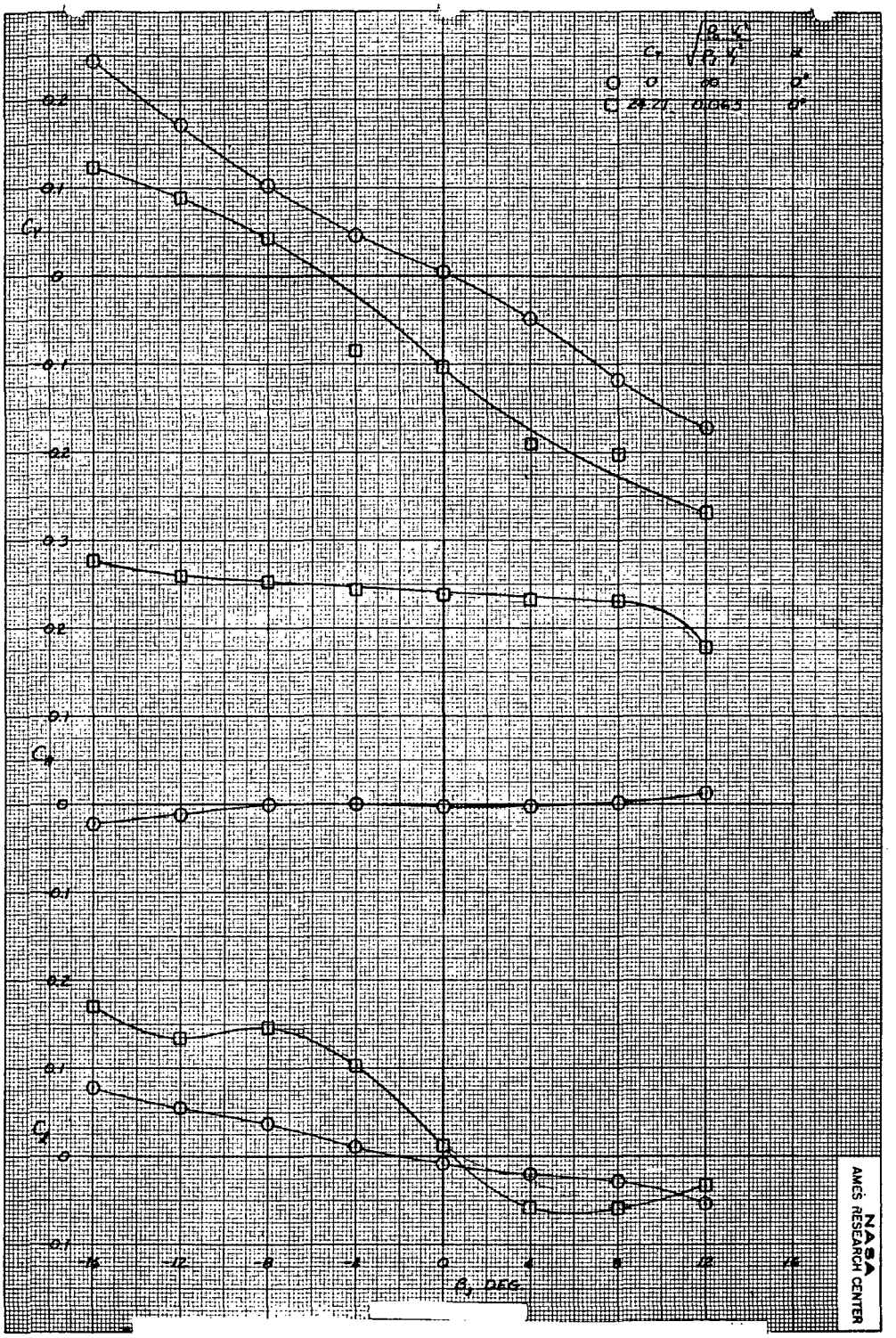

Figure 29.- Effect of sideslip angle on the lateral-directional characteristics of the model. $\sigma = 90°$. $i_t = 0°$. All engines set at equal thrust, $\delta_f = 45°, \delta_s = 25°$.

(a) $\alpha = 0°$.

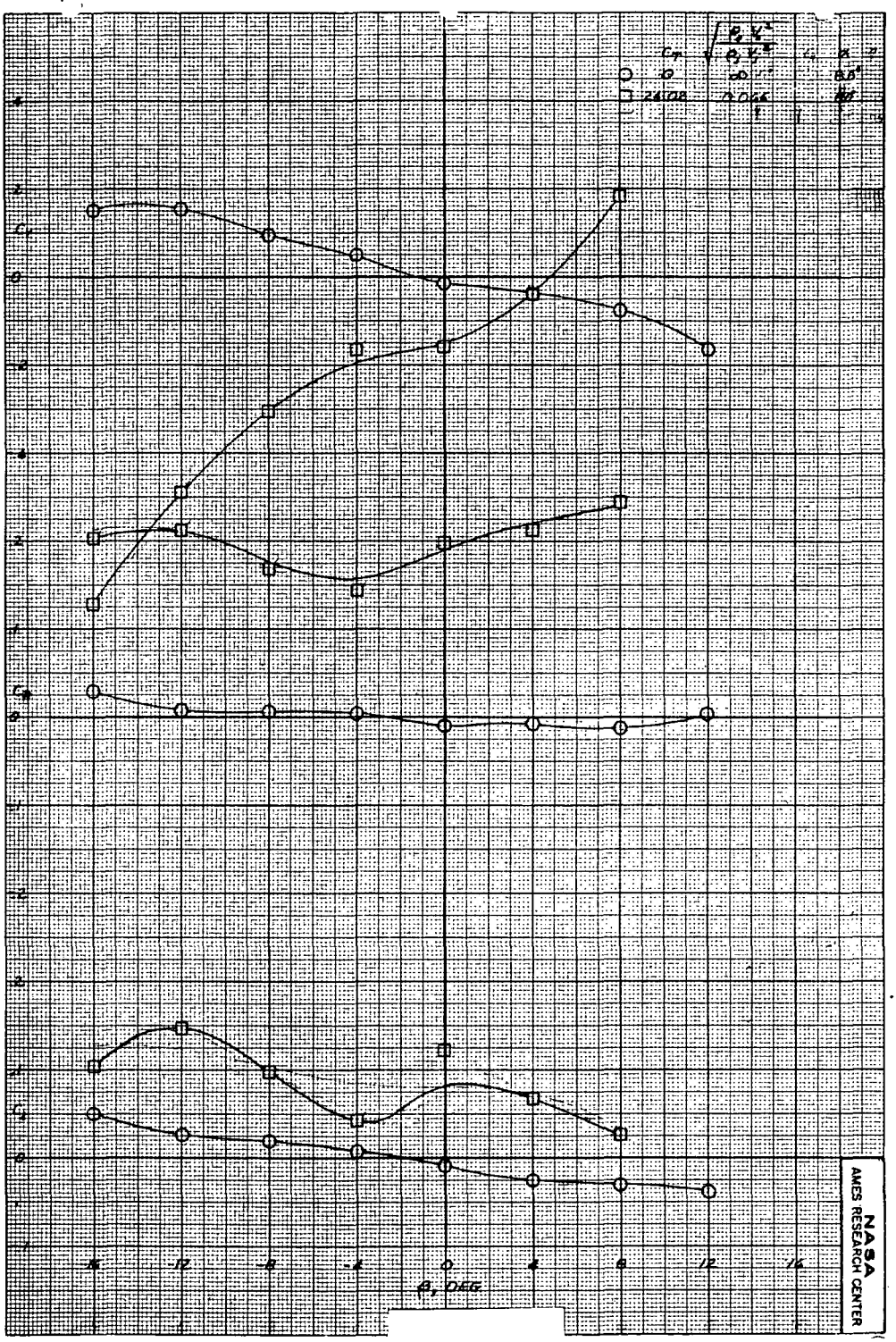

(b) α = 8°.

Figure 29.- Continued.

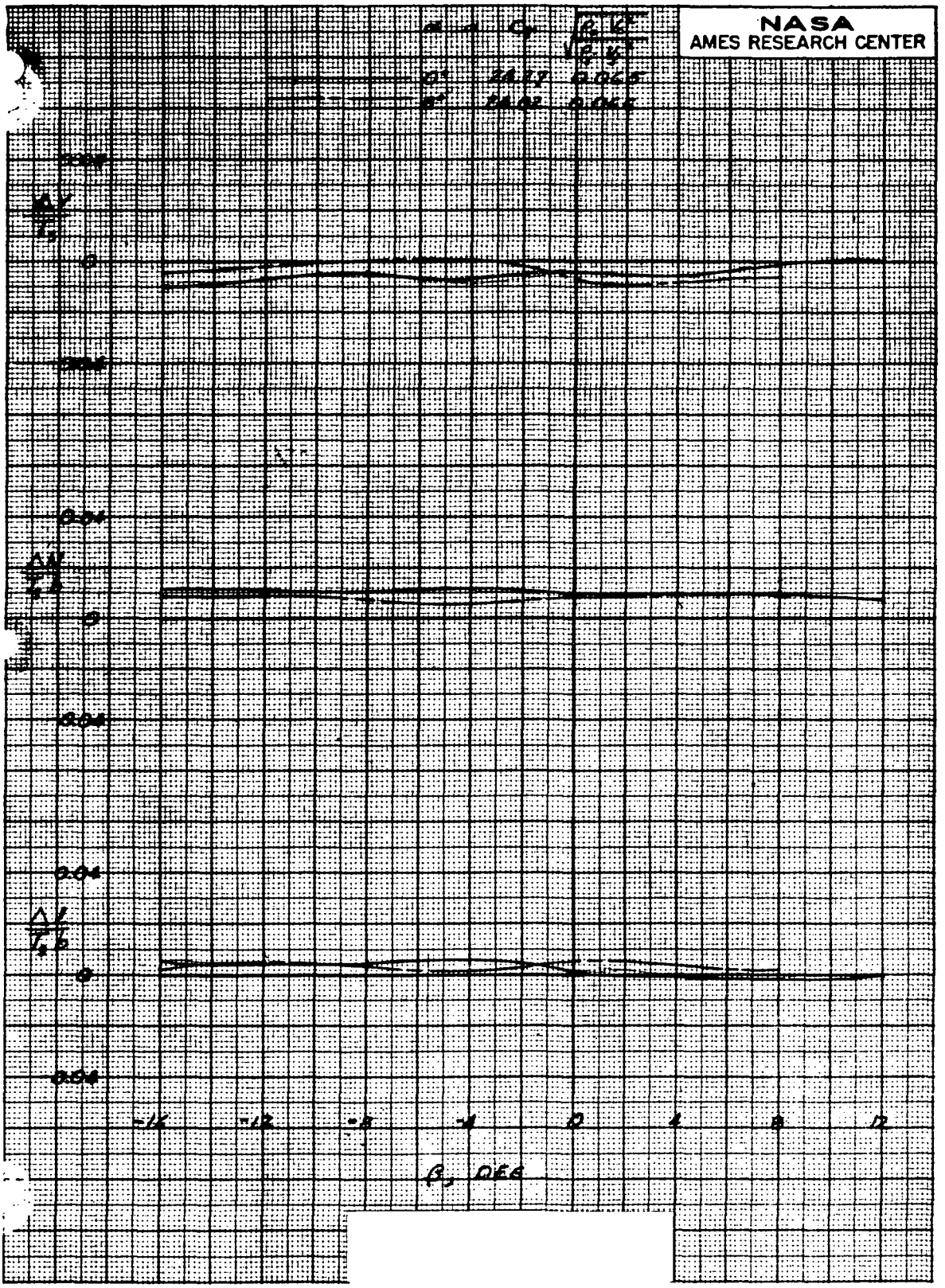

Figure 29.- Concluded.

(c) Interference increments

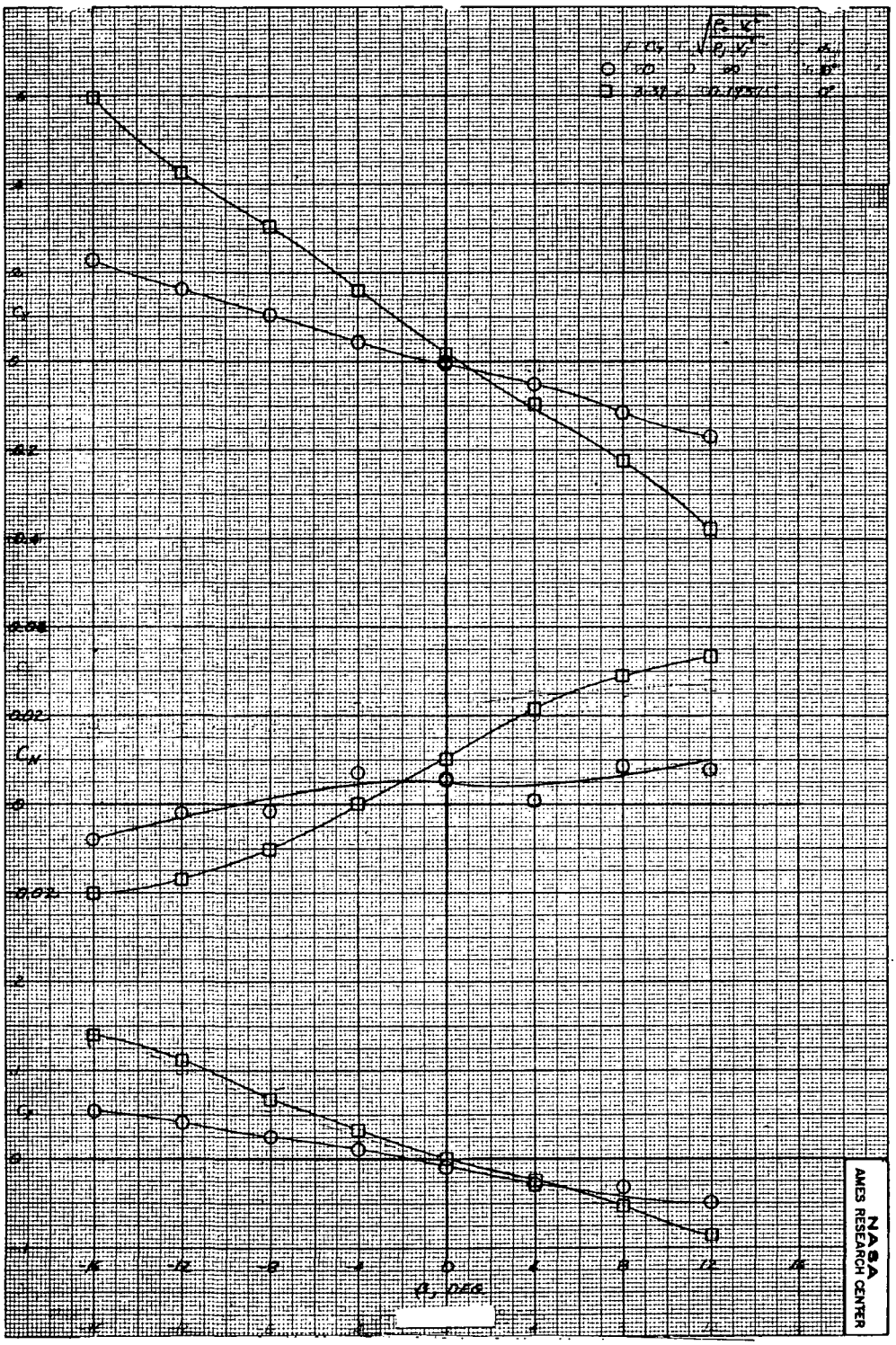

Figure 30.- Effect of sideslip angle on the lateral-directional characteristics of the model. $\sigma = 75°$. $i_t = 0°$. All engines set at equal thrust, $\delta_f = 45°$, $\delta_s = 25°$.

(a) $\alpha = 0°$.

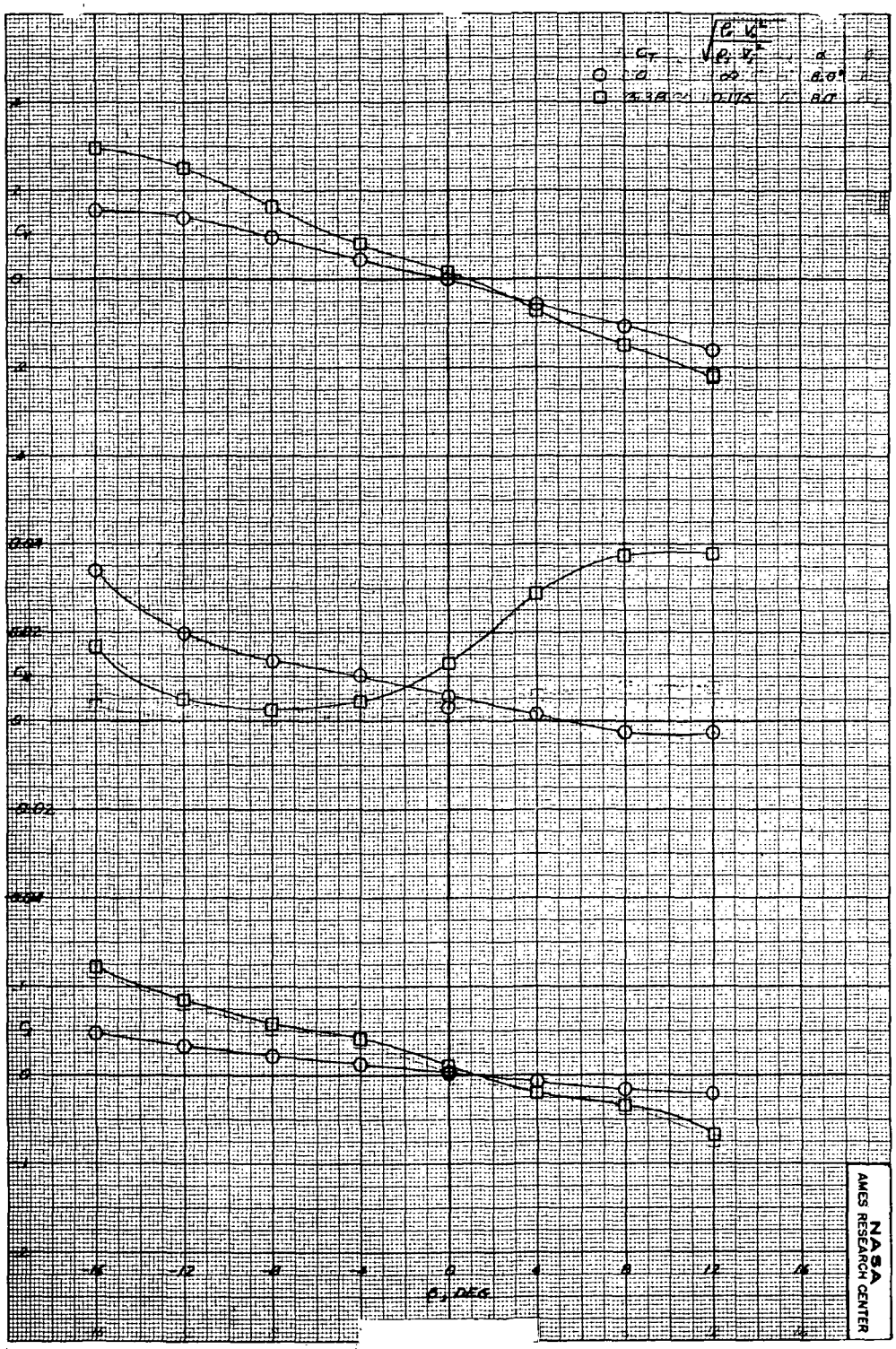

(b) $\alpha = 8°$.

Figure 30.- Continued.

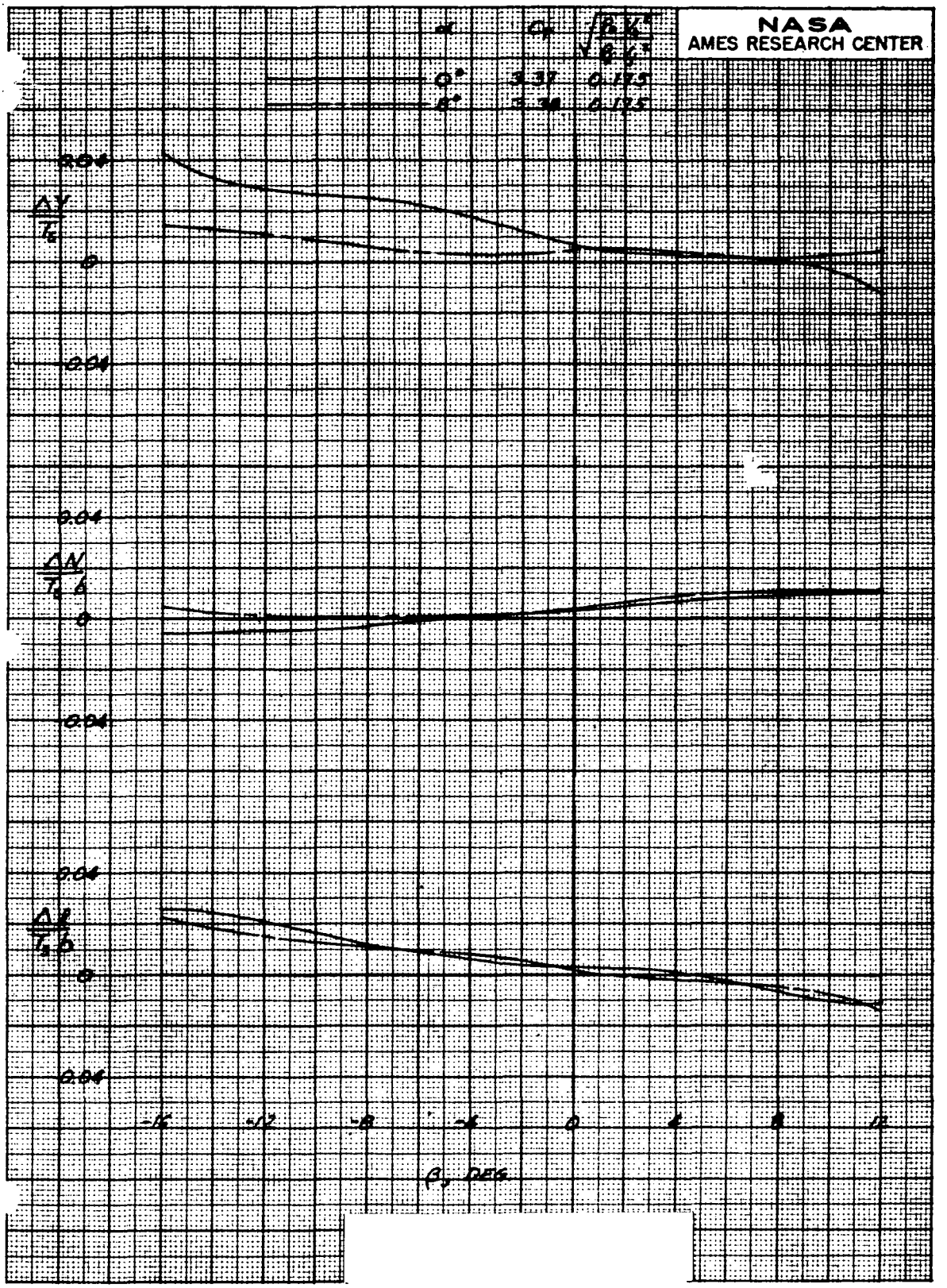

Figure 30.- Concluded.

(c) Interference increments.

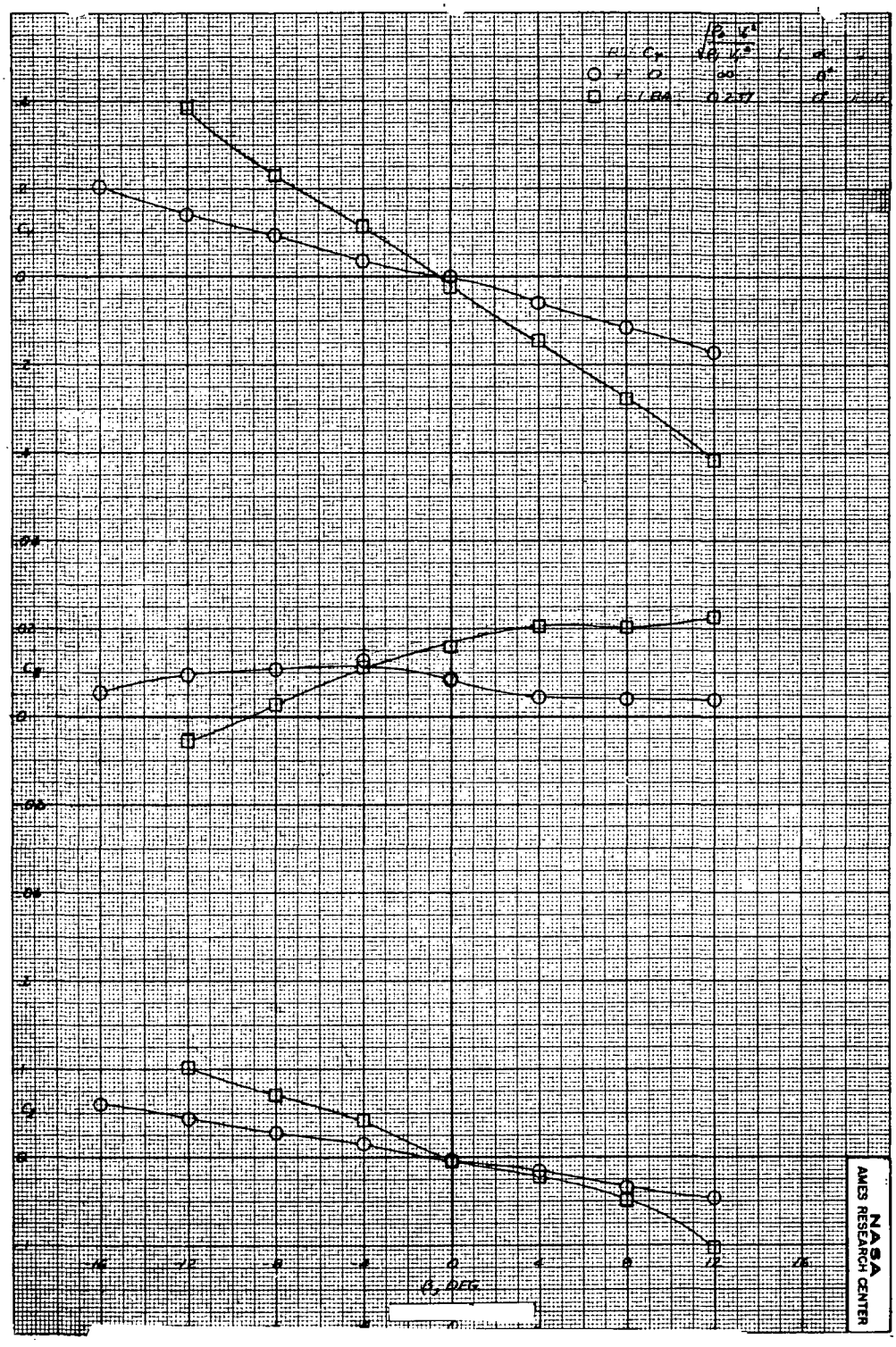

Figure 31. Effect of sideslip angle on the lateral-directional characteristics of the model. $\sigma = 60°$. $i_t = 0°$. All engines set at equal thrust, $\delta_f = 45°$, $\delta_s = 25°$.

(a) $\alpha = 0°$.

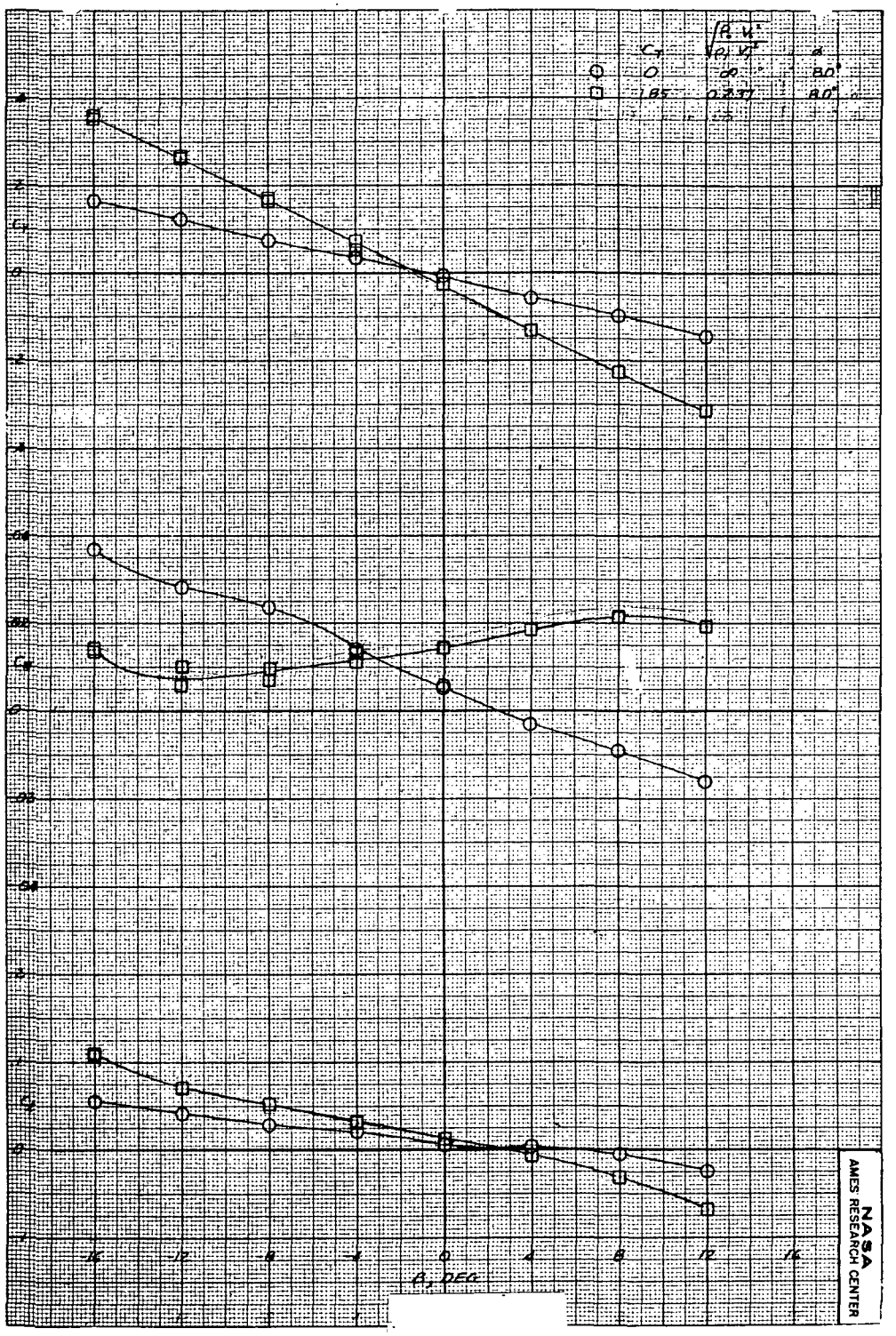

(b) $\alpha = 8°$.

Figure 31.- Continued.

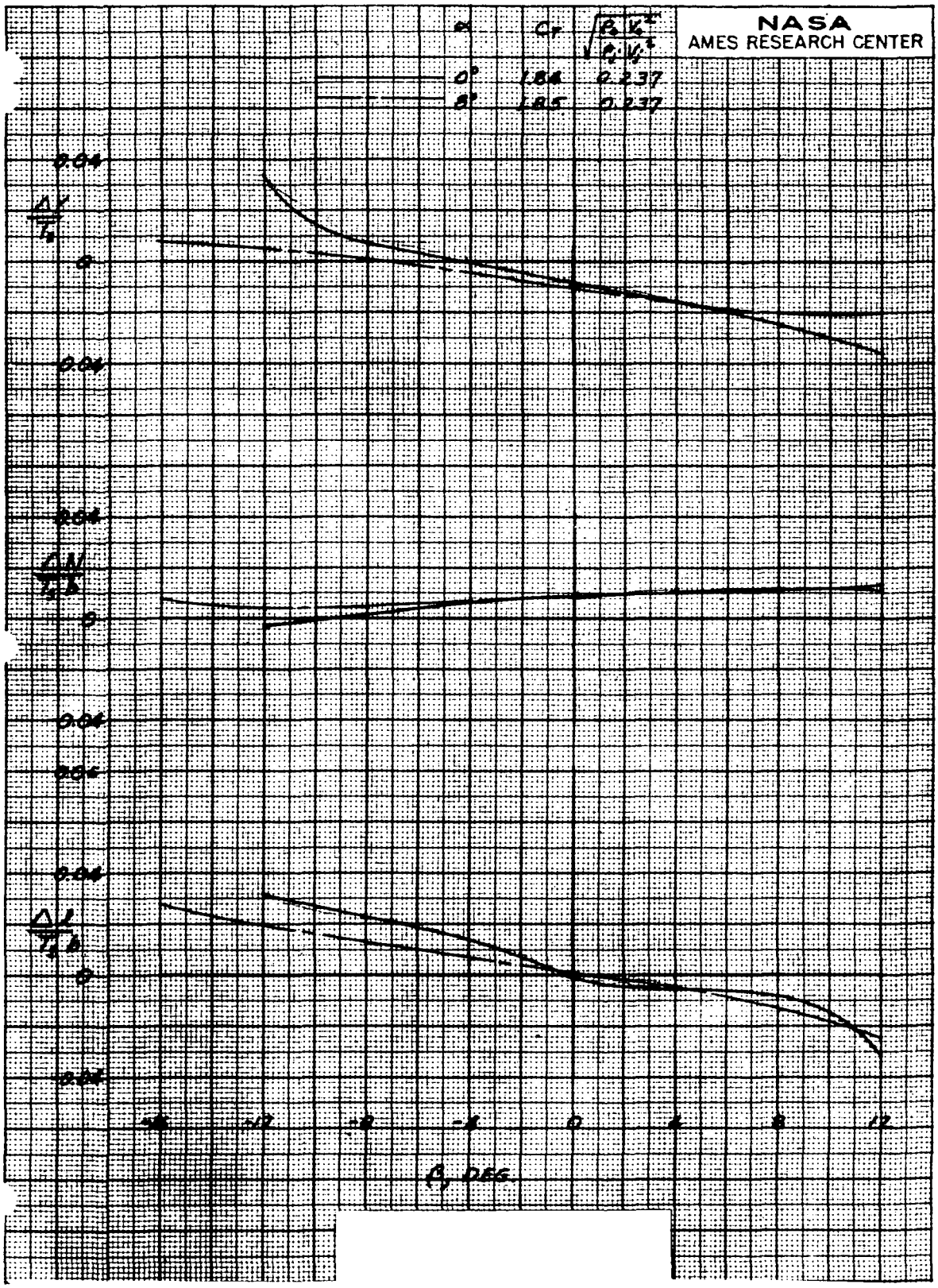

Figure 31.- Concluded.

(c) Interference increments.

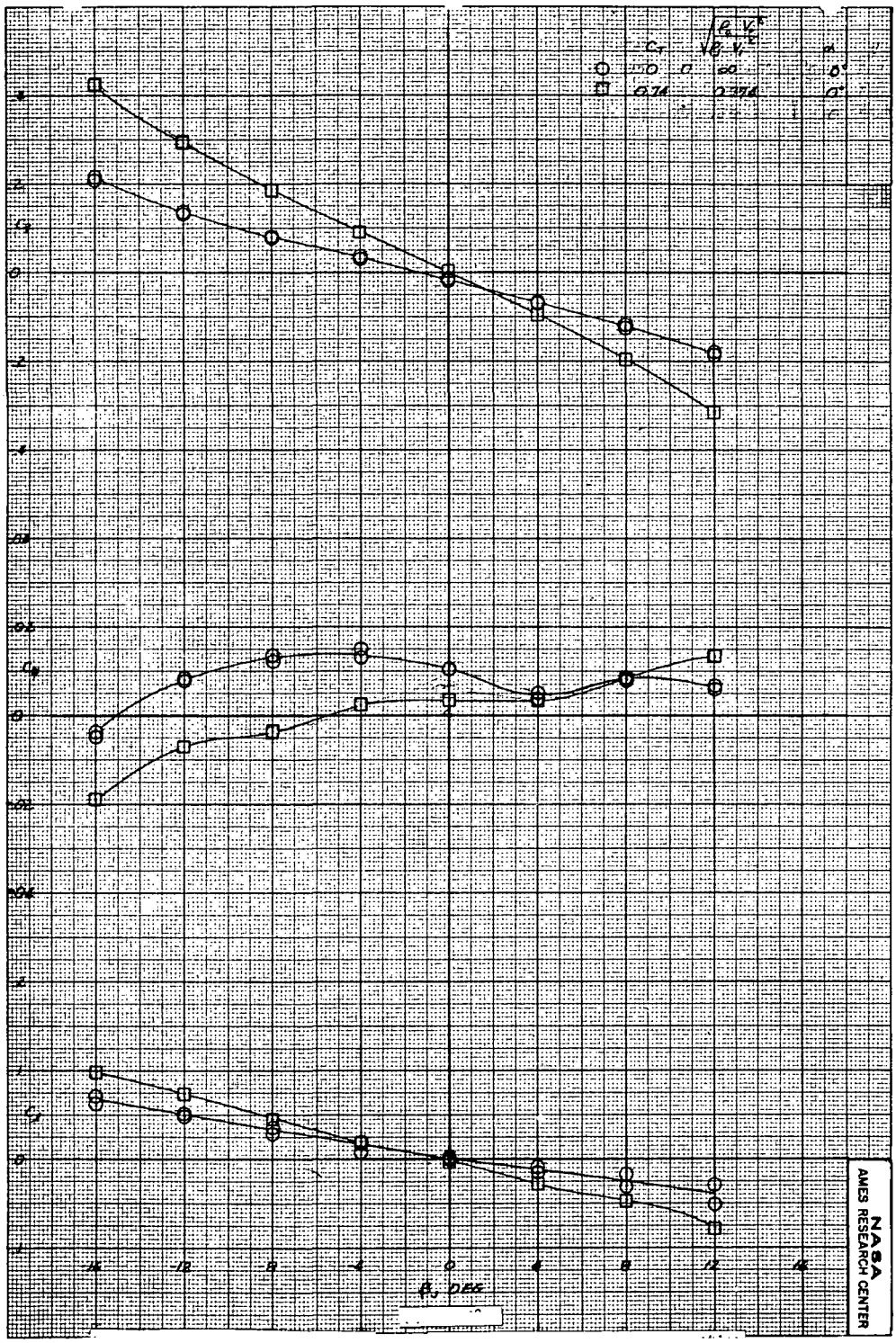

Figure 32.- Effect of sideslip angle on the lateral-directional characteristics of the model. $\sigma = 45°$. $i_t = 0°$. All engines set at equal thrust.

(a) $\alpha = 0°$.

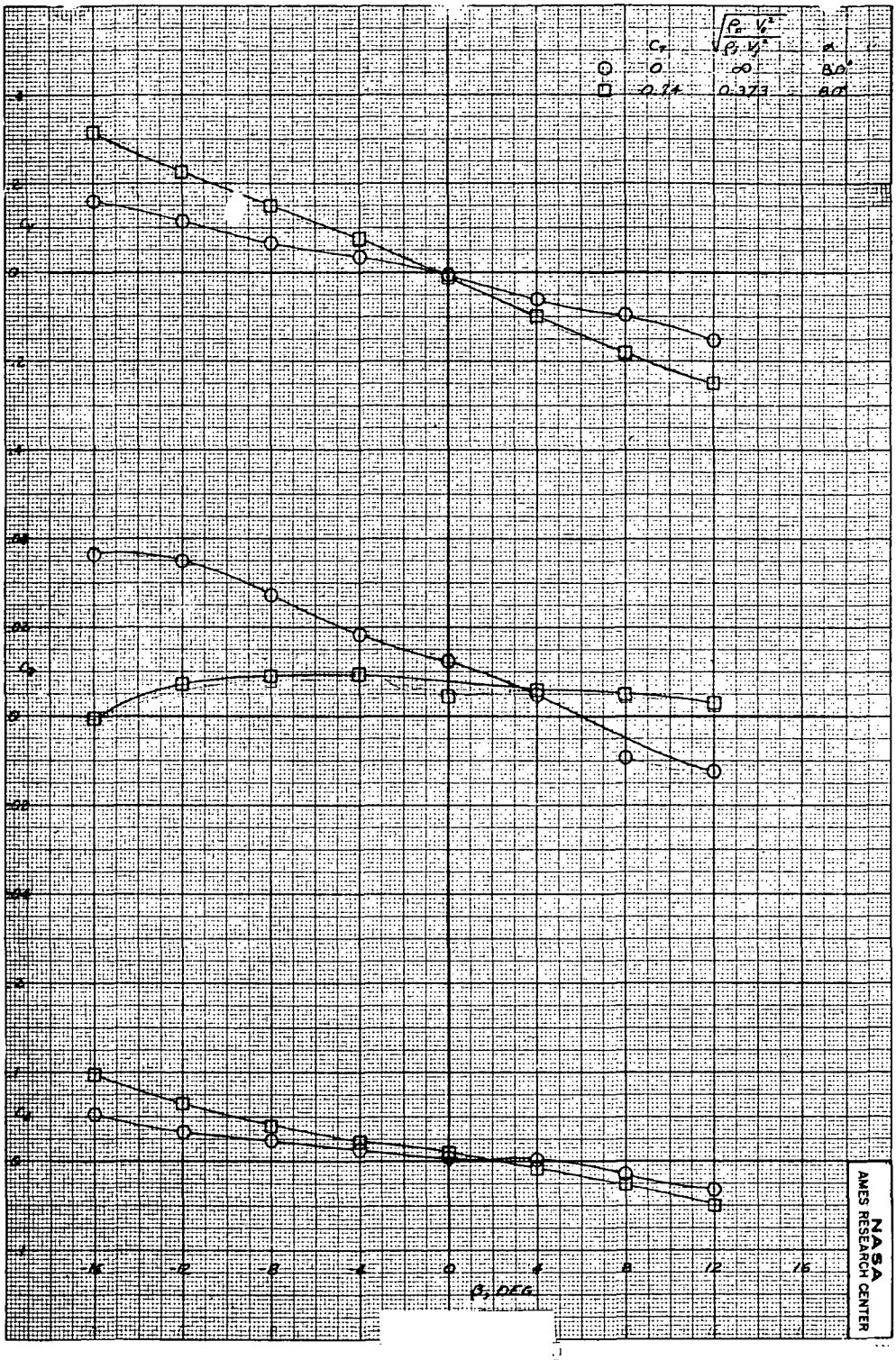

(b) $\alpha = 8°$.

Figure 32.- Continued.

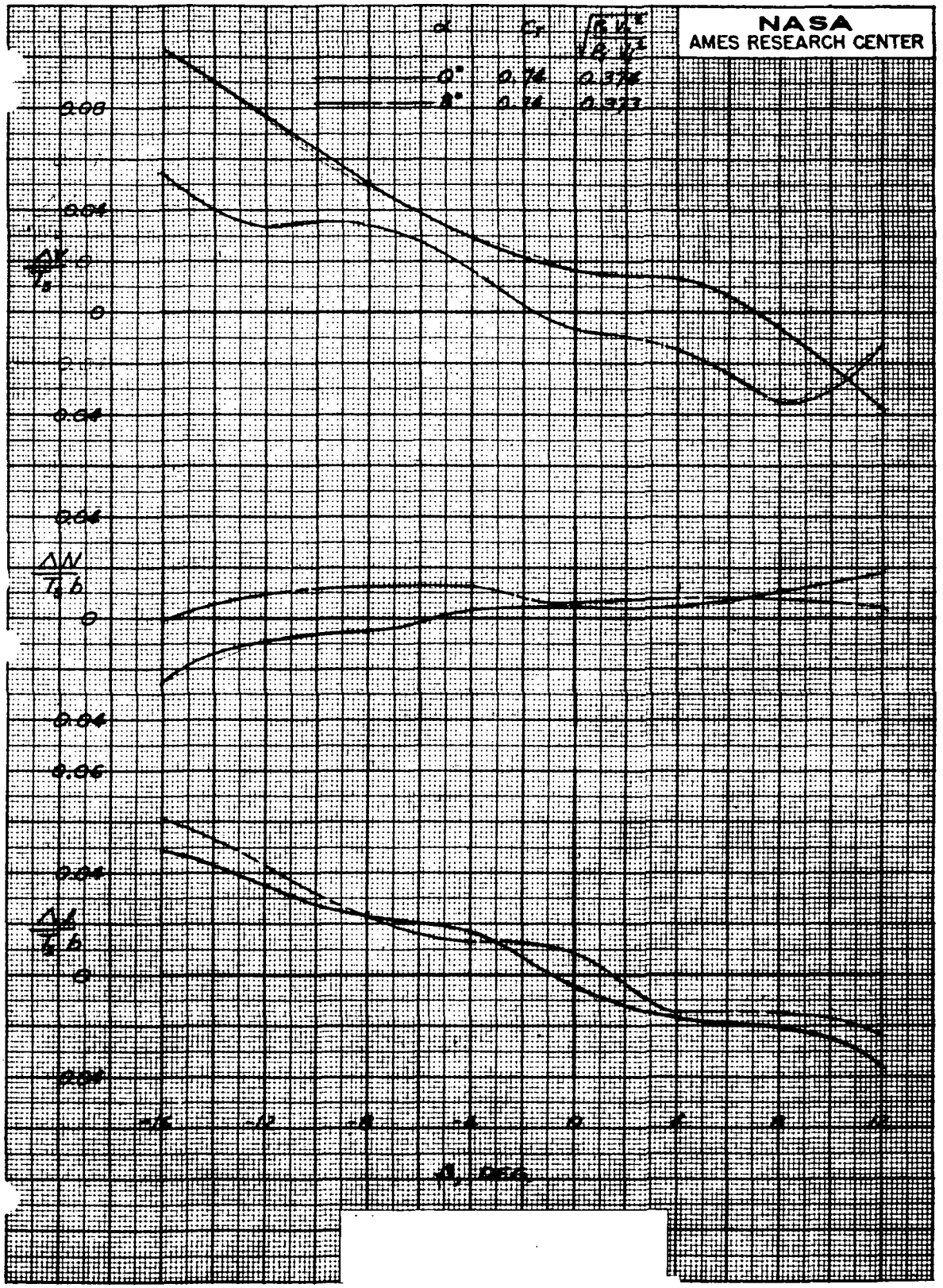

Figure 32.- Concluded.

(c) Interference increments.

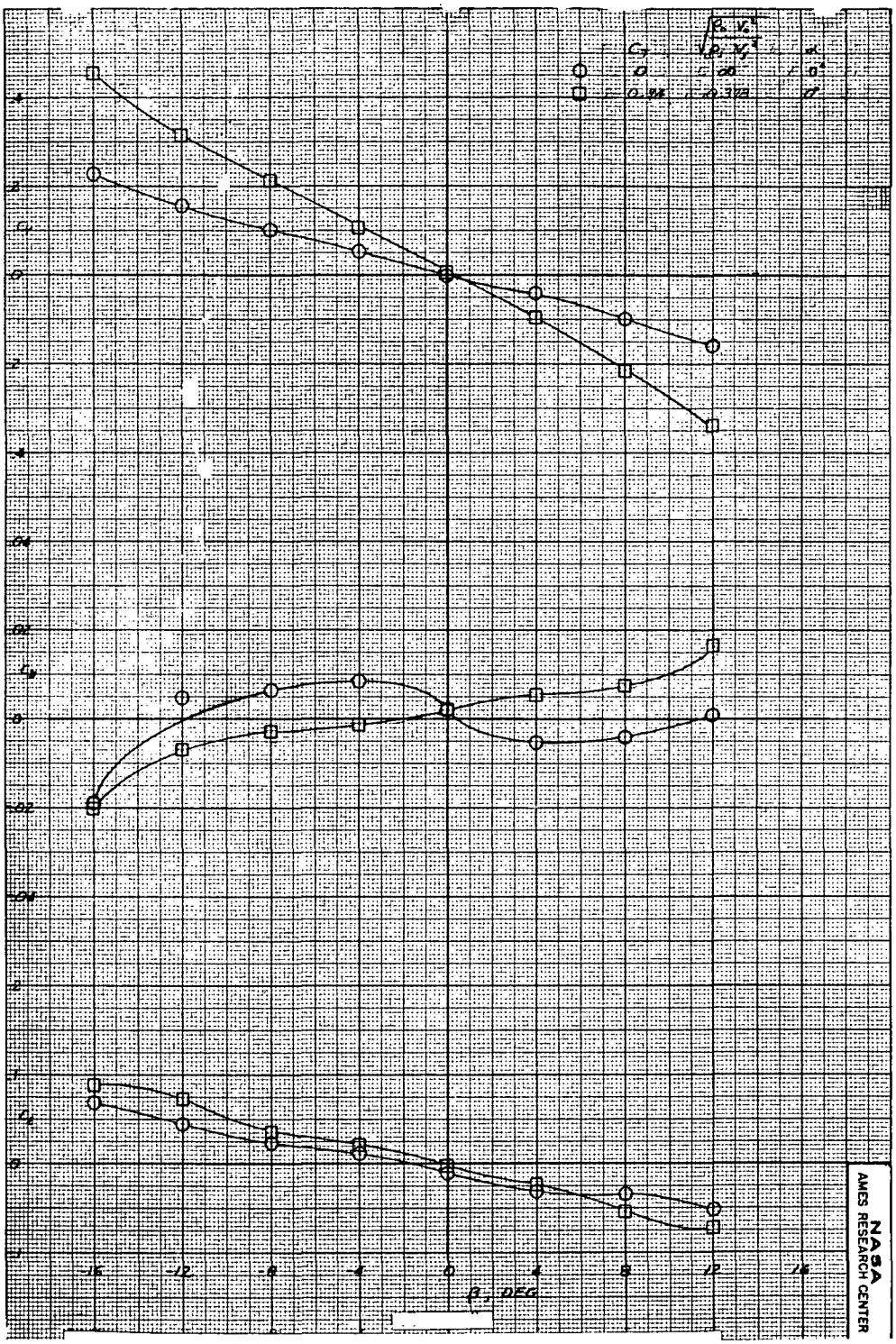

Figure 33.- Effect of sideslip angle on the lateral-directional characteristics of the model. $\sigma = 30°$. $i_t = 0°$. All engines set at equal thrust, $\delta_f = 45°$, $\delta_s = 25°$.

(a) $\alpha = 0°$.

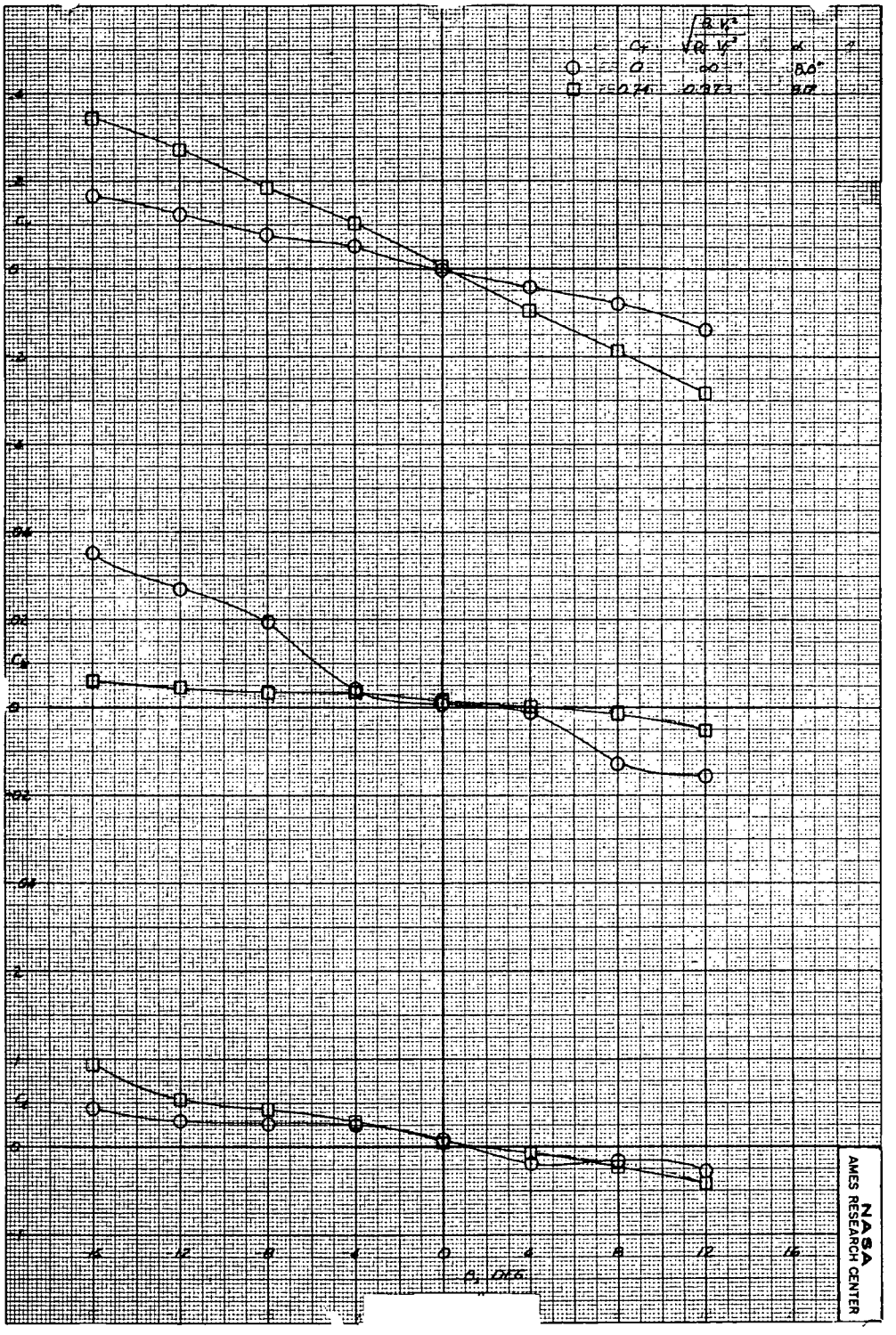

(b) $\alpha = 8°$.

Figure 33.- Continued.

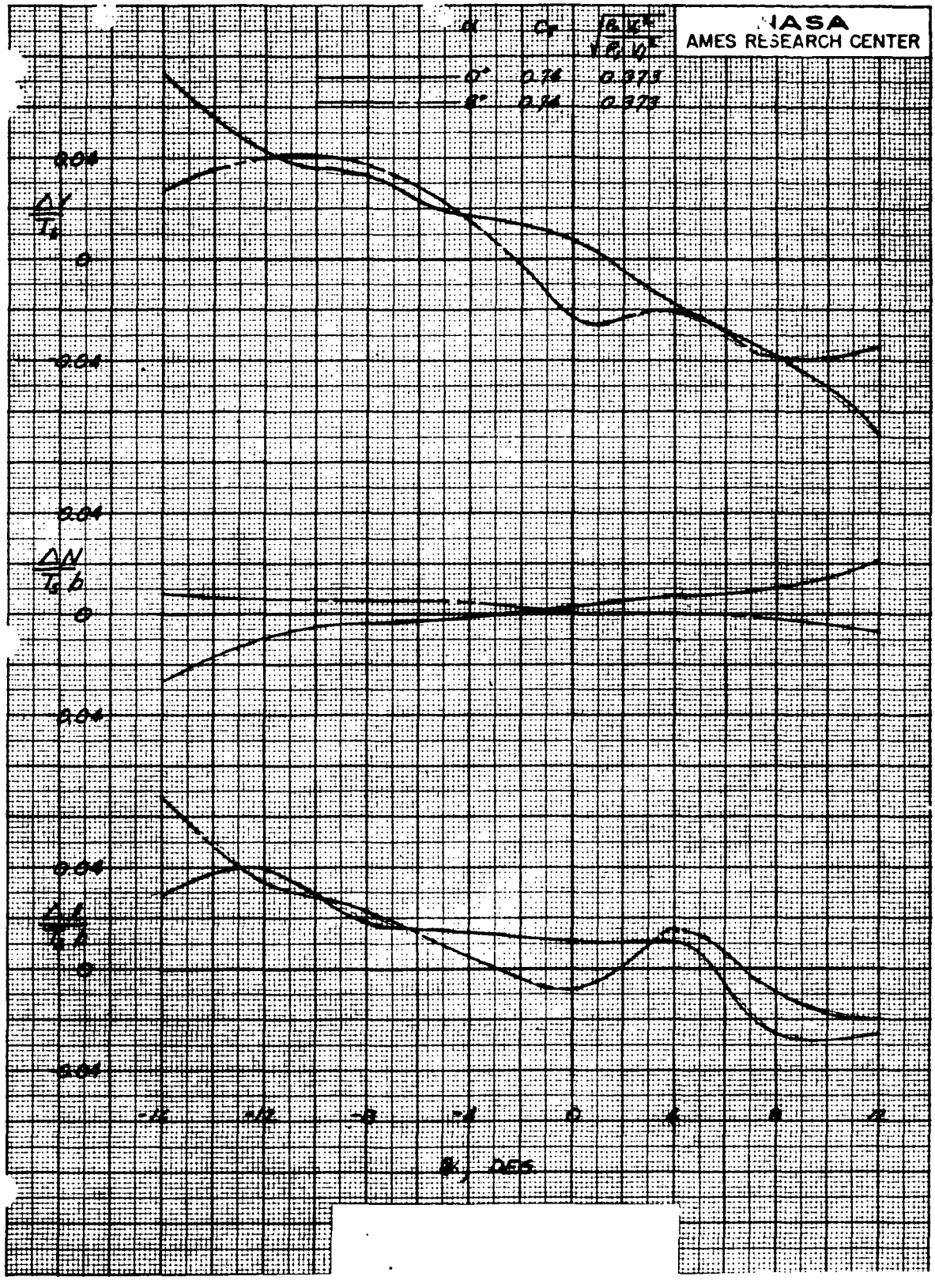

Figure 33.- Concluded.

(c) Interference increments.

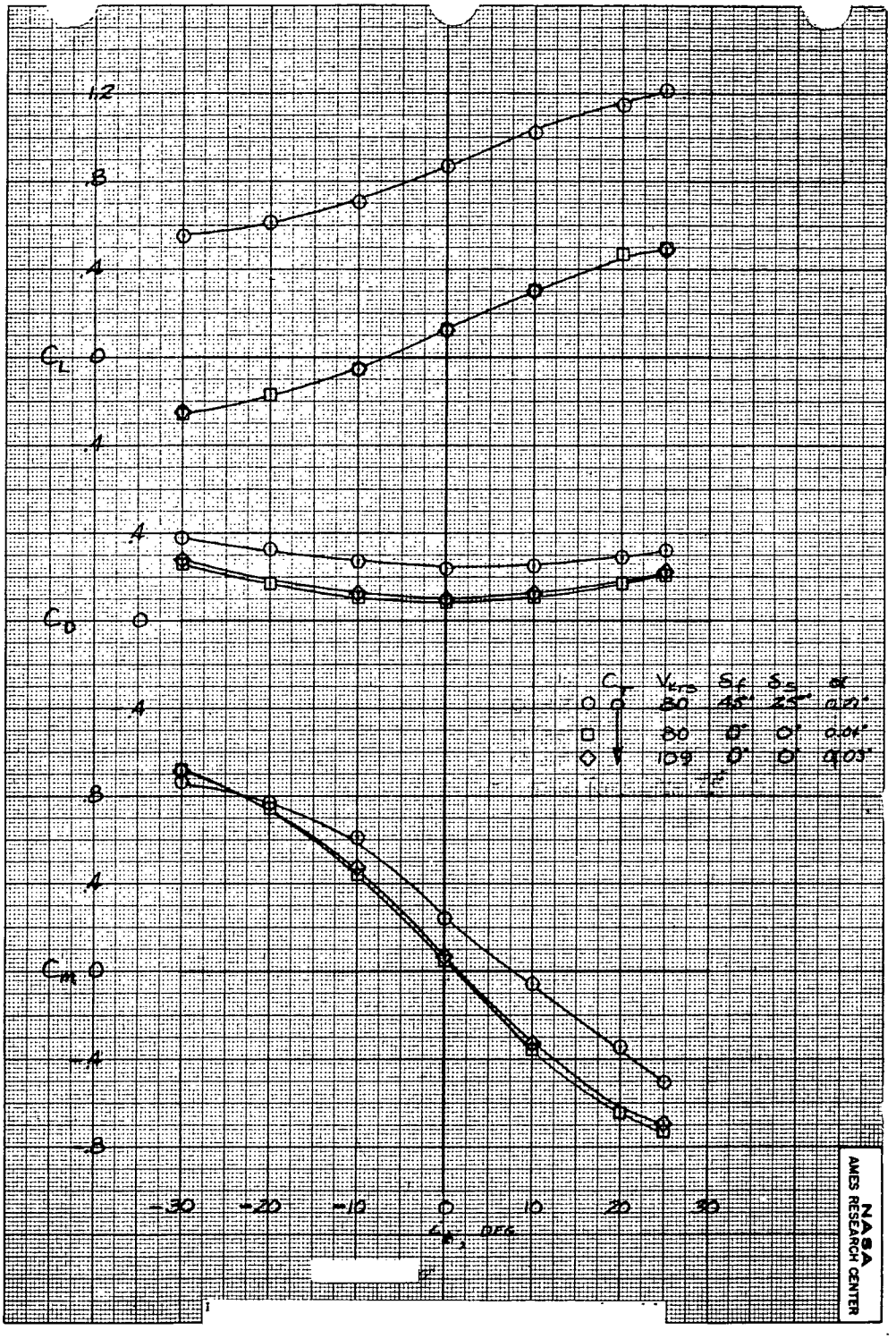

Figure 34.- Effect of horizontal tail deflection on the model longitudinal aerodynamic characteristics; $\beta = 0°$, Lift engines and cruise engine nozzles removed, Power off.

(a) $\alpha = 0°$.

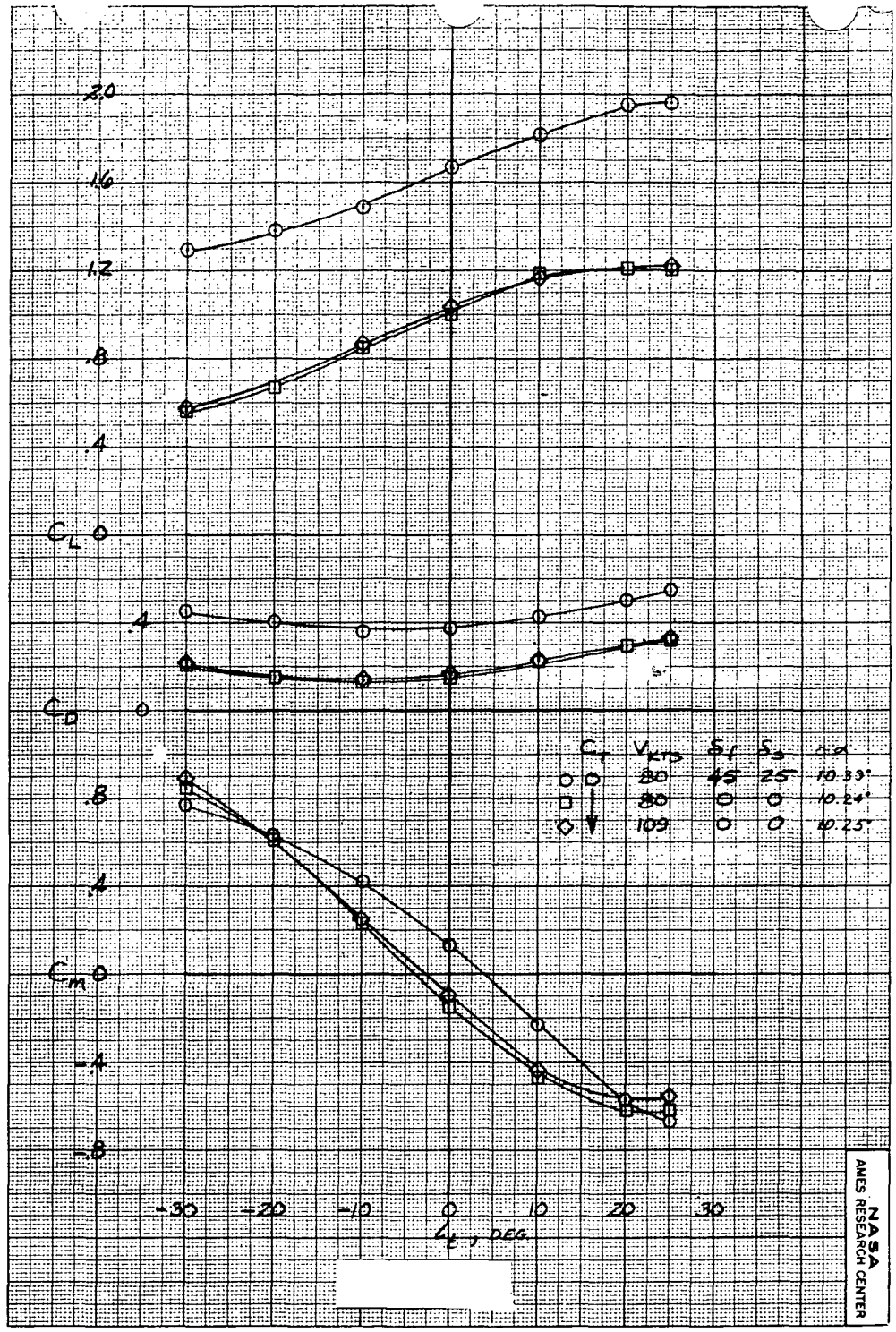

(b) $\alpha = 10°$.

Figure 34.- Concluded.

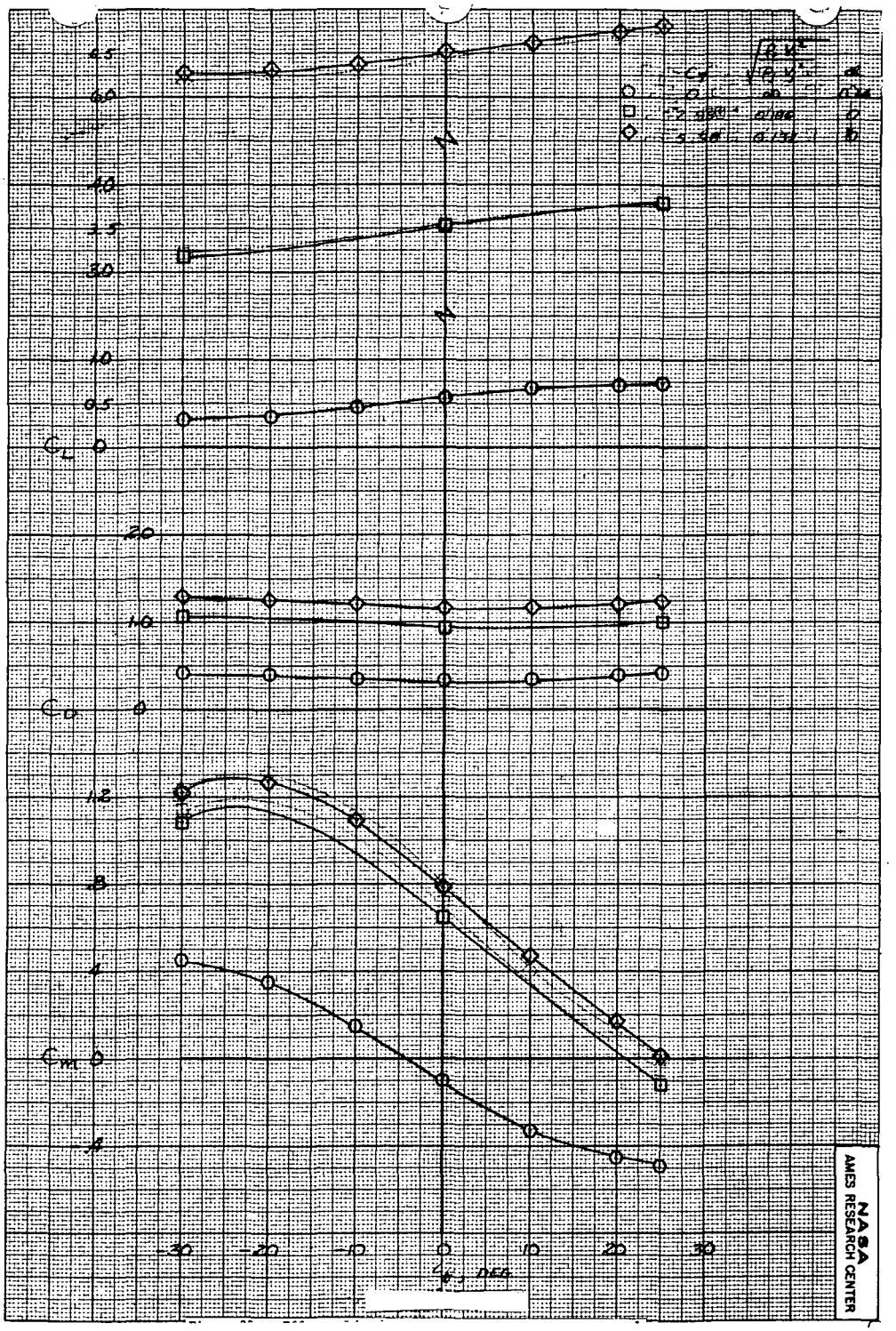

Figure 35.- Effect of horizontal tail deflection on the model longitudinal aerodynamic characteristics, $\beta = 0°$, $\sigma = 90°$, $\delta_f = 45°$, $\delta_s = 25°$.

(a) $\alpha = 0°$.

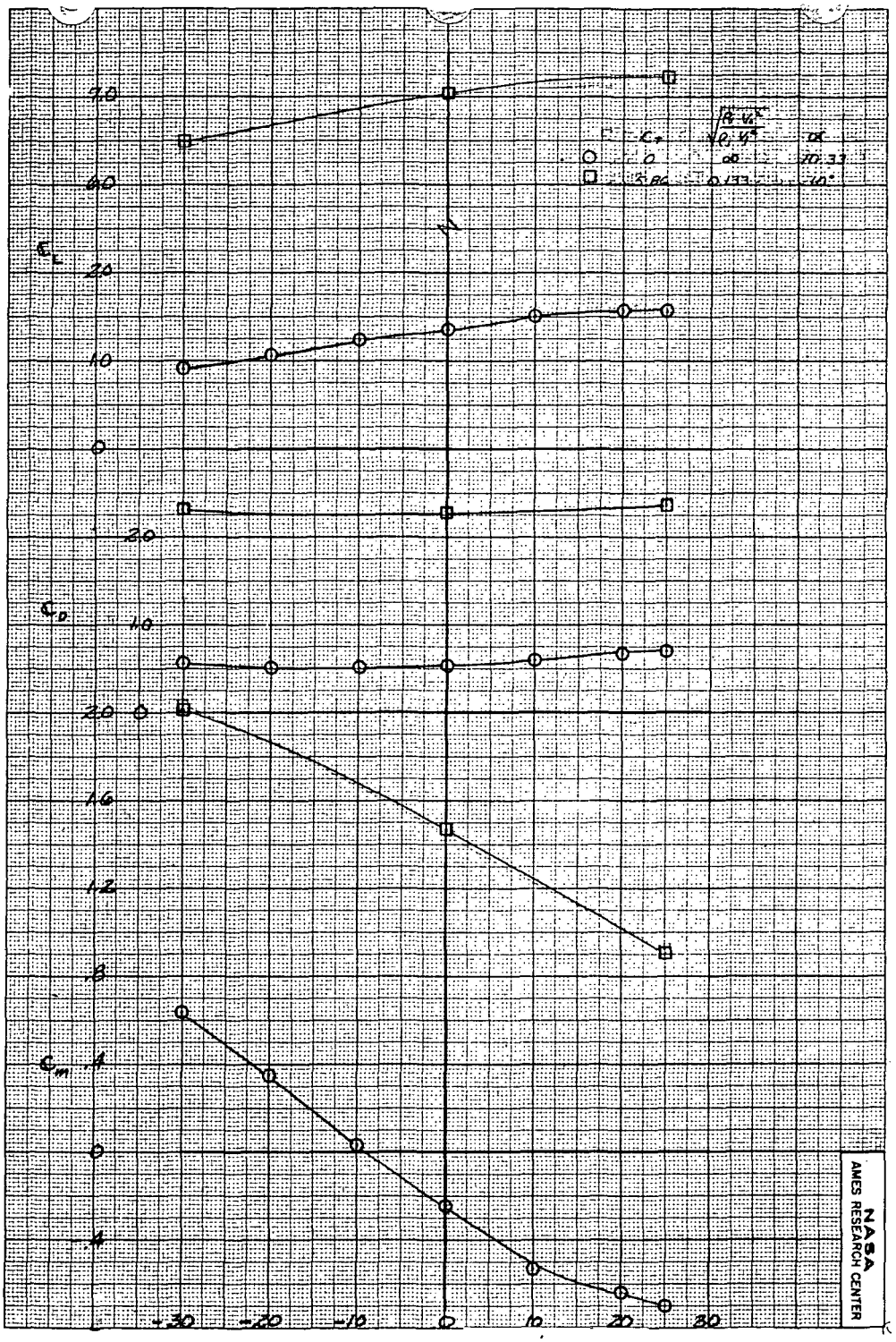

(b) $\alpha = 10°$.

Figure 35.- Concluded.

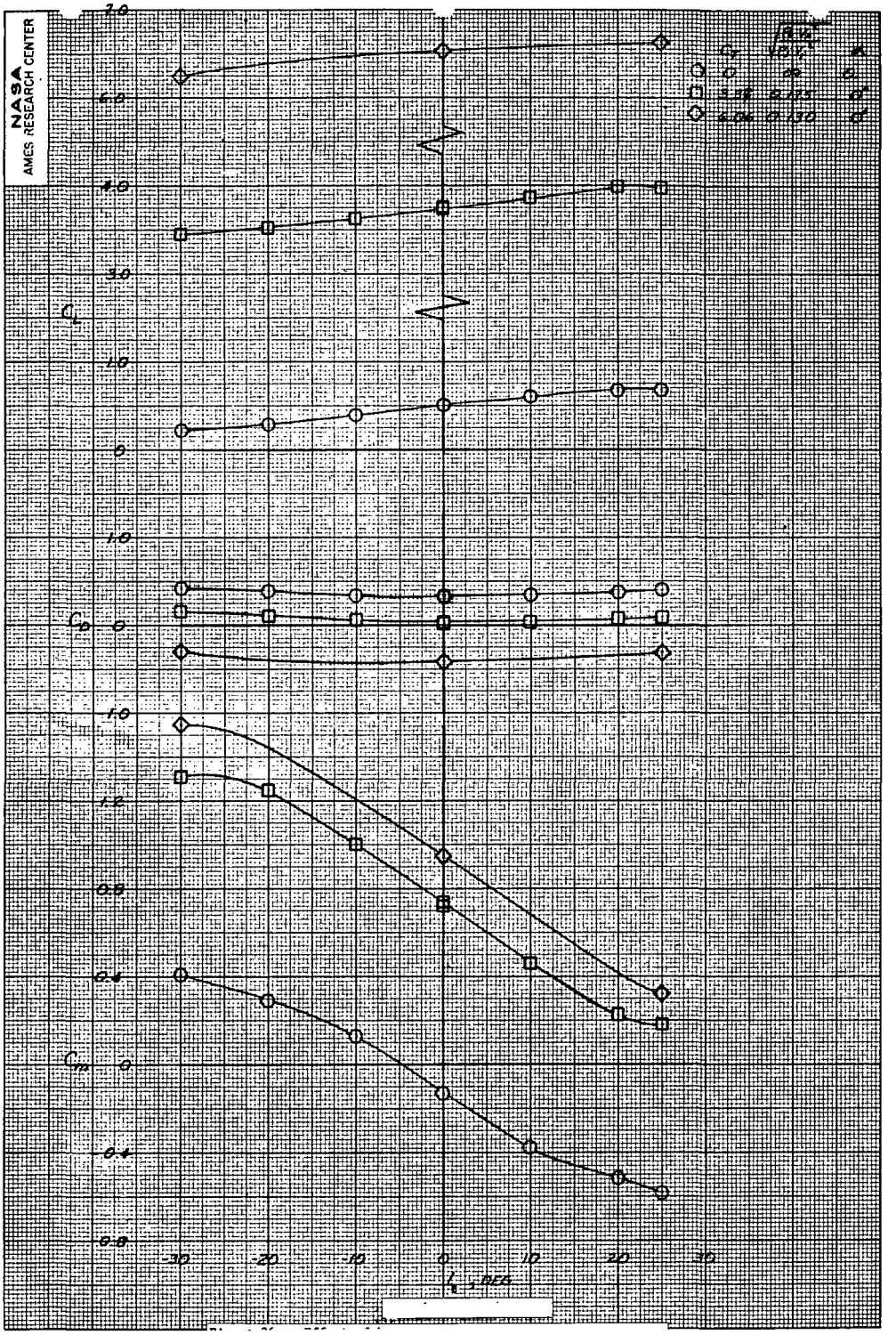

Figure 36.- Effect of horizontal tail deflection on the model longitudinal aerodynamic characteristics, $\beta = 0°$, $\sigma = 75°$, $\delta_f = 45°$, $\delta_s = 25°$.

(a) $\alpha = 0°$.

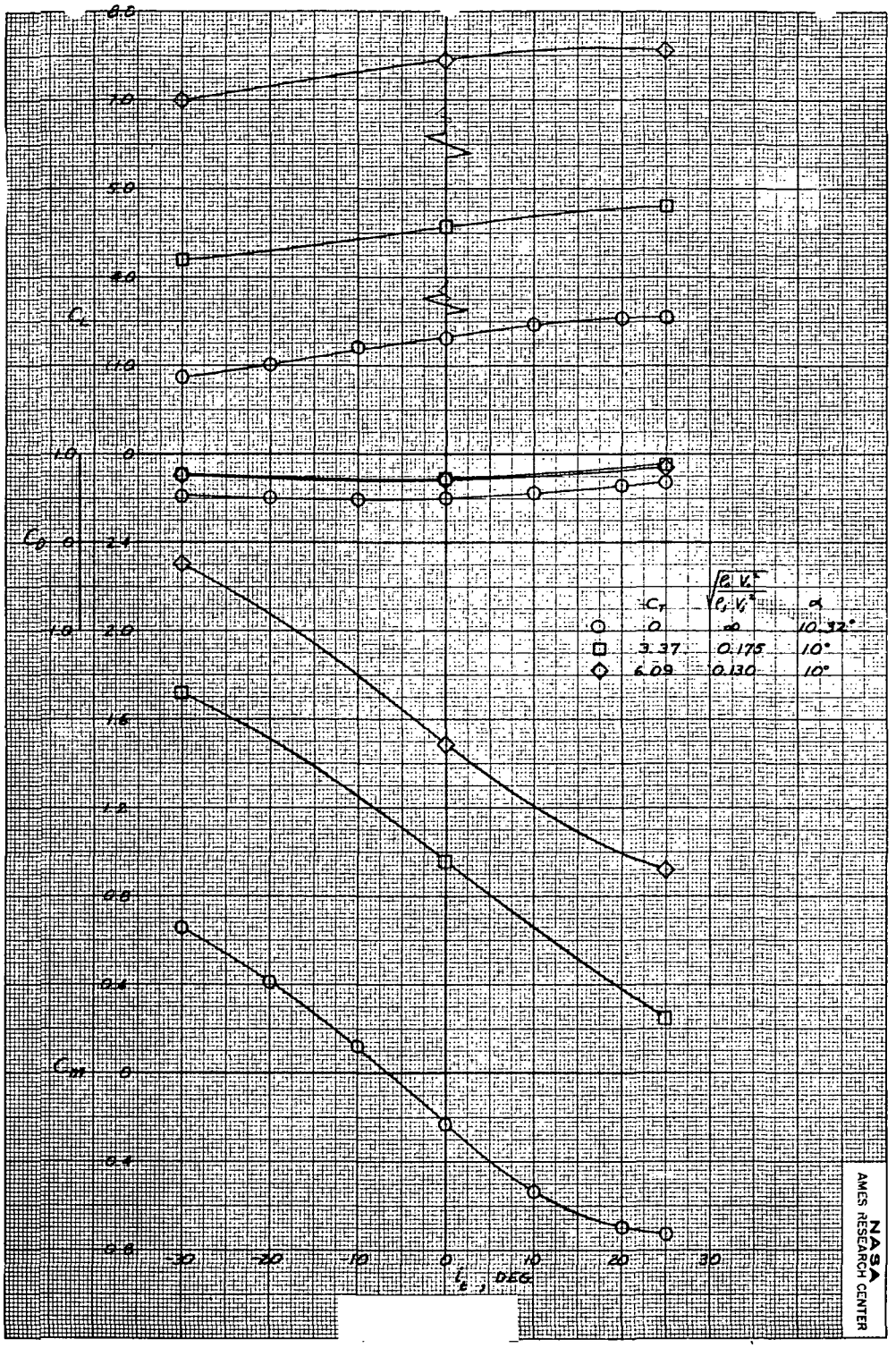

(b) $\alpha = 10°$.

Figure 36.- Concluded.

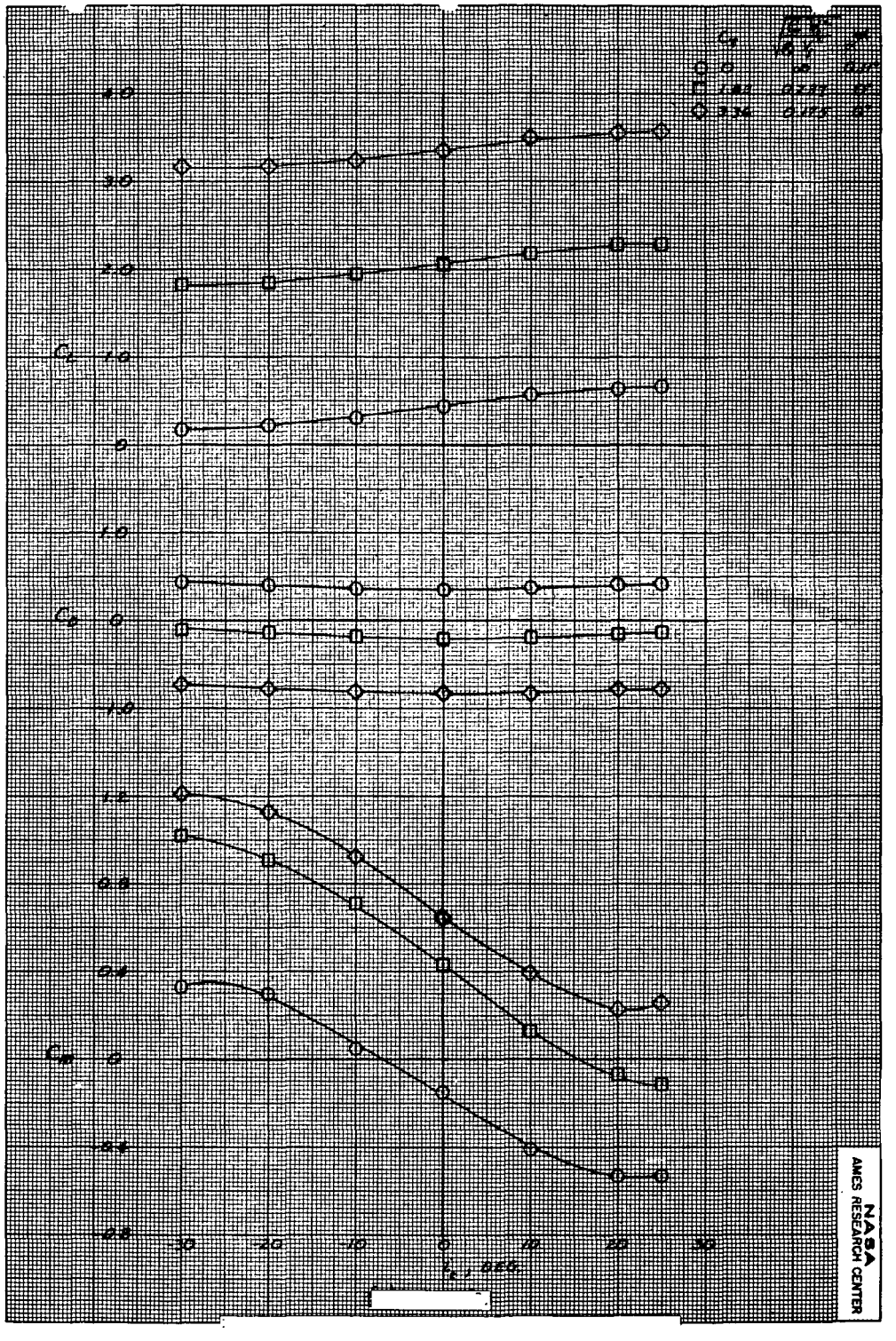

Figure 37.- Effect of horizontal tail deflection on the model longitudinal aerodynamic characteristics; $\beta = 0°$, $\sigma = 60°$, $\delta_f = 45°$, $\delta_s = 25°$.

(a) $\alpha = 0°$.

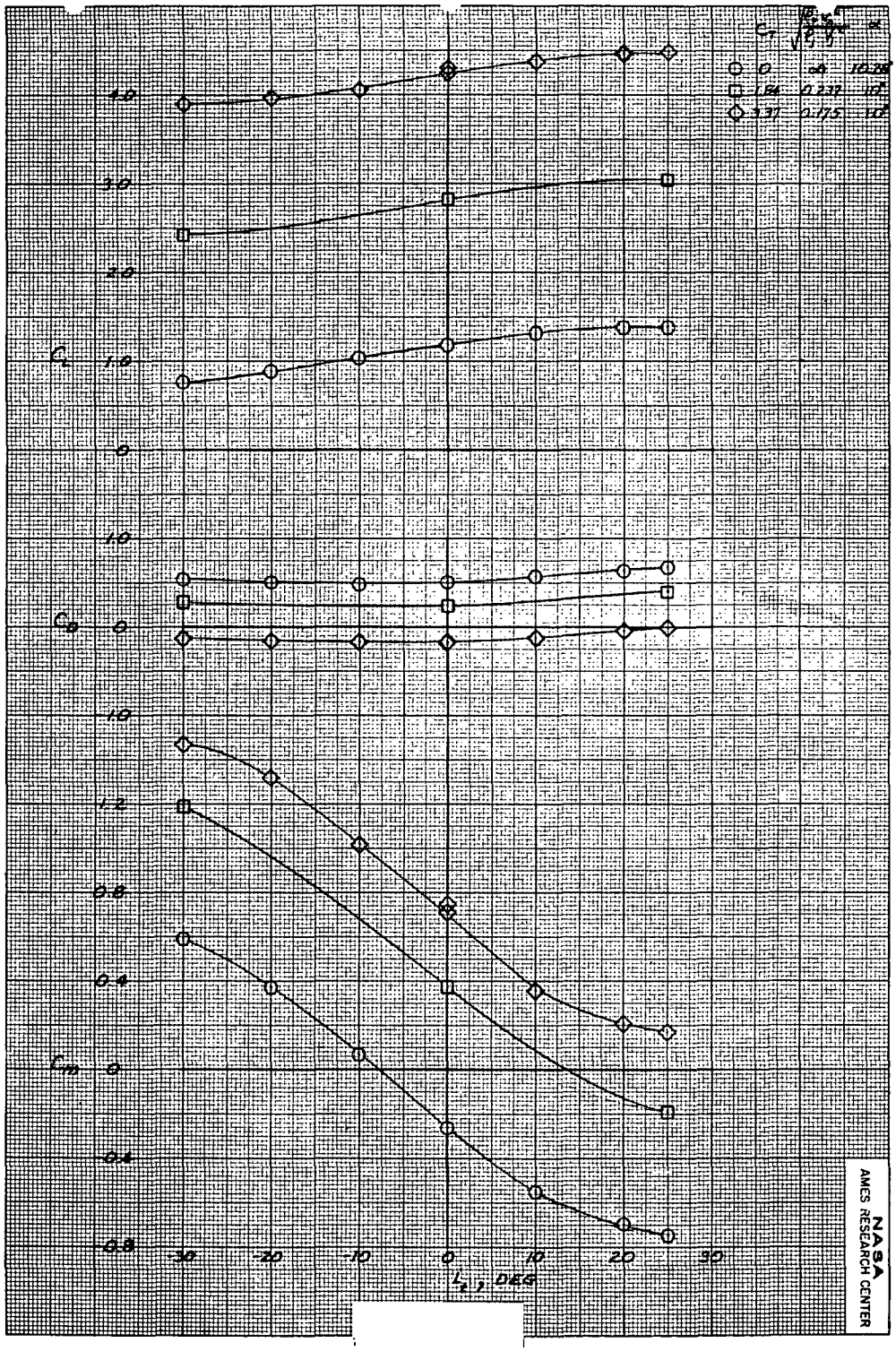

(b) $\alpha = 10°$.

Figure 37.- Concluded.

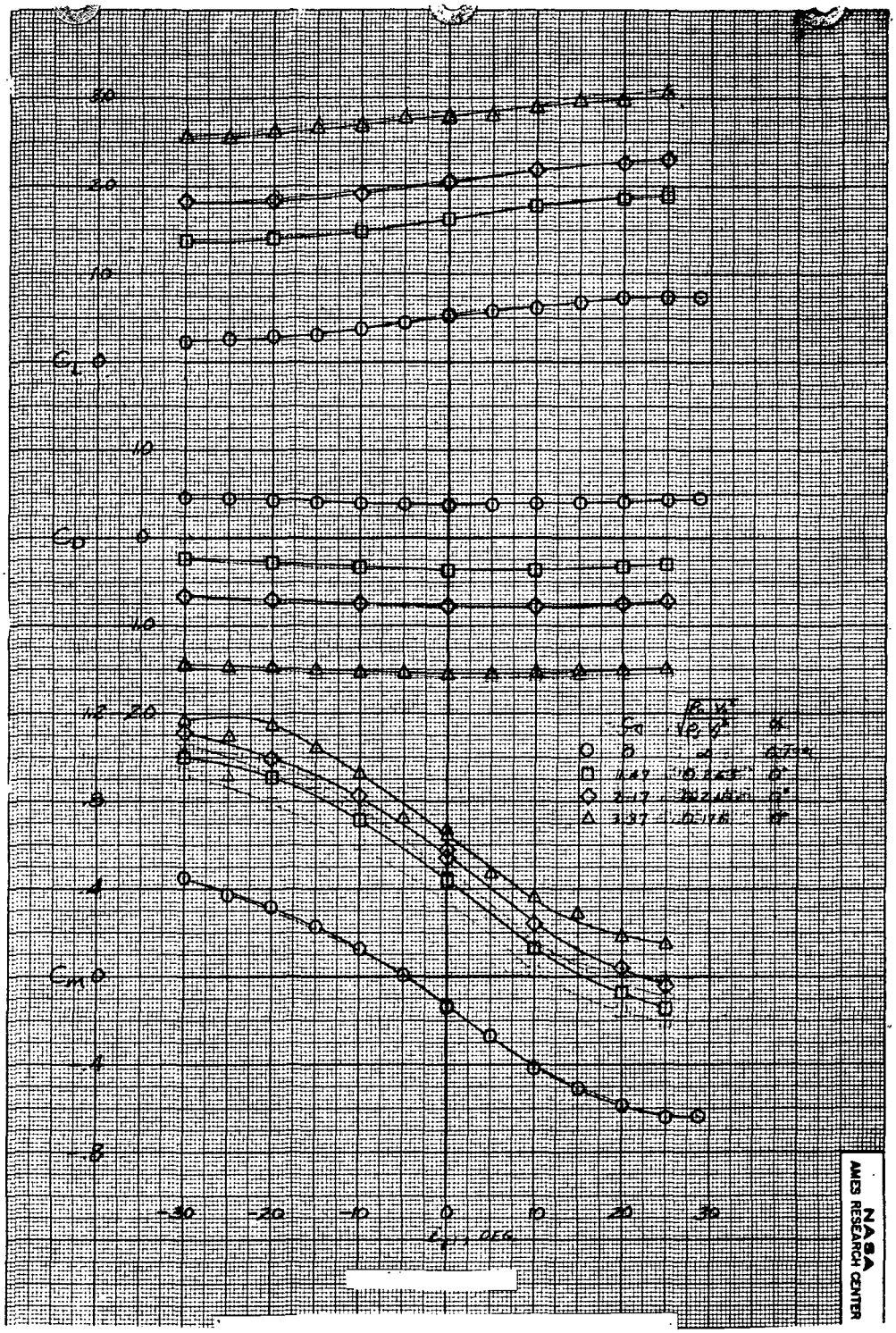

Figure 38.- Effect of horizontal tail deflection on the model longitudinal aerodynamic characteristics; $\beta = 0°$, $\sigma = 45°$, $\delta_f = 45°$, $\delta_s = 25°$.

(a) $\alpha = 0°$.

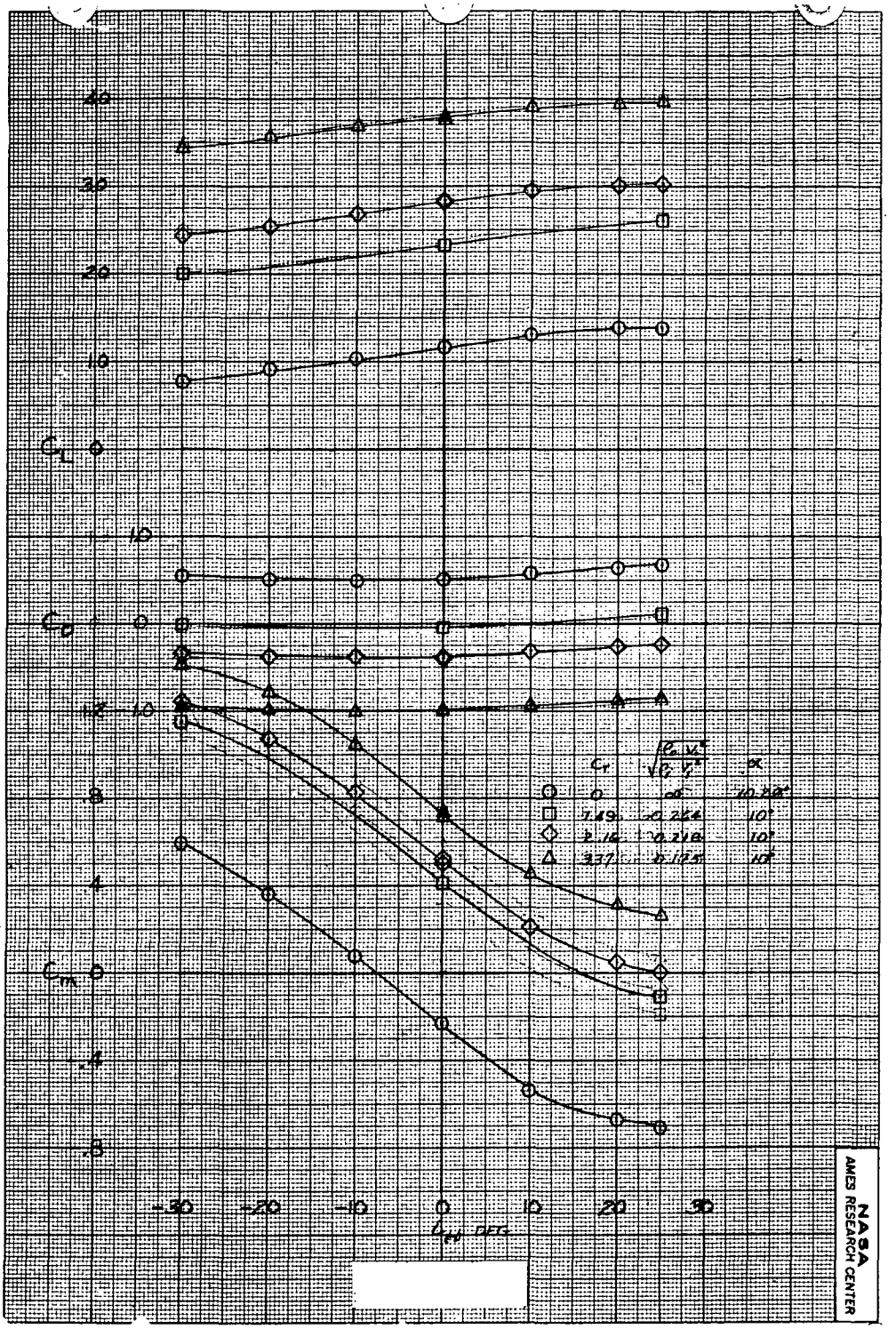

(b) $\alpha = 10^\circ$.

Figure 38.- Continued.

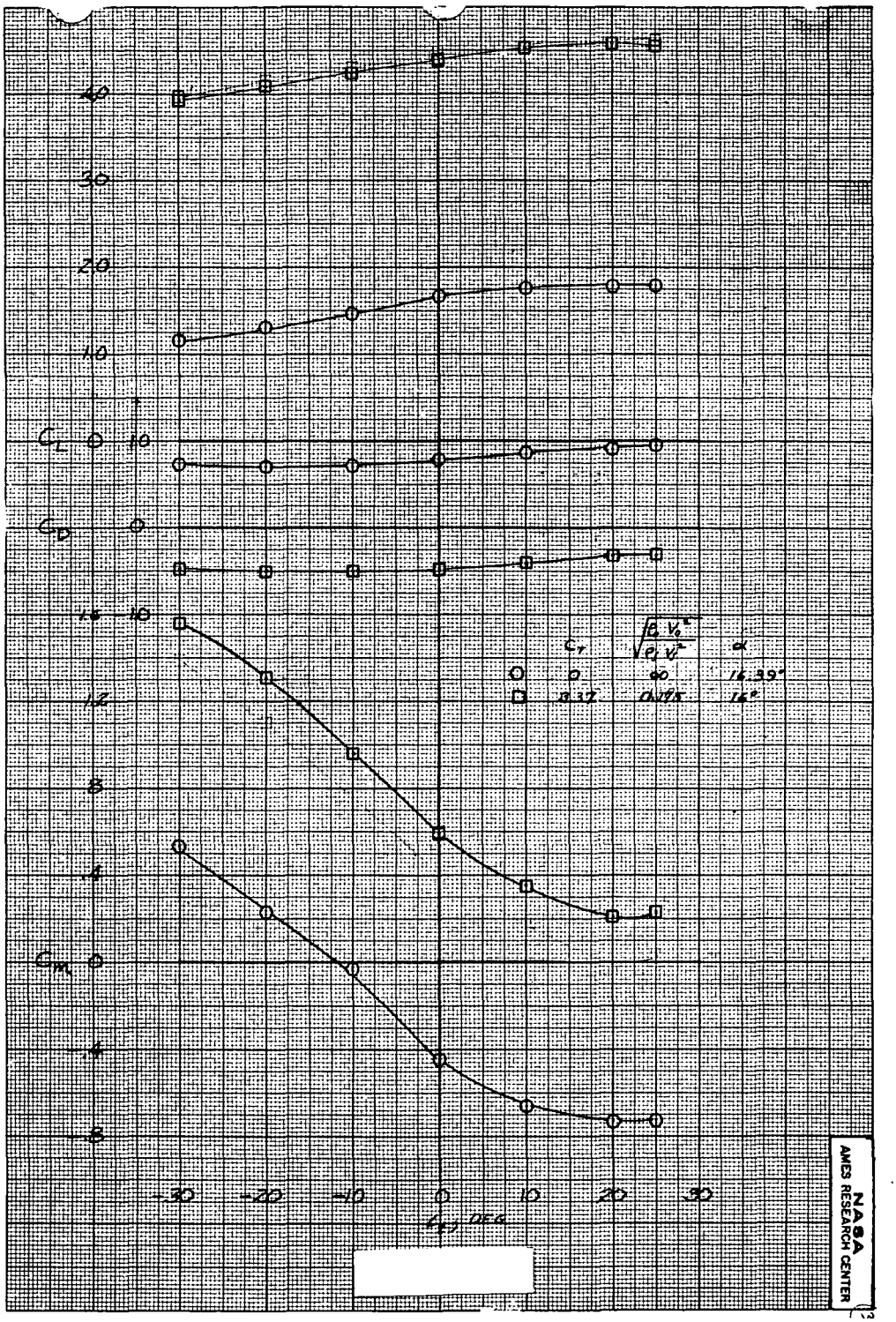

(c) $\alpha = 16°$.

Figure 38.- Concluded.

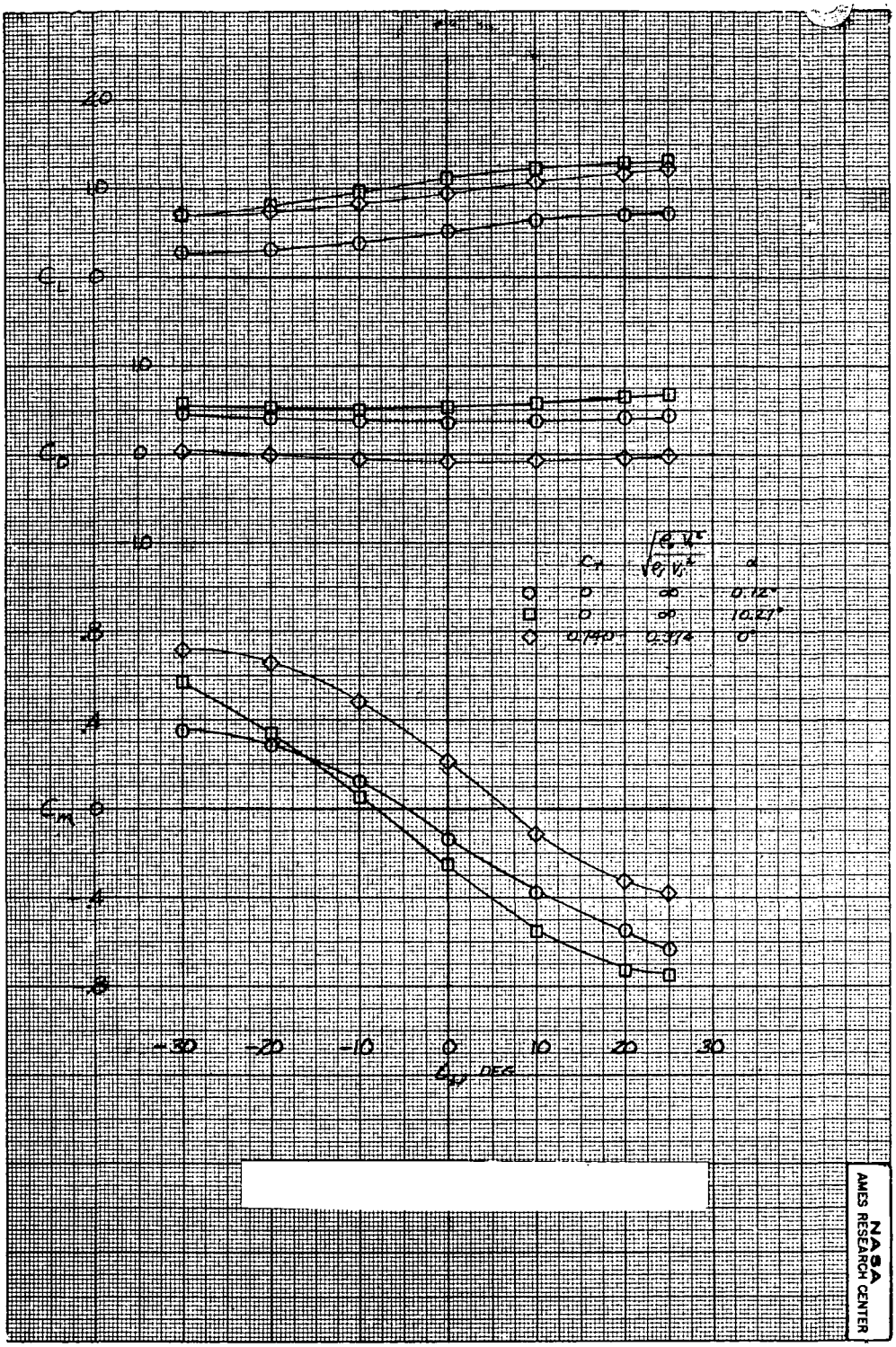

Figure 39.- Effect of horizontal tail deflection on the model longitudinal aerodynamic characteristics; $\beta = 0°$, $\alpha = 30°$, $\delta_f = 45°$, $\delta_s = 25°$.